Extracellular Matrix Effects on Hepatocyte Functioning: A Multivariate Regression Approach

BY

LIOUDMILA VALERYEVNA SOROKINA
B.S., University of Illinois at Chicago, 2017

THESIS

Submitted as partial fulfillment of the requirements
for the degree of Master of Science in Bioengineering
in the Graduate College of the
University of Illinois at Chicago, 2018

Chicago, Illinois

Defense Committee:

Salman R. Khetani, Chair and Advisor
Michael A. Stroscio
Thomas J. Royston

This thesis is dedicated to all who believed I could fly when I could barely crawl. You are the wind beneath my wings.

TABLE OF CONTENTS

List of Figures

List of Figures

List of Figures

List of Tables

LIST OF ABBREVIATIONS

DILI	drug-induced liver injury
MPCC	micropatterned co-culture
TCPS	tissue culture polystyrene
PHH	primary human hepatocyte
iHeps	induced pluripotent stem cells-derived human hepatocyte-like cells
ECM	extracellular matrix
LBM	liver biomatrix
TGF-β	transforming growth factor beta
PEMs	polyelectrolyte multilayers
CYP	cytochrome P450
CAR	constitutive androstane receptor
AHR	aryl hydrocarbon receptor
PXR	pregnane X receptor
GST	glutathione – S transferases
ATP	adenosine phosphate
ABC	adenosine phosphate binding cassette
MRP	multidrug resistant protein
iPSCs	induced pluripotent stem cells
FPH2	functional proliferation hit 2
ELISA	enzyme-linked immunosorbent assay
BSA	bovine serum albumin
GF	growth factor
GAG	glycosaminoglycan
FGF-2	fibroblast growth factor 2

SUMMARY

The use of *in vitro* liver models represents an important step in drug discovery and disease modeling. In the United States, 11% of acute liver cases are due to idiosyncratic drug-induced liver (DILI) injury, yet presently used animal models are a poor predictor of idiosyncratic DILI. Micropatterned co-cultures (MPCCs), composed of primary human hepatocytes (PHHs) and 3T3-J2 murine embryonic fibroblasts, demonstrate stable, long-term hepatic functions by controlling substrate geometry and cell-cell interactions *in vitro*. Yet present MPCC model is not fully human-relevant due to the use of both animal-derived cells and substrate. Furthermore, PHHs used in MPCCs are source-limited cells. To address these challenges, MPCCs using induced pluripotent stem cells-derived human hepatocyte-like cells (iHeps) in place of PHHs were designed and tested on various extracellular matrix (ECM) proteins. In a separate study, an ECM screen was performed in a traditional MPCC format to elucidate the effects of human ECM components on cell functioning and to compare them to mixed-ECM substrates such as decellularized human and porcine liver biomatrices. The presence of collagen I at 50% concentration showed upregulation of most tested hepatocyte functions. Finally, a platform was designed for *in vitro* delivery of transforming growth factor beta (TGF-β), a cytokine that plays a significant role in regulation of many chronic liver diseases. Present *in vitro* models of TGF-β employ soluble methods of delivery, which are not physiologically relevant and cost prohibitive. Fibronectin – coated polyelectrolyte multilayers (PEMs) of chitosan and heparin were used for adsorption and delivery of TGF-β to PHHs to discern the effect of microenvironmental cues on cell functioning. Multivariate regression analysis was employed to identify the contributing variables that can be used in the design of next generation *in vitro* liver

models. In particular, adsorbed TGF-β and the presence of co-culture upregulated PHH functions in PEMs.

1. INTRODUCTION

1.1 Inside the Liver

Human liver is a fascinating organ responsible for a variety of important functions such as the synthesis of plasma proteins, drug metabolism, and blood purification. Structurally, the liver is composed of hexagonal functional units known as lobules, which originate at the central vein and end with the hepatic artery, portal vein, and bile duct, collectively known as the portal triad (Juza and Pauli 2014; Lemaigre, Duncan, and Si-Tayeb 2010). The mixture of venous and arterial blood takes place in the liver sinuses and travels to the central vein via a network of sinusoidal capillaries, where it subsequently exits the lobule (Juza and Pauli 2014; Demetris and Bellamy 2016). This movement from periportal to perivenous zones demarcates liver zonation, with differences in important components of liver functions such as oxygen levels, nutrients, and various metabolic players (Birchmeier 2016).

Many metabolic processes in the liver are zonated as well. Specifically, drug metabolism involving cytochrome P450 (CYP) enzymes and glutathione conjugation occurs in the perivenous zone while bile acid, urea and albumin production occurs in the periportal zone (Lindros 1997; Jungermann and Keitzmann 1996; Gebhardt and Matz-Soja 2014). Additionally, assessment of albumin, a protein that helps maintain colloid osmotic pressure in the vasculature, and urea, a byproduct of the breakdown of amino acids in the liver, may indicate a presence of a potential disease (Bernardi, Maggioli, and Zaccherini 2012; Krebs 1942). Metabolism of xenobiotics and drugs occurs in three phases. Phase I is most commonly characterized as drug oxidation or reduction by CYP enzymes, with the most prominent CYPs such as CYP 3A, CYP 1A2, and CYP 2C (Amacher 2010). Such enzymes are found in the smooth endoplasmic reticulum of the hepatocytes (Williams et al. 2001). The activation of

nuclear receptors in phase I such as constitutive androstane receptor (CAR), aryl hydrocarbon receptor (AHR), and pregnane X receptor (PXR) is due to the ligands from xenobiotics binding to said receptors and inducing target gene expressions (Amacher 2010; Tien and Negishi 2006; Aleksunes and Klaassen 2012). The induction of CYP 3A4 activity is specifically due to PXR receptor (Aleksunes and Klaassen 2012). Phase II is centered on the conjugation via superfamilies of drug metabolizing enzymes such as glutathione – S transferases (GST) and results in enhanced excretion of the drug (Xu, Li, and Kong 2005). Phase III relies on adenosine phosphate (ATP) binding cassette (ABC) transporters such as P-glycoprotein (P-gp) and multidrug resistant protein (MRP) family to eliminate the drugs using energy stores (Xu, Li, and Kong 2005; Borst et al. 2018).

Most significant liver functions including drug metabolism happen in primary hepatocytes, which are the parenchymal cells and compose at least 70-80% of all liver cells (Bale et al. 2016; Juza and Pauli 2014; Wang and Kaufman 2014; Lemaigre, Duncan, and Si-tayeb 2010; Gordillo, Evans, and Gouon-Evans 2015). Non-parenchymal cells include sinusoidal endothelial cells, Kupffer cells, stellate cells, portal fibroblasts and cholangiocytes and provide both the support for primary hepatocytes as well as specific functions (Bale et al. 2016; Juza and Pauli 2014; Dranoff and Wells 2010). Specifically, endothelial cells that line the sinusoidal capillaries allow for the portal blood to reach the hepatocytes via fenestrae. Kupffer cells are resident macrophages in the sinusoids and perform phagocytic functions, stimulated by exposure to bacteria (Juza and Pauli 2014; Klein et al. 2018; Seki et al. 2000). Cholangiocytes line the biliary tract and maintain liver immunity through the use of pathogen recognition receptors and subsequent release of cytokines (Chen, Hara, and Larusso 2008). Cholangiocytes share a common progenitor with hepatocytes (Gordillo, Evans, and Gouon-

Evans 2015). Hepatic stellate cells are primarily known for their role in hepatic injury as they activate into myofibroblasts upon injury as well as storage of vitamin A in quiescent state (Juza and Pauli 2014; Gordillo, Evans, and Gouon-Evans 2015; Friedman 2018). They are found in the subendothelial space, between the endothelial cells and hepatocytes and comprise approximately 15% of all liver cells (Friedman 2008). Similarly to stellate cells, portal fibroblasts, which are adjacent to the bile duct, also differentiate into myofibroblasts in case of chronic injury (Dranoff and Wells 2010). Together, the aforementioned cell types work to perform essential liver functions and as a consequence, understanding their functioning and interactions is essential when designing *in vitro* models.

At the heart of cellular functions lies the extracellular matrix (ECM), an intricate network which provides the nearby cells with scaffolding as well as an environment to exercise basic cellular functions such as adhesion, migration, signaling, and proliferation (Baiocchini et al. 2016). ECM structural composition can be defined in terms of two types of macromolecules: proteoglycans and fibrous proteins such as collagens, laminins, fibronectins, and elastins, with collagen I being most prevalent (Frantz, Stewart, and Weaver 2018; Watanabe et al. 2016). The hallmark of collagen structure is the three polypeptides, such as two αI chains and one αII chain in collagen I, coiled in a right-handed triple helix formation (Shoulders and Raines 2009; Schuppan 1990). Fibronectin is a glycoprotein made of two monomers with covalent sulfide bond bridges (Johansson et al. 1997). Fibronectin is used to anchor other ECM components such as collagens by binding to integrins, which span across the cellular membrane. The cells secrete soluble fibronectin dimer of types I, II, and III modules, which is then converted into insoluble fibrils extracellularly (Wierzbicka-Patynowski and Schwarzbauer 2003). Laminin is another type of noncollogenous glycoprotein and is

composed of α, β, and γ subunits, forming three arms on the amino terminals and intertwined through coil interactions on carboxy-terminals (Matlin, Myllyma, and Manninen 2018; Carlsson et al. 1981). Laminins are found in the basement membrane, with laminin – 1 most frequently observed (Mak and Mei 2017; Clément et al. 1988).

Predominant location of ECM proteins in the liver is also zonated and corresponds to the functional needs of the cell types located in each part of the liver. For example, collagens I and III are found in the portal triad, central vein, Glisson's capsule, and the space of Disse (Martinez-Hernandez and Amenta 1995). Collagen IV is present in abundance in the space of Disse and also found in the portal triad, central vein, and basement membrane. Collagens IV and VI are the only network collagen type present in the liver; other collagen types are fibril-forming (Schuppan 1990). In addition to collagen IV, basement membrane contains laminins, entactins, and perlicans (Hahn et al. 1980; Martinez-Hernandez and Amenta 1995). Collagen V has a greater presence around the portal triad and central vein (Martinez-Hernandez and Amenta 1995). Collagen VII acts as an anchoring structure in the portal triad. Fibronectin is most abundantly present in the space of Disse and follows a distribution pattern similar to collagen I.

Changes in ECM composition often mark the presence of pathogenic processes and chronic liver diseases such as fibrosis, which is characterized in part by increased collagen deposition (Bataller and Brenner 2005; Williams et al. 2001; Friedman 2003). Thus, experimental methods to mitigate fibrosis include prevention of fibronectin fibril assembly that is necessary to support collagen deposition (Altrock et al. 2015). Ultimately, understanding cell-matrix interactions is crucial to designing therapies for chronic liver diseases.

Of special interest in understanding and eradicating chronic liver diseases are cell-cell signaling such as cytokines, for example transforming growth factor beta (TGF-β). TGF-β is actively involved in liver transformation from conception, by directing whether a progenitor cell becomes a hepatocyte or a cholangiocyte (Kaylan et al. 2016).

TGF-β is also involved in the remodeling response of the liver post-injury, causing the destruction of hepatocytes, transformation of HSCs into myofibroblasts, and subsequent excessive production of ECM proteins (Bataller and Brenner 2005; Dooley and Dijke 2012; Sanderson et al. 1995; Shek and Benyon 2004). TGF-β binds to receptors on proteoglycans, namely types I, II, and III, activating macrophages such as Kupffer cells (Bissell, Roulot, and George 2001; Nguyen-Lefebvre and Horuzsko 2015). One of the present challenges in designing *in vitro* models using TGF-β is mimicking the native-binding state of said cytokine.

1.2 Current Perspectives On In Vitro Models

The complexities of cell-matrix interaction as well as the surrounding environmental cues have long been a target for *in vitro* liver models. Since liver transplantation, a costly and donor-limited procedure, remains the only viable long-term solution for chronic liver diseases such as cirrhosis and hepatitis, continuing research efforts target design of viable *in vitro* models. In addition, idiosyncratic drug-induced liver (DILI) injury is responsible for 11% of acute liver failure cases in the United States and may have a variety of factors such as age, gender, and presence of chronic liver disease that contribute to its occurrence (Leise, Poterucha, and Talwalkar 2014; Reuben, Koch, and Lee 2010; Kaplowitz 2004). It is particularly important to develop platforms to identify DILI in humans since many compounds that contribute to DILI are tested in animal models that are not representative of the human-specific metabolic response. In fact, using animals for the prediction of human DILI only works 50% of the time,

which could be attributed to the species-specific difference in metabolic response as well as poor genetic diversity in lab animals (Lin and Khetani 2016). The aforementioned challenges contribute to the fact that it takes at least a decade to bring a drug to the market and call for species-specific screening strategies in pre-clinical studies (Stevens and Baker 2009).

Present two dimensional strategies for high-throughput *in vitro* testing are comprised of conventional cell cultures and micropatterned co-cultures (MPCCs) while some three dimensional approaches include spheroids, liver slices, and perfusion systems (Lin and Khetani 2016). Cancerous cell lines such as HepG2 have been used for decades and are advantageous in high-throughput screens due to their virtually unlimited sourcing. However, they are problematic due to their single donor origin and subsequently, anomalous outputs of liver functions. By contrast, primary human hepatocytes (PHHs) most closely represent liver functioning in an *in vitro* format as well as result in more accurate toxicity results (Lin and Khetani 2016; Westerink and Schoonen 2007). Despite these advantages, PHH monocultures are not ideal for studying DILI due to their downregulation of functions after a few days in culture as well as donor variability. Three dimensional spheroids have been used to mitigate the problems presented by two dimensional monocultures as they demonstrated improved functions when compared to traditional monoculture (Lin and Khetani 2016). Spheroids have been constructed using both primary hepatocytes and cell lines as well as both natural and synthetic biomaterials, resulting in improved cell-cell and cell-matrix interactions (Lin and Khetani 2016; Thomas et al. 2005; Lin and Chang 2008; Ramaiahgari et al. 2014). Although liver slices contain all liver cell types and native tissue architecture, they are best suited for short term studies of 24-72 hours due to rapid decrease in functioning (Lin and Khetani 2016; Khetani and Bhatia 2008). Perfusion systems may be used for re-creating functions based on zonation,

tissue-like mechanical forces, and architecture to allow for particular cell-cell interactions (Lin and Khetani 2016; Allen, Khetani, and Bhatia 2018; De Bartolo et al. 2009; Andria et al. 2010). Yet the increased number of variables and long-term maintenance of steady state make perfusion systems challenging to become an industry standard.

MPCC platform was developed to better control cellular microenvironment, specifically cell-cell interactions, by controlling the geometry of hepatocyte islands as well as the interaction with non-parenchymal cell types. Thus, MPCC captures the organizational structure relevant at the tissue level, rather than the randomized cellular distribution seen in conventional co-culture models. The MPCC system utilized in experiments detailed further in this thesis was developed using soft lithography by Khetani and Bhatia (Khetani and Bhatia 2008). The patterning is created by exposing ECM protein coated tissue culture polystyrene (TCPS) multi-well plate to oxygen plasma. A polydimethylsiloxane (PDMS) mask is used to protect portions of ECM protein coating, allowing the plasma to etch away the unprotected parts. Hepatocytes are seeded onto the remaining ECM islands ~500 μm in diameter with ~ 1200 μm spacing in between (Khetani and Bhatia 2008; Berger et al. 2015). Non-parenchymal 3T3-J2 murine fibroblasts are seeded approximately 24 hours later. The use of MPCC demonstrated maintenance of hepatocyte functions such as CYP450, phase II genes, and canalicular transport over several weeks (Khetani and Bhatia 2008). Although MPCC was subsequently commercialized by Hepregen, improvements to this model are needed (Bale et al. 2014). Specifically, the limitations of using PHHs and the need for a more human-relevant ECM substrate are addressed in chapters 2 and 3 of this thesis. Chapter 4 describes a novel approach for delivery of TGF-β using fibronectin-coated polyelectrolyte multilayers (PEMs) (Lin et al. 2017). PEMs are created using layer-by-layer assembly of aqueous materials of opposite charge as a result of their

electrostatic interactions (Costa and Mano 2014). Ionic strength is of particular significance to the design of PEMs with specific functionality as charge densities of weak polyelectrolytes depend upon the pH of the solution (Schlenoff and Dubas 2001; Choi and Rubner 2005; Salomäki, Vinokurov, and Kankare 2005). A variety of properties due to surface modification coupled with low cost of fabrication make PEMs use possible with a plethora of biologically-favorable substrates. The studies presented in this thesis explored the long-term delivery of TGF-β to PHHs *in vitro* using chitosan-heparin PEMs coated with fibronectin (Lin et al. 2017). The overall aims of this thesis are to present novel methods of modification of cell functioning as well as to create more physiologically relevant improvements upon the existing MPCC model.

2. ECM EFFECTS ON INDUCED PLURIPOTENT STEM CELLS-DERIVED HUMAN HEPATOCYTE-LIKE CELLS IN MPCC

2.1 Motivation

As the areas of drug discovery and personalized medicine become more reliant on *in vitro* models for new breakthroughs, the sourcing of cells for species and physiologically relevant models becomes a limiting factor. In 2012, the Nobel Prize winners Drs. Gurdon and Yamanaka delivered an exciting possible solution by establishing that mature cells are in fact reversible and that they may be reprogrammed to become pluripotent. Induced pluripotent stem cells (iPSCs) have several distinct advantages over donor-obtained human hepatocytes: they are a nearly unlimited cell source that can be tailored to individual patients, they can help reduce lot to lot variability, and they are not obtained from human embryos and can be considered an ethical cell source. As the protocols for generating induced pluripotent stem cells-derived human hepatocyte-like cells (iHeps) demonstrating functions comparable to hepatocytes continue to be optimized, MPCC with Matrigel overlay was used to significantly increase iHep functions (Berger et al. 2015; Du et al. 2014; Si-Tayeb et al. 2010).

The presented study was used to verify the long-term effects of individual ECM matrix components on MPCC iHeps functioning over a course of 35 days. As this study was a continuation of prior work done by Mr. Dustin Berger and Dr. Matthew Davidson, it was used to confirm the top performing ECM proteins and their combinations for long-term functionality of iHeps. Based on prior work, human collagens I, III, III + IV and gold standard, rat tail collagen I, were chosen to serve as controls. For combinations of ECM proteins, Mr. Berger and Dr. Davidson used a concentration of 25 µg/mL per protein in combinations of the aforementioned proteins, thus varying the final concentration. In this study, a concentration of

25 µg/mL total was used to see whether the final protein concentration may be kept constant while maintaining high, long-term iHeps functionality and reducing materials cost. Protocol comparisons were entitled and are thereafter referred as “Berger/Davidson” for variable final protein concentration protocol and “Lin/Sorokina” for constant final protein concentration protocol used. ECM combinations used to compare the two protocols included human collagen IV + fibronectin, human collagen III + IV + fibronectin, and human collagen III + IV + fibronectin + laminin. Fibronectin and laminin were taken out as experimental controls and attempted to re-pattern in subsequent studies. iHeps were cultured with murine 3T3-J2 fibroblasts in MPCC format. iHeps functionality was assessed via albumin, urea, CYP1A2, CYP2A6, CYP2C9, and CYP3A4 screens.

2.2 Methods

2.2.1 Formation of ECM MPCCs

MPCCs were created using soft lithography in a process outline by Khetani and Bhatia (Khetani and Bhatia 2008). In addition to using rat tail collagen I as a substrate, human collagens I, III, III + IV, laminin, and fibronectin were used as substrates at concentrations of 25 µg/mL per total protein concentration. Protein combinations of human collagen IV + fibronectin, human collagen III + IV + fibronectin, and human collagen III + IV + fibronectin + laminin were coated at 25 µg/mL per total protein concentration following the “Lin/Sorokina” protocol and at 25 µg/mL per individual protein concentration following the “Berger/Davidson” protocol. 24-well plates were coated with respective ECMs, incubated for 2 hours at 37ºC, patterned using PE-25 oxygen plasma machine (PlasmaEtch, Carson City, NV) and sterilized with 70% ethanol. Plates were coated with 0.2% bovine serum albumin (BSA) and incubated at 37ºC for 45 minutes prior to iHeps seeding.

2.2.2 Cell Culture

Cryopreserved iHeps (iHep 2.0 iCell, CDI Lot 1029, PHC-100-020-001-P7, WS/BRW/7/28/15), were thawed in previously made thaw media, consisting of 47.5 mL RPMI with l-glutamine, 1 mL B27, 1 mL CDI iHep 2.0 Media Supplement, 500 µL pen/strep, and 0.5 µL dexamethasone. iHeps were re-suspended in plating media, consisting of 47.5 mL RPMI with l-glutamine, 1 mL B27, 1 mL CDI iHep 2.0 Media Supplement, 500 µL pen/strep, 0.5 µL dexamethasone, and freshly spiked OSM at the concentration of 2.5 ng/mL, ROCK inhibitor at the concentration of 5 µM, and 10 µM FPH2. Following a cell count and assessing percent viability at 88.99%, the cells were seeded in plating media at 223,000 cells per 300 µL, gently agitated every 20 minutes, and incubated at 37ºC overnight. The next day the cells were washed three times with warm RPMI with l-glutamine and incubated in maintenance media, consisting of 47.5 mL RPMI with l-glutamine, 1 mL B27, 1 mL CDI iHep 2.0 Media Supplement, 500 µL pen/strep, 0.5 µL dexamethasone, and freshly spiked OSM at the concentration of 2.5 ng/mL and 10 µM FPH2.

Maintenance media was changed and collected for further analysis every other day for 35 days. At day 5, previously cryopreserved and expanded 3T3-J2 murine fibroblasts were seeded at the density of 90,000 cells per 300 µL in iH2M2 medium plus 10% bovine serum (lot # 1424960). The co-cultures were gently agitated every 30 minutes for 2 hours and incubated at 37ºC overnight. H2M2 medium consisted of 42.25 mL DMEM, 1 mL B27, 750 µL Hepes buffer, 500 µL ITS+, 500 µL pen/strep, 0.5 µL dexamethasone, and 0.5 µL glucagon. Fresh OSM at the concentration of 2.5 ng/mL and 10 µM FPH2 were added in at every media change. From day 9 onwards, medium was changed to iH2M2 plus 5% knock out serum plus 5 % DMEM as well as freshly spiked OSM and FPH2 at the aforementioned concentrations. At day

29, medium was changed to 1% bovine serum medium. To assess morphology, images were taken at 4X magnification using phase contrast imaging.

2.2.3 Biochemical Assays

Cell functions were assessed via albumin and urea production as well as CYP1A2, CYP2A6, CYP2C9, and CYP3A4. Albumin levels were detected using a competitive enzyme-linked immunosorbent assay (ELISA) with the use of horseradish peroxidase detection and the substrate of 3,3',5,5'-tetramethylbenzidine (TMB), as previously outlined by Khetani and Bhatia (Khetani and Bhatia 2008). Urea assessment of collected media was performed using diacetylmonoxime with acid and heat in a colorimetric endpoint assay, also previously presented in a work by Khetani and Bhatia (Khetani and Bhatia 2008). For CYP450 analysis, supernatant was collected on days 11, 19, 25, and 33. PGlo medium for iHeps used in CYP assays constituted of 48.75 mL of 1X DMEM – phenol red + glucose, 750 µL Hepes buffer, and 500 µL pen/strep. CYP activity was measured via luminescence for CYPs 3A4 (luciferin – IPA) and 2C9 (luciferin – H), as outlined by Berger et al. (Berger et al. 2015). CYP activity was also measured via fluorescence for CYPs 2A6 (7-hydroxy-coumarin) and 1A2 (Resorufin). Post-rinse in PGlo medium outlined above, the cultures were incubated for either 1 hour (CYPs 3A4 and CYP 2A6) or 3 hours (CYPs 1A2 and CYP 2C9) with the diluted substrate at 37ºC. Supernatants were collected, processed, and analyzed using a spectrophotometer.

2.2.4 Data Analysis

Microsoft Excel was used for graphing.

2.3 Results and Discussion

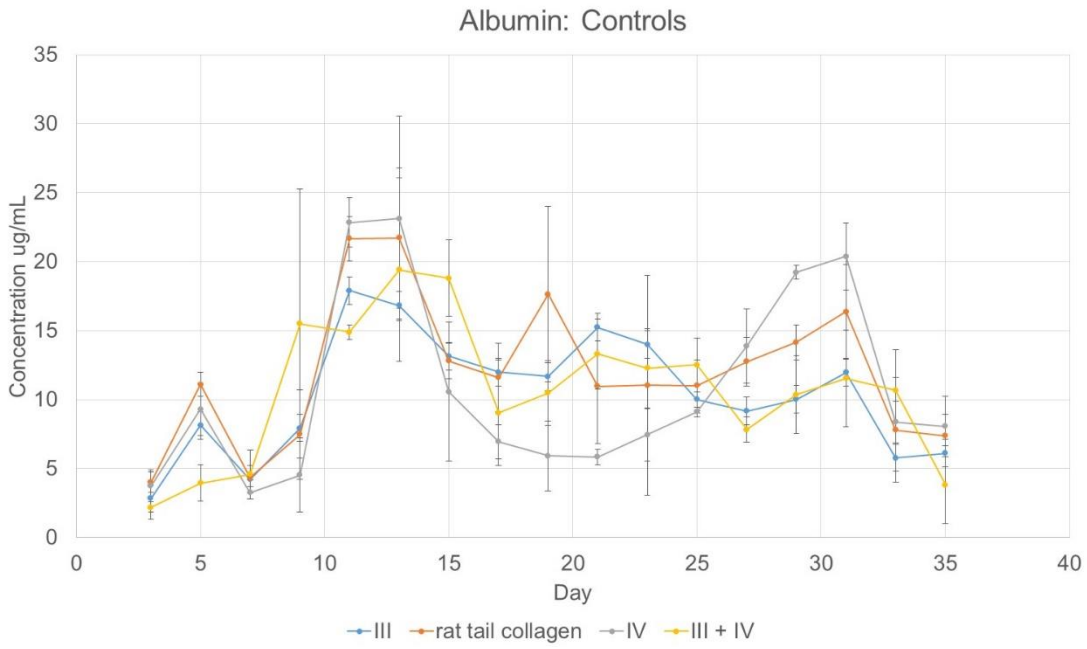

Figure 1 Albumin production in control conditions.

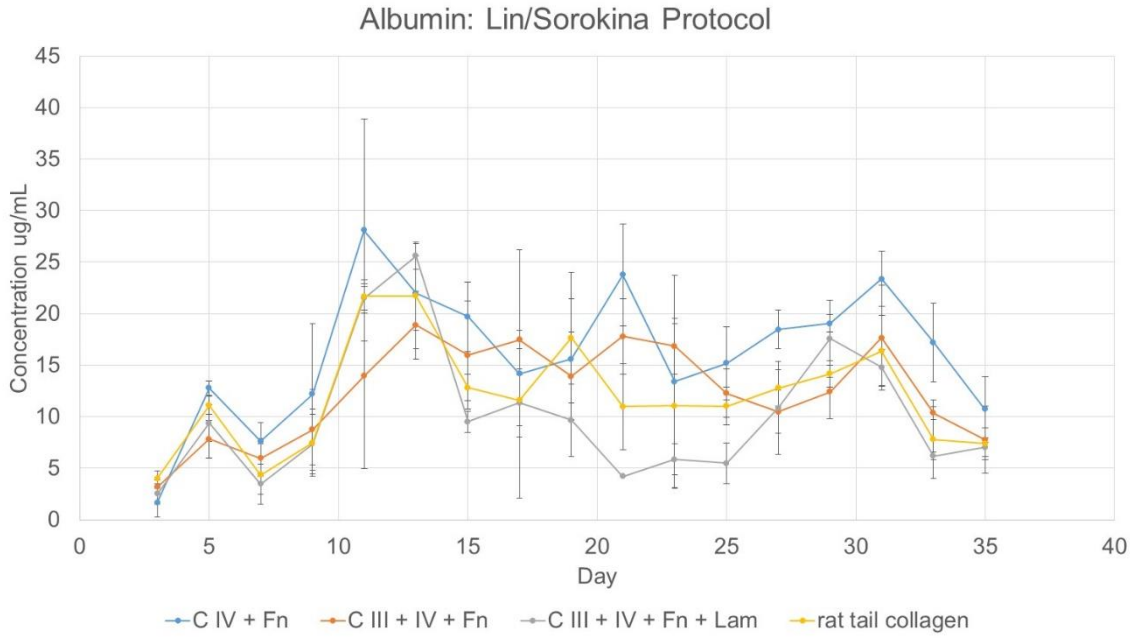

Figure 2 Albumin production in conditions following the Lin/Sorokina protocol.

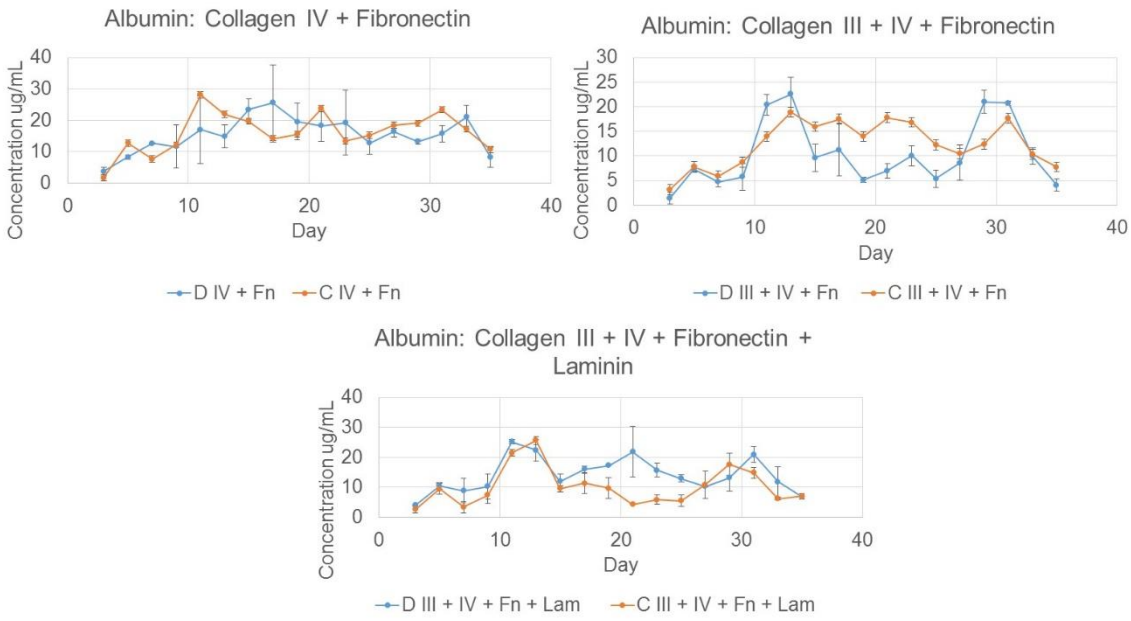

Figure 3 Comparison in albumin production between Berger/Davidson and Lin/Sorokina protocols.

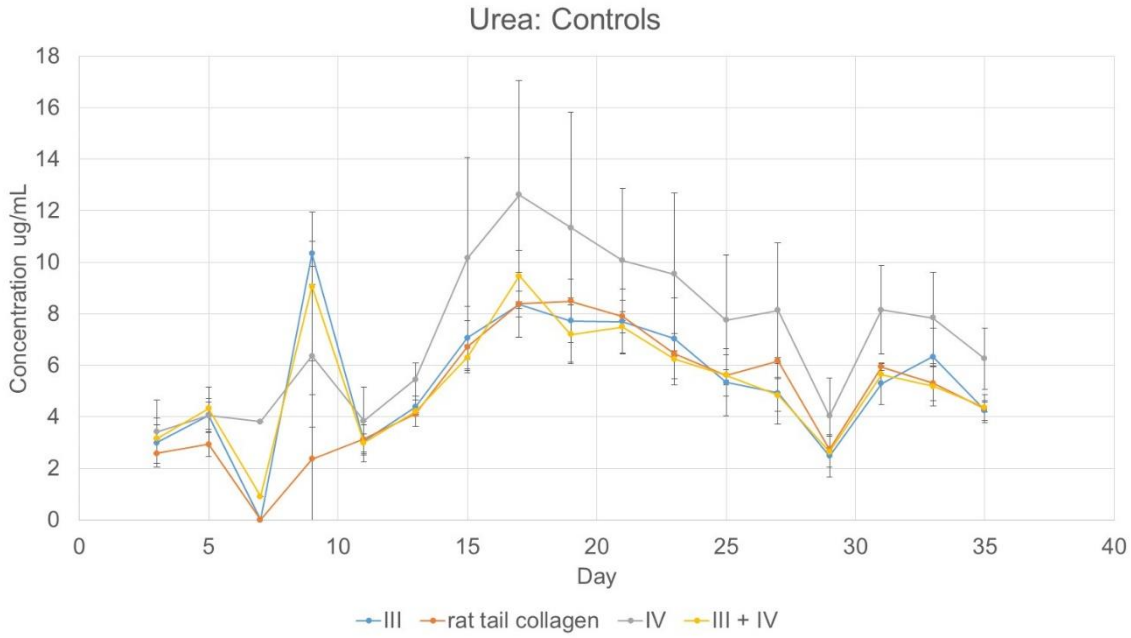

Figure 4 Urea production in control conditions.

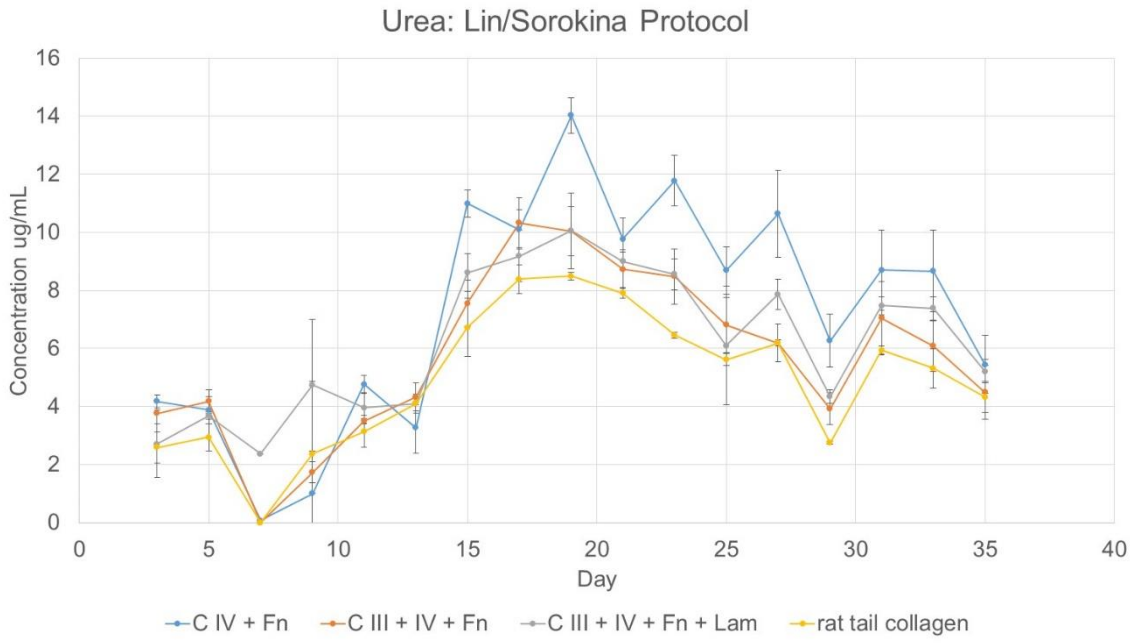

Figure 5 Urea production in conditions following the Lin/Sorokina protocol.

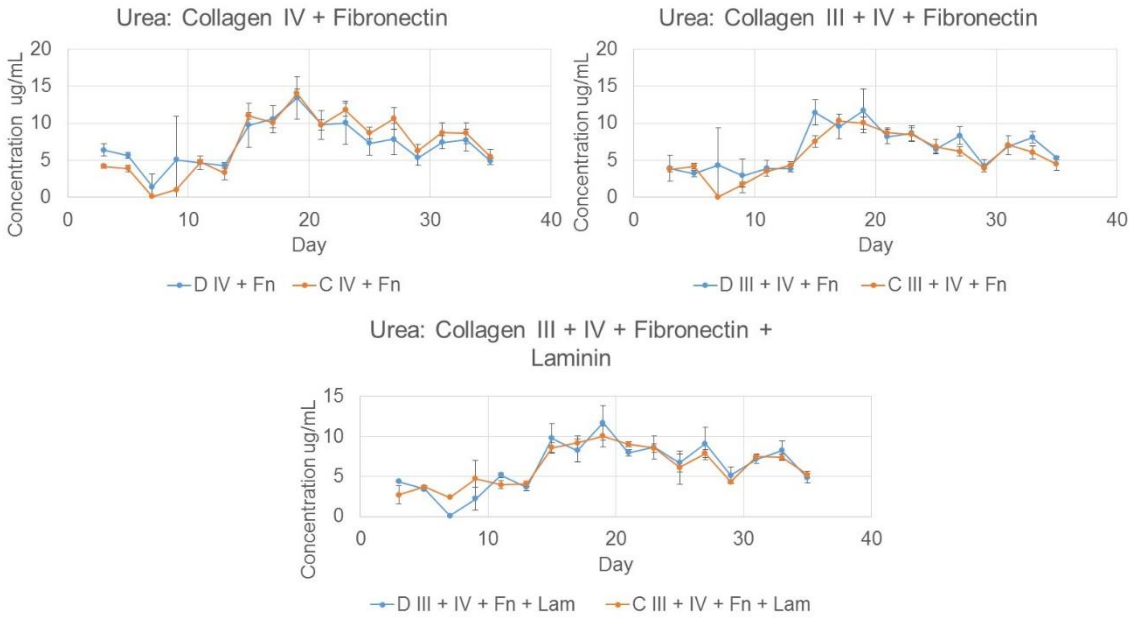

Figure 6 Comparison in urea production between Berger/Davidson and Lin/Sorokina protocols.

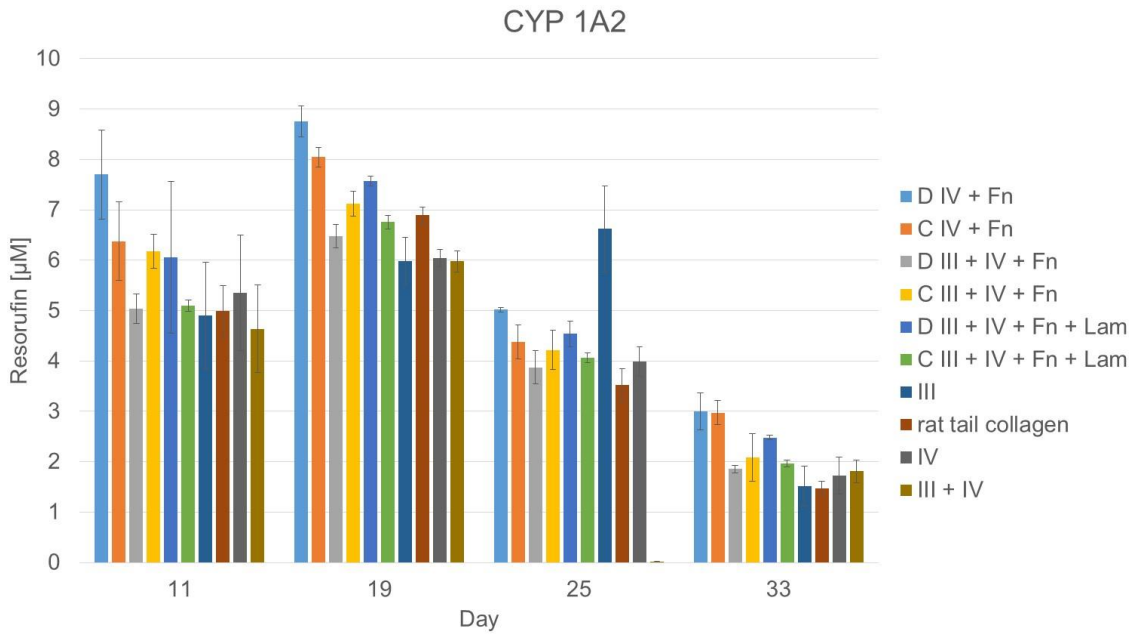

Figure 7 CYP 1A2 activity for all conditions.

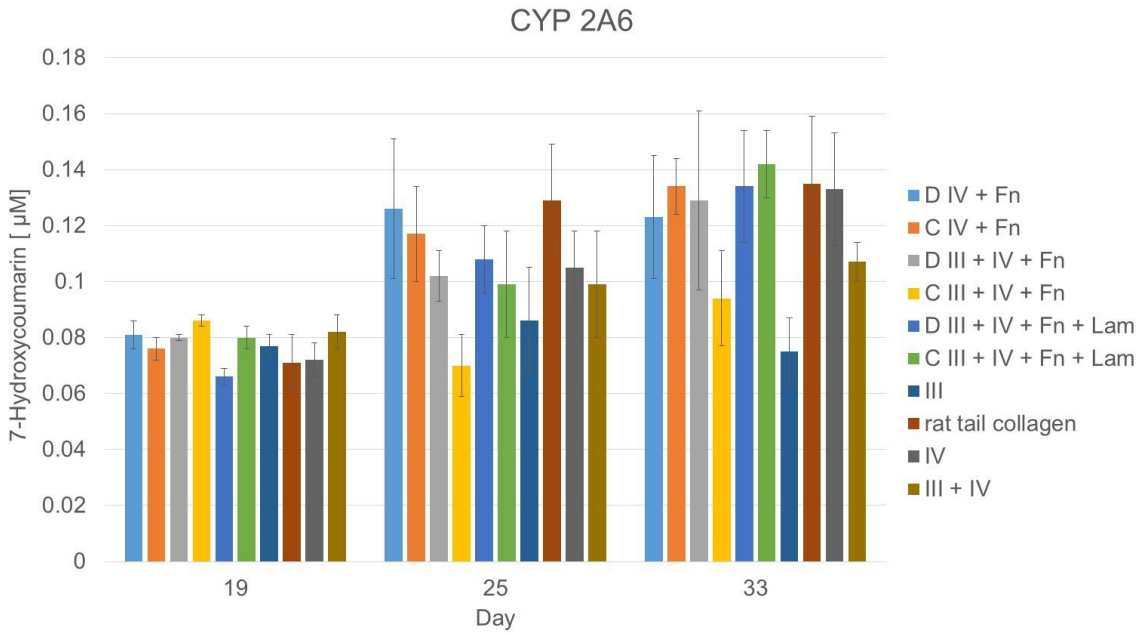

Figure 8 CYP 2A6 activity for all experimental conditions.

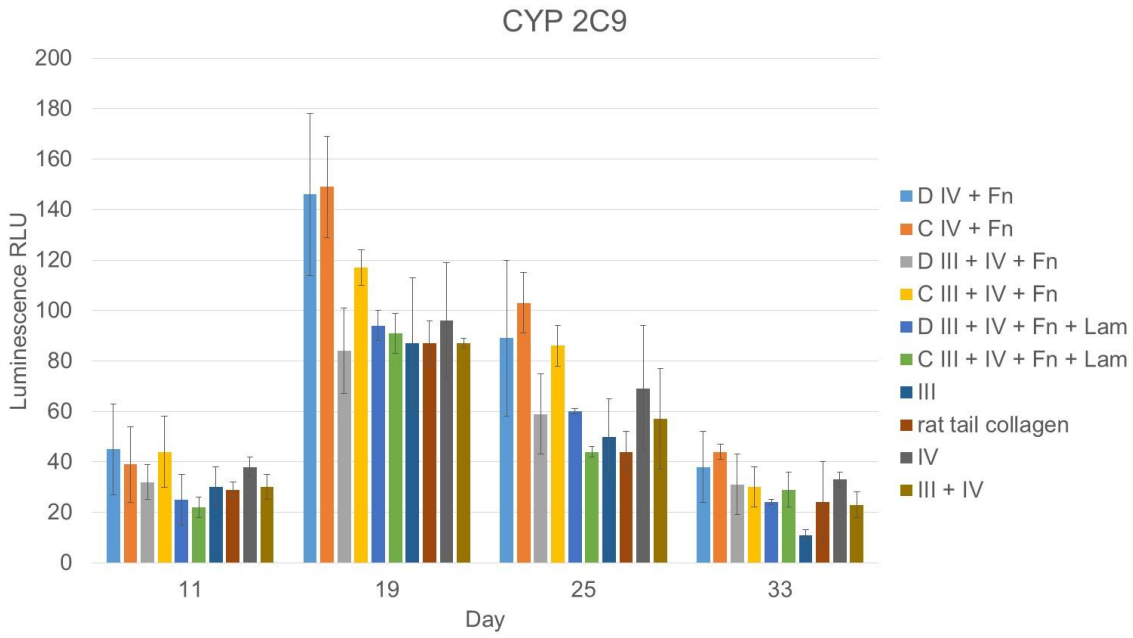

Figure 9 CYP 2C9 activity for all conditions.

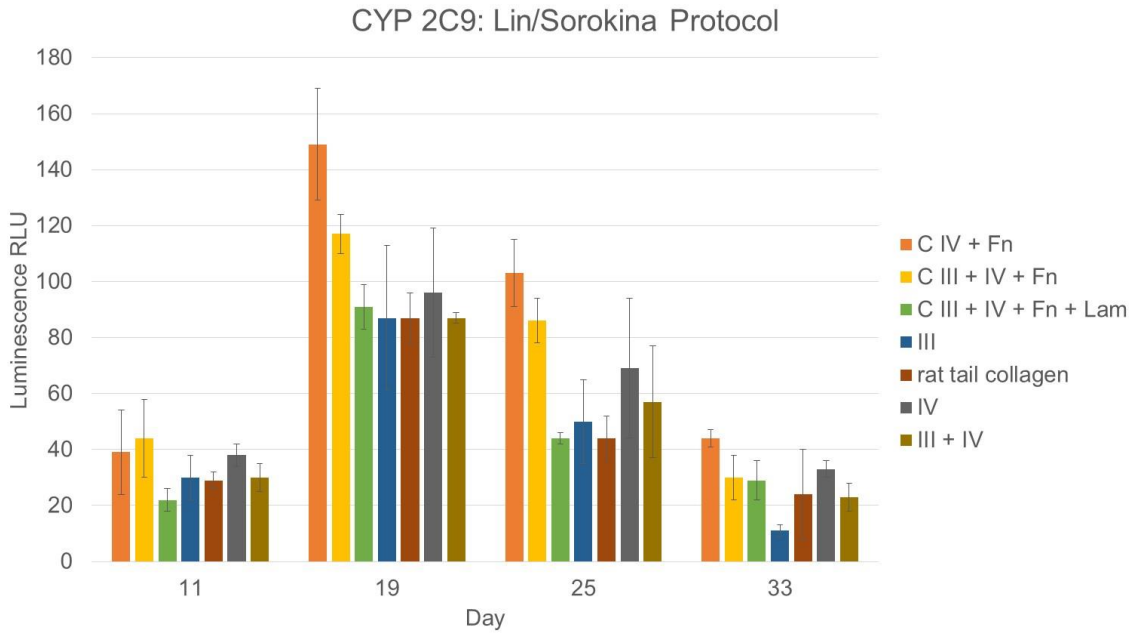

Figure 10 CYP 2C9 activity for conditions following Lin/Sorokina protocol.

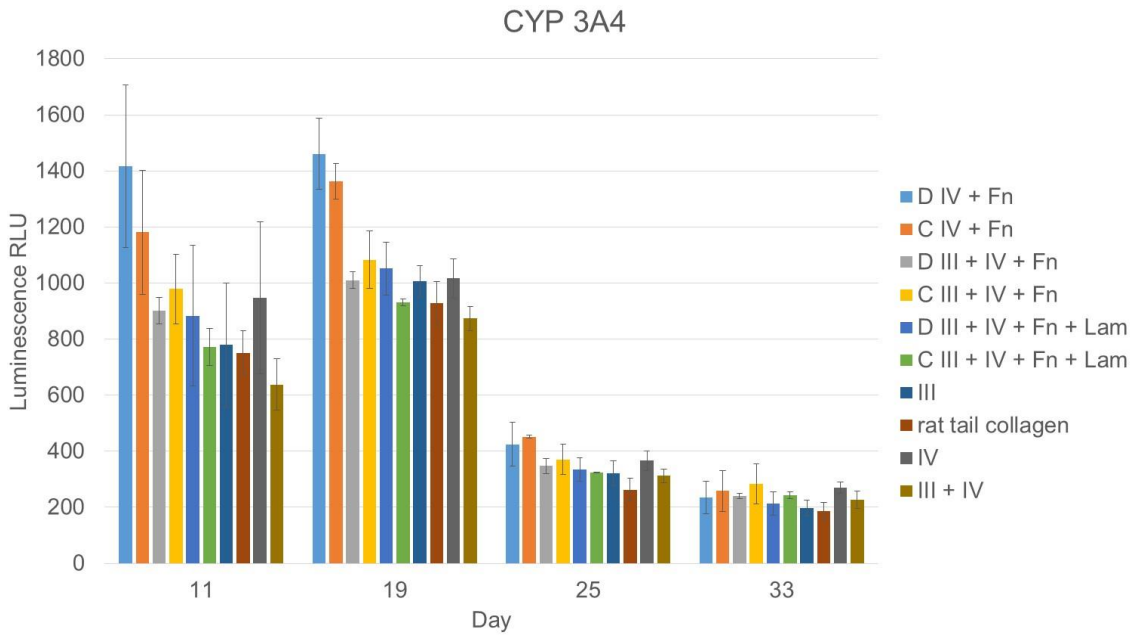

Figure 11 CYP 3A4 activity for all experimental conditions.

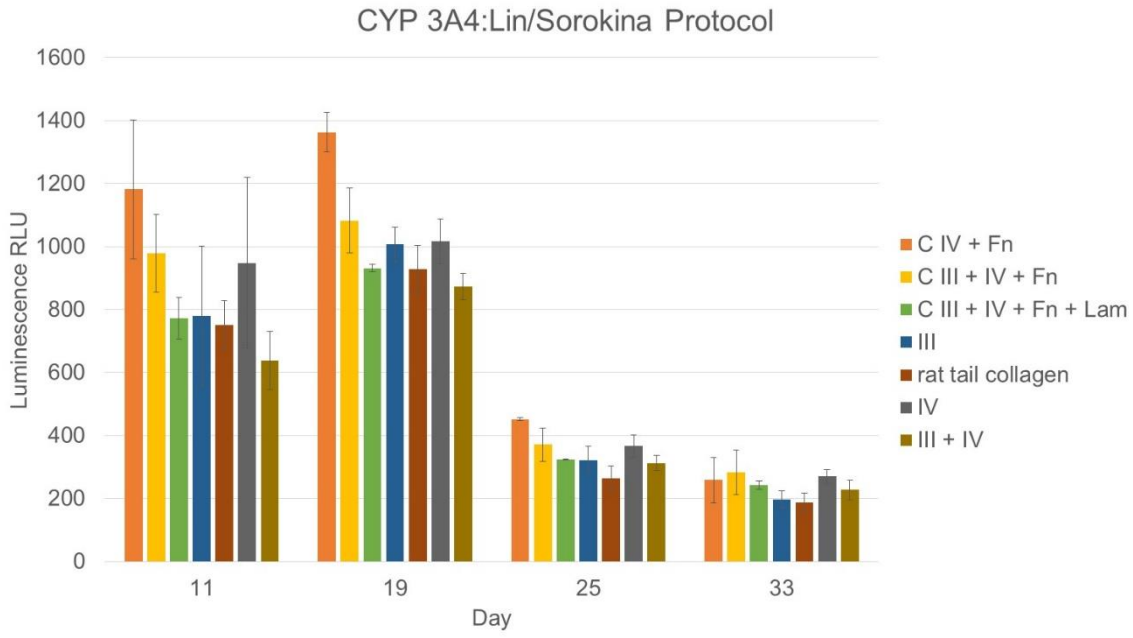

Figure 12 CYP 3A4 activity for conditions following Lin/Sorokina protocol.

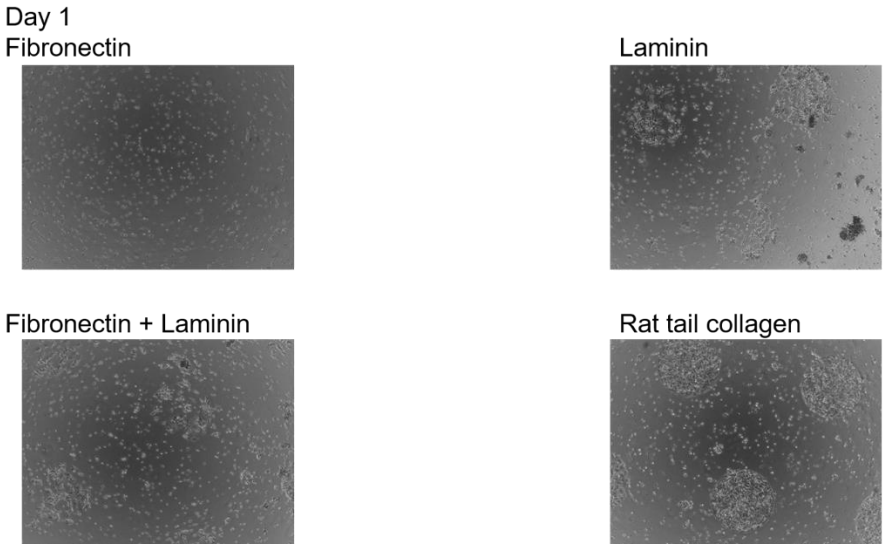

Figure 13 Images showing unspecific attachment in conditions patterned on fibronectin, laminin, and fibronectin + laminin as compared to gold standard rat tail collagen.

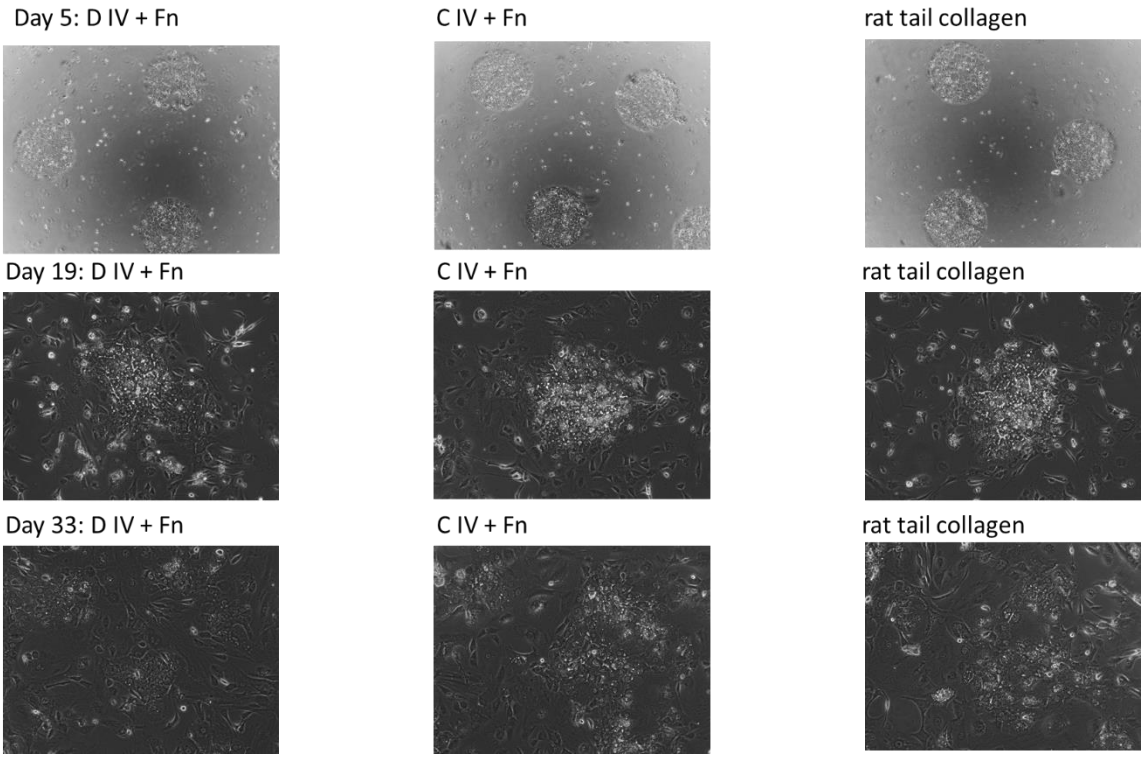

Figure 14 Comparison of top performing condition, collagen IV + fibronectin across Berger/Davidson protocol (D) and Lin/Sorokina protocol (C). Rat tail collagen is the gold standard.

This study was used to assess the effectiveness of using various ECM substrates to enhance long-term iHeps functioning in MPCC. To discern the impact of an overall protein concentration, two separate protocols were compared. In the Berger/Davidson protocol, the individual protein concentration was kept at 25 µg/mL, for total protein concentrations varying between 25-100 µg/mL. In the Lin/Sorokina protocol, the final protein concentration was kept constant at 25 µg/mL, with individual protein concentrations varying between 6.25 - 25 µg/mL. Rat tail collagen I had a similar albumin output than other controls such as collagen III, collagen IV, and collagen III + IV, shown in Figure 1. Albumin production for two protocols is compared in Figure 3, with collagen IV + fibronectin performing similarly across two protocols. Collagen III + IV + fibronectin demonstrated more stable performance at 17 µg/mL from days 13 – 31 following Lin/Sorokina protocol. Collagen III + IV + fibronectin + laminin showed improved performance following Berger/Davidson protocol. Overall, the trends suggest that the two protocols are comparable in albumin production. Within the Lin/Sorokina protocol, collagen IV + fibronectin showed superior performance and stability, followed by collagen III + IV + fibronectin; both conditions perform approximately the same as rat tail collagen, as shown in Figure 2. Collagen III + IV + fibronectin + laminin seems to be the worst performing condition for albumin production following Lin/Sorokina protocol. It is interesting to note that with the addition of each new ECM protein to collagen IV + fibronectin combination, the output of albumin seems to decrease. Possible explanations include competitive binding of ECM proteins or interactions due to events such as binding together. Figure 4 demonstrates that for control conditions, the output of urea was approximately the same. Similar trend continues when examining urea production across the two protocols in Figure 6. In conditions following the Lin/Sorokina protocol, collagen IV + fibronectin appears to be the top condition for urea

production, with the rest of the conditions performing approximately the same, as shown in Figure 5. Figure 7 demonstrates results of CYP 1A2 assay, specifically that none of the ECM combinations are helpful in preventing the decline in function in long-term. However, collagen IV + fibronectin from Lin/Sorokina protocol performed better than rat tail collagen I and the rest of the conditions from that protocol performed about as well as rat tail collagen I. CYP 2A6 data, shown in Figure 8, indicates improved performance for collagen IV + fibronectin over rat tail collagen I, yet the overall trend is difficult to discern due to high error bars. CYP 2C9 activity is shown for all conditions in Figure 9 and for Lin/Sorokina protocol compared with controls in Figure 10. Collagen IV + fibronectin seemed to continue to outperform the rest of the conditions, with the overall trend being a decline in functions across all conditions starting from day 19. Similar trend is observed in CYP 3A4 activity, shown in Figures 11 and 12. Figure 14 shows collagen IV + fibronectin patterning across two conditions and compared to rat tail collagen I. Collagen IV + fibronectin filled out the island in a manner similar to rat tail collagen, with limited non-specific attachment for both conditions. In addition, the use of lower total protein concentration in the Lin/Sorokina protocol as compared to the Berger/Davidson protocol resulted in comparable patterning. Thus, the data shows that it feasible to keep total protein concentration at 25 µg/mL and still maintain hepatic functions in iHeps MPCCs, with collagen IV + fibronectin being the desired combination. It should be noted, however, that statistical analyses, such as two-way ANOVA or regression, would be useful in determining which of the above-mentioned functional trends are statistically significant. Nonetheless, the trends observed are encouraging and can be potentially useful for drug screening applications.

One of the unexpected challenges faced in this study was the inability to pattern conditions that included fibronectin, laminin, and fibronectin + laminin since they have

appeared as one of the top ECMs in iHeps studies done by Mr. Berger and Dr. Davidson. Figure 13 shows in contrast to well-defined and filled out islands in the rat tail collagen I control condition, fibronectin did not pattern at all. Similarly, fibronectin + laminin as well as only laminin showed merely outlines of islands, but were unable to fill in. Thus, the aforementioned conditions were excluded from further analysis. Several follow-up studies were conducted to assess the potential roles of BSA concentration, seeding densities, age of fibronectin, and patterning process on the attachment of iHeps. The results are summarized below.

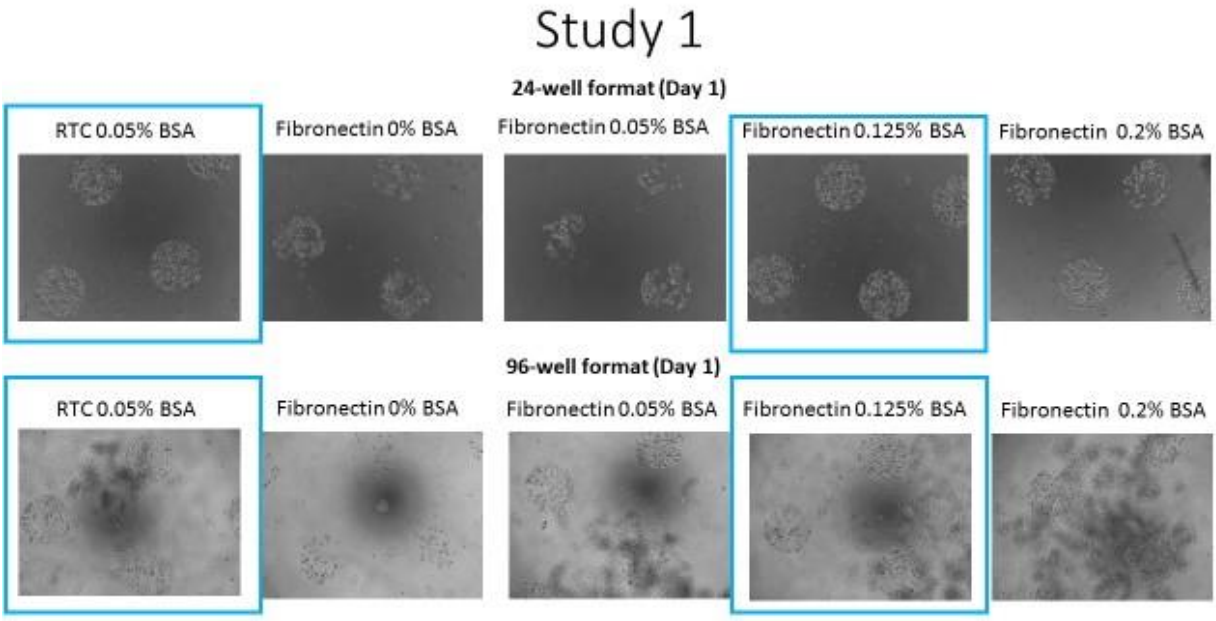

Figure 15 The effect of BSA concentration on cell attachment in 24- and 96-well format.

Figure 16 The effect of age of fibronectin on attachment.

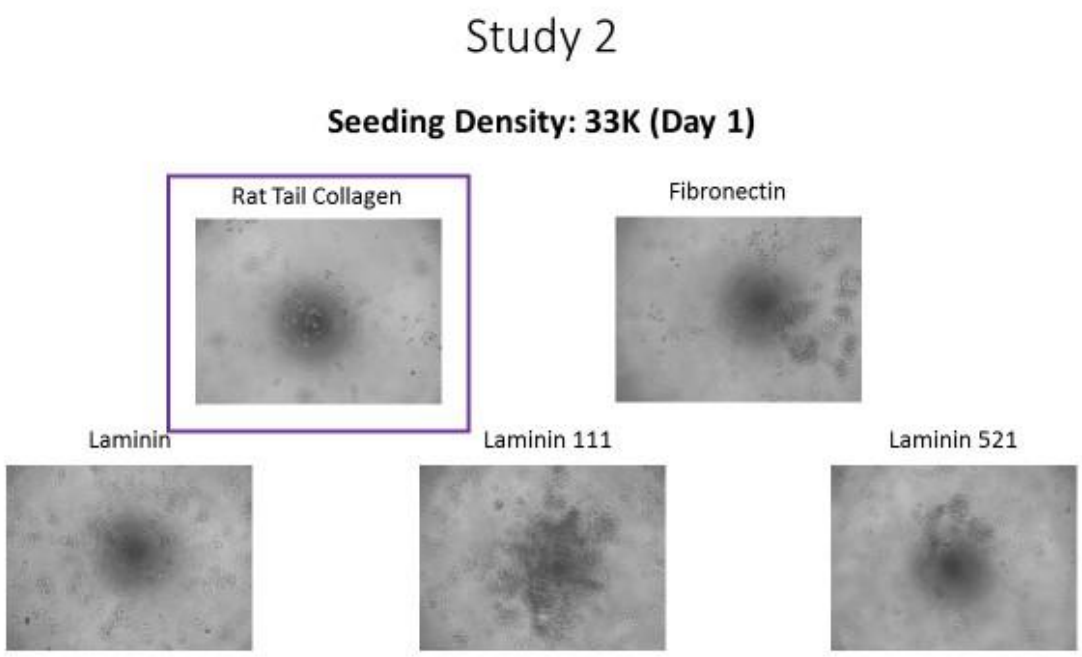

Figure 17 The effect of 33k seeding density on iHeps attachment.

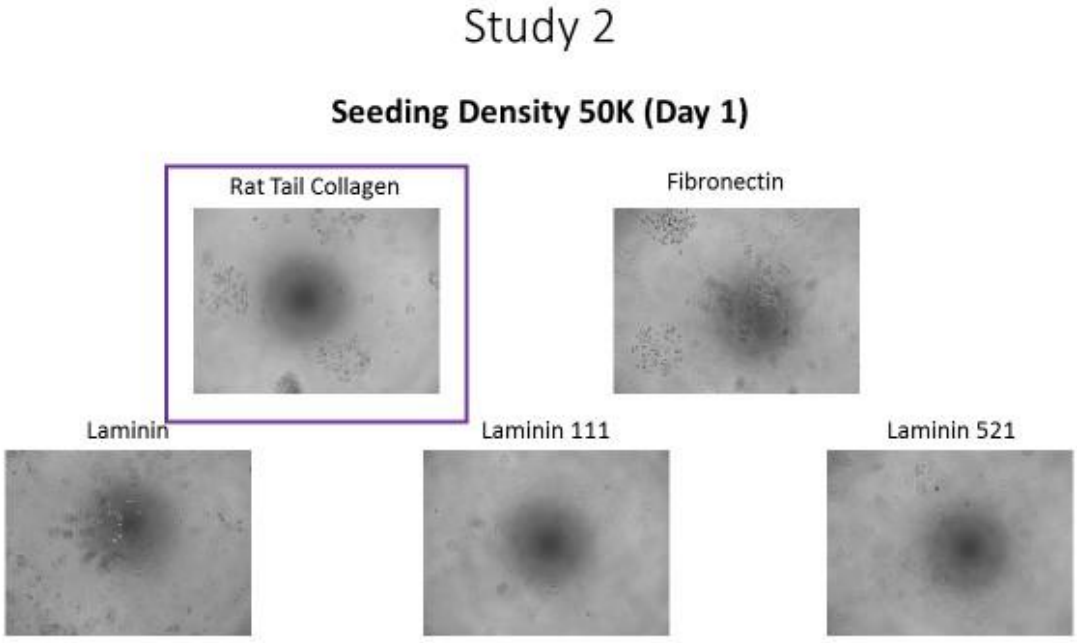

Figure 18 The effect of 50k seeding density on iHeps attachment.

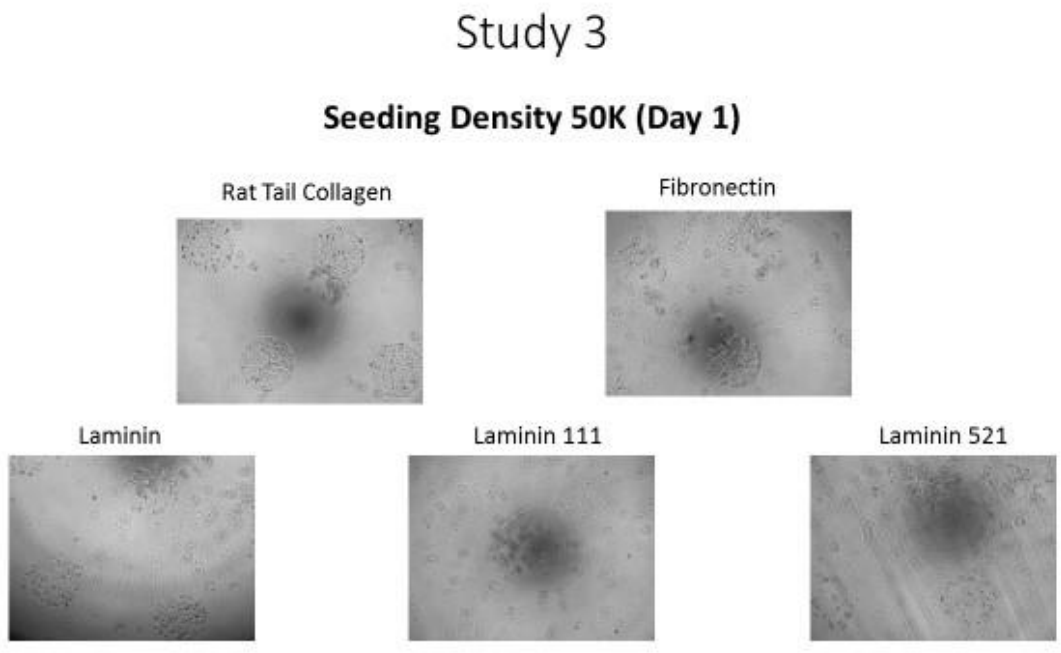

Figure 19 Verification of Study 2 results

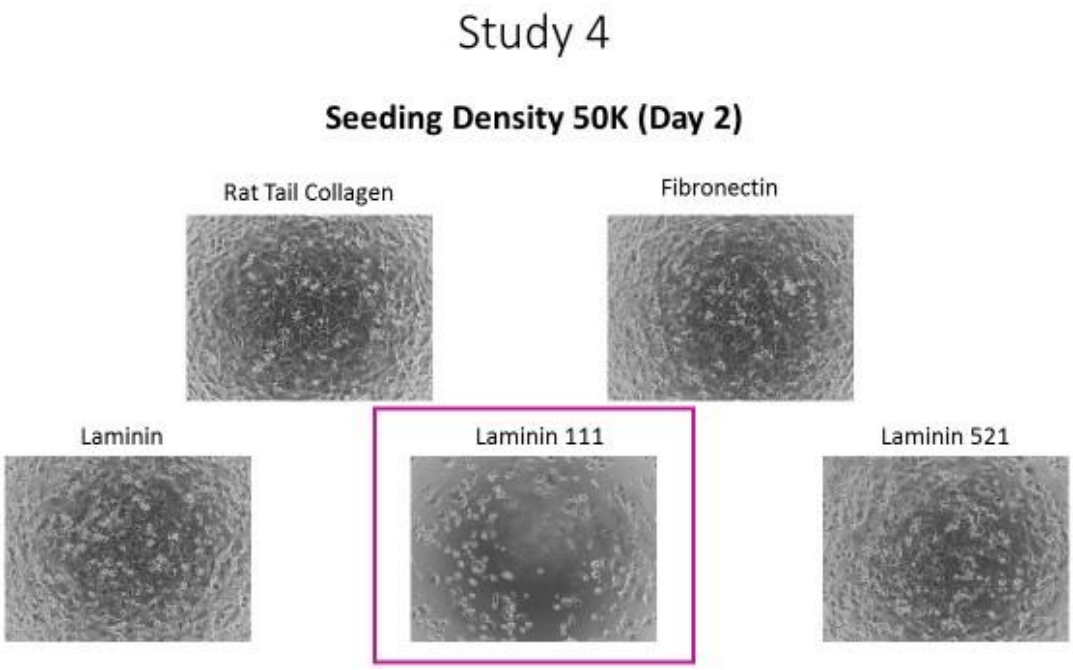

Figure 20 Verification of patterning studies using monoculture.

Study 1 was used to elucidate the effects of BSA concentration on attachment of iHeps on fibronectin as well as whether the plate format had an effect, as shown in Figure 15. Based on qualitative assessment, fibronectin at 0.125% BSA patterned similarly to rat tail collagen at 0.05% BSA in both formats; other BSA concentrations tested performed worse for fibronectin attachment. Furthermore, two types of plates, 24- and 96-well format, were used to eliminate format as a contributing factor since Mr. Berger and Dr. Davidson were able to pattern fibronectin and laminin in a 96- well format yet their results could not be replicated in the iHeps study. Additionally, Study 1 was performed using a fresh batch of fibronectin and this could have potentially contributed to the successful patterning outcome, as seen in Figure 16. The aim of Study 2, shown in Figures 17 and 18, was to discern the difference between iHeps seeding densities of 33K and 50K and potential effect on attachment. In addition to testing fibronectin and laminin, laminin 111 and 521 were tested based on work of Cameroon et al. with the aim of

using them in later studies (Cameron et al. 2015). There was very little attachment observed at seeding density of 33K and partial patterning at 50K. It is likely that the quality of cells used for Study 2 was subpar since there was only partial attachment on rat tail collagen I, a previously tested and reliable control. Study 3 repeated the 50K seeding density portion of Study 2, as shown in Figure 19. While there was a clear improvement in patterning in fibronectin and laminin in addition to the cultures lasting 7 days instead of 1-2 days as in Studies 1 and 2, it was still unclear as to why there was variability in patterning laminin 521 and difficulty in any patterning of laminin 111. Study 4, shown in Figure 20, tested attachment in monoculture to clarify whether the patterning process or the proteins themselves contributed to inconsistent patterning. Study 4 confirmed that with all other conditions such as protein concentration and cell seeding density being equal, cells do not attach to laminin 111 as well as they do to the other substrates. Since in work by Cameroon et al. laminin 111 was used in combination with laminin 521 and it showed poor attachment here, it may be that laminin 111 is used to increase the number of binding sites but by itself is a poor substrate.

3. EXTRACELLULAR MATRIX SCREEN FOR LONG-TERM CULTURE OF PRIMARY HUMAN HEPATOCYTES

3.1 Motivation

One of the primary challenges of creating long-term *in vitro* models to study liver diseases and for drug development is the dedifferentiation of PHHs which occurs once the cells have been removed from the liver and placed on a culture plate of harder stiffness. Loss of hepatocyte-specific functions such as albumin secretion, urea production, polarity and cytochrome P450 activity takes place followed by apoptosis in the absence of appropriate environmental cues (Sellaro et al. 2010; Skardal et al. 2014). As a consequence, identifying preferred ECM for culturing hepatocytes has been of great interest as a diverse and complex ECM microenvironment is responsible for the modification of the hepatocyte functions *in vivo* (Zeisberg et al. 2006; DiPersio, Jackson, and Zaret 1991; Moghe et al. 1996). Prior studies included using individual ECM proteins such as collagen I as substrates as well as multi-component substrates, perhaps the most famous being Matrigel (Moghe et al. 1996; Gross-Steinmeyer 2005; Hamilton et al. 2001; Silva, Day, and Nicoll-Griffith 1999). Decellularized liver matrices have also been employed as scaffolds for hepatocyte culture due to their native, tissue-specific composition (Khetani and Bhatia 2008; Enat et al. 1984; Lang et al. 2011; Lin et al. 2004)**.** Thus, the motivation for this study was to determine if there is an ECM protein or a combination of proteins that can be used to enhance *in vitro* PHH functions in MPCC greater than the current gold standard, rat tail collagen I.

Of special significance in hepatocyte interaction is the ability of the cells to communicate with one another, an attribute that may be controlled via specific geometry *in vitro*. To account for this important detail, MPCC platform was used to ensure a consistent cell count for each

sample as well as to elicit specific cell-cell interaction by controlling the substrate geometry (Khetani and Bhatia 2008). The ECM screen was composed of 32 ECM proteins and their combinations, as well as human decellularized biomatrix and porcine decellularized biomatrix. Rat tail collagen I served as the control. The ECM proteins selected for this study included collagens I, III, IV, laminin and fibronectin. The selection was made based on literature search as well as on prior work done in the lab. The addition of each ECM protein was tested by including combinations of two, three, four, and five of the aforementioned proteins. Based on the results from the iHeps study outlined in Chapter 2 of this thesis, total protein concentration was selected to remain constant at 25 µg/mL. PHH functions were assessed though albumin, urea, CYP 1A2, CYP 2A6, CYP 2C9, and CYP 3A4 assays over a period of 28 days.

3.2 Methods

3.2.1 Formation of ECM MPCC's

MPCCs were created using soft lithography in a process established by Khetani and Bhatia (Khetani and Bhatia 2008). In addition to using rat tail collagen I, human collagens I, III, IV, laminin, fibronectin, human decellularized biomatrix, and porcine decellularized biomatrix were used as substrates at concentrations of 25 µg/mL total protein concentration per condition. Human collagens I, III, IV, laminin, and fibronectin were also combined in two, three, four, and five protein combinations, with the total protein concentration per condition also kept at 25 µg/mL. 96-well plates were coated with respective ECMs, incubated for 2 hours at 37ºC, patterned using PE-25 (PlasmaEtch, Carson City, NV) and sterilized with 70% ethanol. Plates were coated with 0.05% bovine serum albumin (BSA) and incubated at 37ºC for 45 minutes prior to PHH seeding.

3.2.2 Cell Culture

Cryopreserved PHH (HUM4055A PHHs, CL/BRW 12/9/15) were thawed in previously made human hepatocyte seeding media, H2SM, consisting of 48.25 William's medium, 750 µL Hepes buffer, 500 µL pen/strep, 500 µL ITS +, 0.5 µL dexamethasone, and 0.5 µL glucagon. Cells were re-suspended at the density of 33,333 per 50 µL and cell viability was assessed using trypan blue at 87%. After gentle agitation every 20 minutes for 6 hours, PHHs were rinsed three times with 1X DMEM and incubated overnight at 37ºC in human hepatocyte overnight media, which consisted of 43.25 mL 1X DMEM, 5 mL of fetal bovine serum, 750 µL Hepes buffer, 500 µL pen/strep, 500 µL ITS +, 0.5 µL dexamethasone, and 0.5 µL glucagon. The following day media was changed to human hepatocyte maintenance media, H2M2, consisting of 43.25 mL 1X DMEM, 5 mL of bovine serum (lot #1648262), 750 µL Hepes buffer, 500 µL pen/strep, 500 µL ITS +, 0.5 µL dexamethasone, and 0.5 µL glucagon. 3T3-J2 murine fibroblasts were seeded also on the day following PHH seeding at the density of 15,000 cells per 50 µL and with viability of 97.5%. The co-cultures were gently agitated every 30 minutes for 2 hours and incubated overnight at 37ºC. Media change and phase contrast imaging were performed every other day for the duration of the study.

3.2.3 Biochemical Assays

Cell functions were assessed based on albumin and urea production as well as CYP1A2, CYP2A6, CYP2C9, and CYP3A4. Albumin levels were detected using a competitive enzyme-linked immunosorbent assay (ELISA) with the use of horseradish peroxidase detection and the substrate of 3,3',5,5'-tetramethylbenzidine (TMB), as previously outlined by Khetani and Bhatia (Khetani and Bhatia 2008). Urea assessment of collected media was performed using diacetylmonoxime with acid and heat in a colorimetric endpoint assay, also previously presented in a work by Khetani and Bhatia (Khetani and Bhatia 2008). For albumin and urea

analysis, supernatant was collected every other day beginning with day 1 until day 29. For CYP450 analysis, supernatant was collected on days 7, 13, 21, and 27 for CYPs 3A4 and 2A6 and on days 9, 15, 23, and 29 for CYPs 1A2 and 2C9. PGlo medium for PHHs used in CYP assays consisted of 48.75 mL Hyclone DMEM/High Modification Medium (lot # AA6205603, + 4.0 mM l-glutamine, 4.500 mg/L glucose, - sodium pyruvate, - phenol red), 750 µL Hepes buffer, 500 µL pen/strep. CYP 3A4 activity was measured via luminescence following 1 hour incubation at 37ºC with luciferin – IPA in PGlo medium. Similarly, CYP 2C9 activity was assessed after 3 hour incubation at 37ºC with luciferin – H and by measuring luminescence. CYP 2A6 output was measured through fluorescence of 7-hydroxy-coumarin after 1 hour incubation at 37ºC of PHHs with coumarin. CYP 1A2 activity was assessed by incubating PHHs with ethoxyresorufin for 3 hours at 37ºC and measuring the fluorescence of resorufin. The detection of all metabolites was performed in accordance with manufacturers' instructions. Samples were analyzed using a plate reader.

3.2.4 Data Analysis

Linear regression analysis was done using RStudio, version 1.1.423. For regression analysis, each input was treated as a categorical variable. Only the ECM conditions that patterned fully or partially were used for regression analysis. Microsoft Excel and GraphPad Prism 7.0 were used for graphing.

3.3 **Results and Discussion**

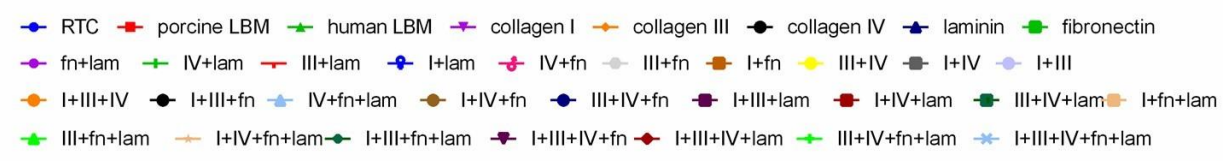

Figure 21 Key for matrix composition

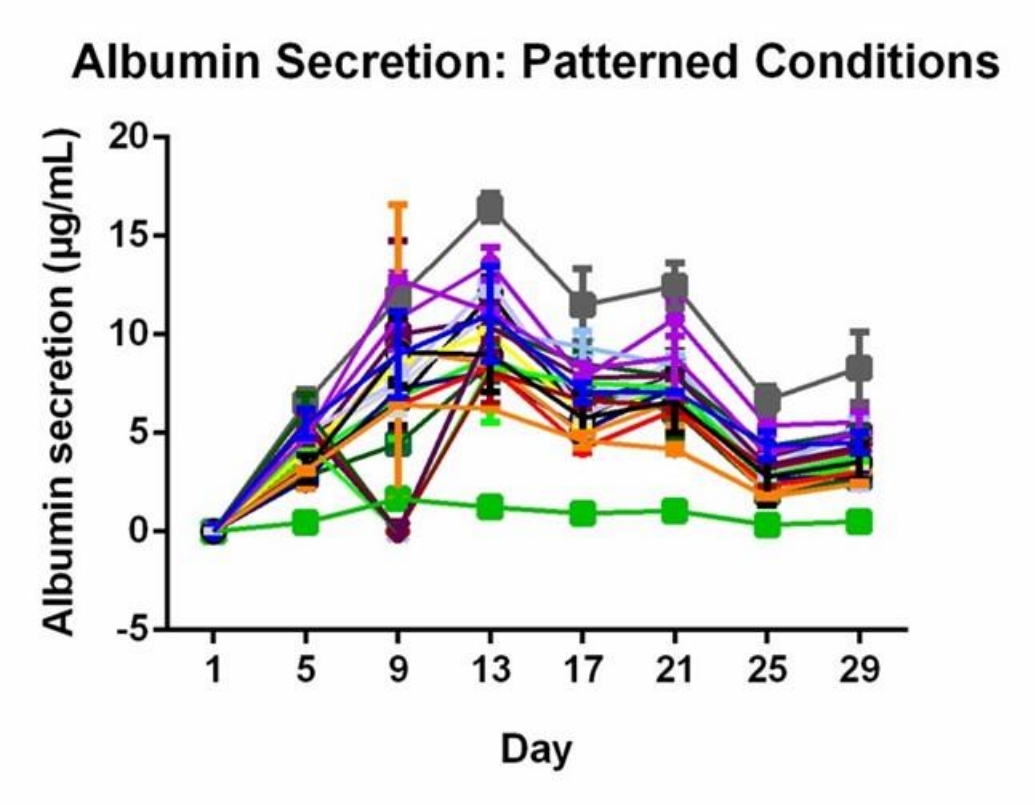

Figure 22 Albumin secretion for patterned conditions

Figure 23 Albumin secretion for liver biomatrix comparison

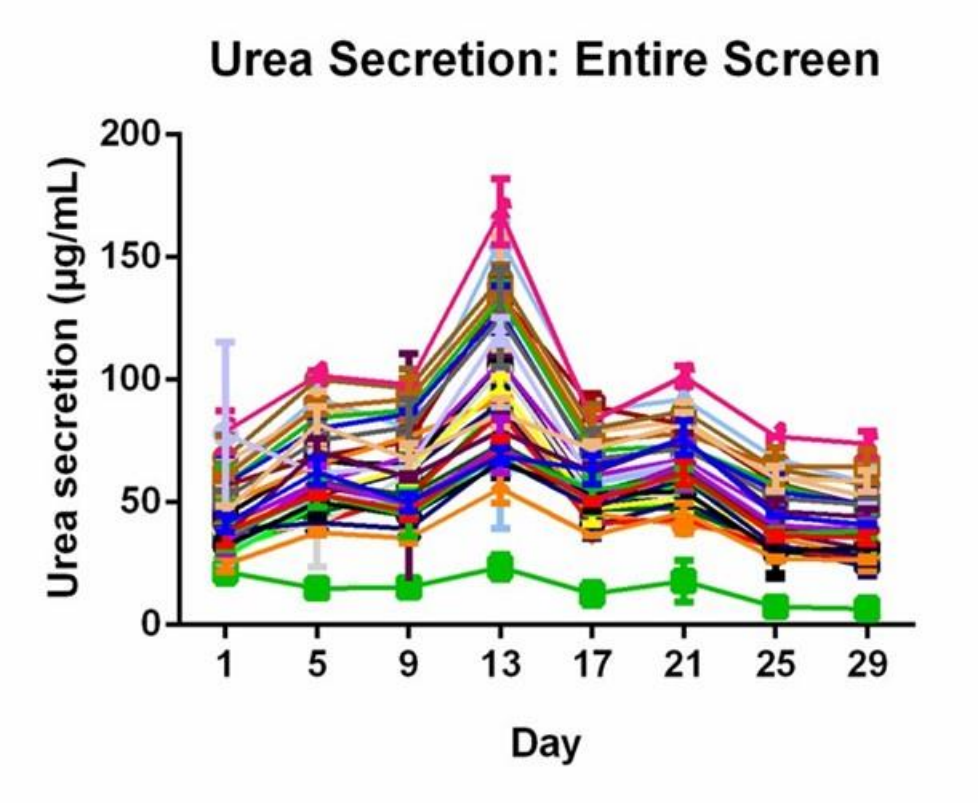

Figure 24 Urea secretion in the entire screen

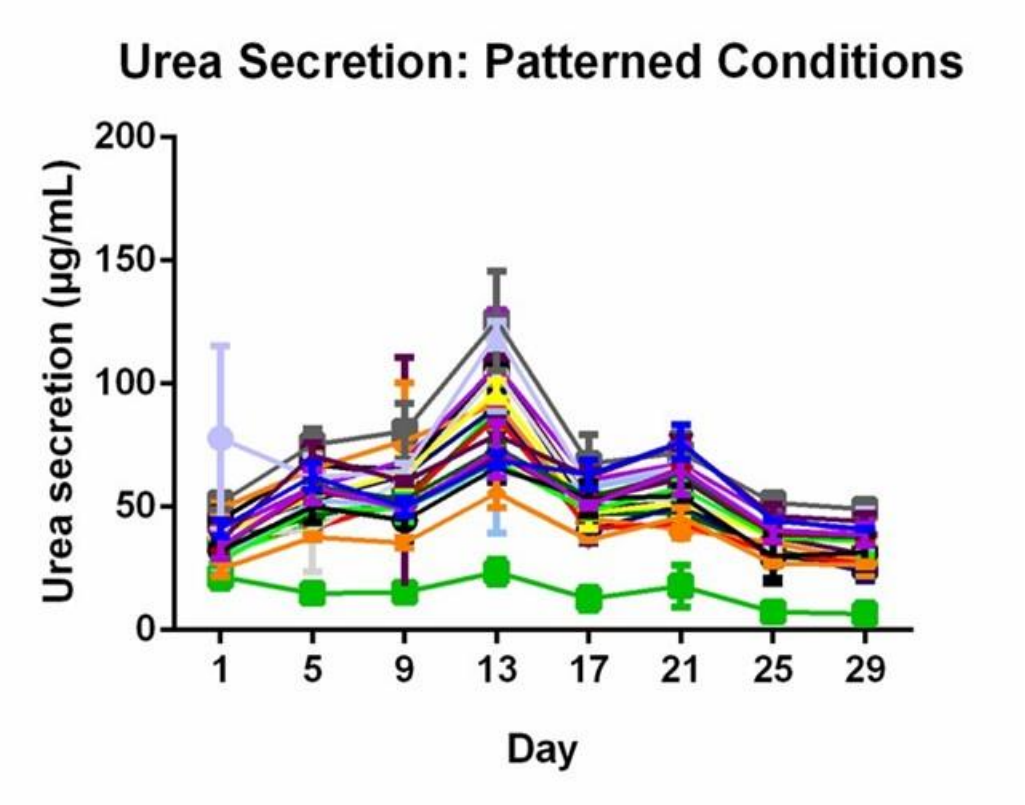

Figure 25 Urea secretion for patterned conditions

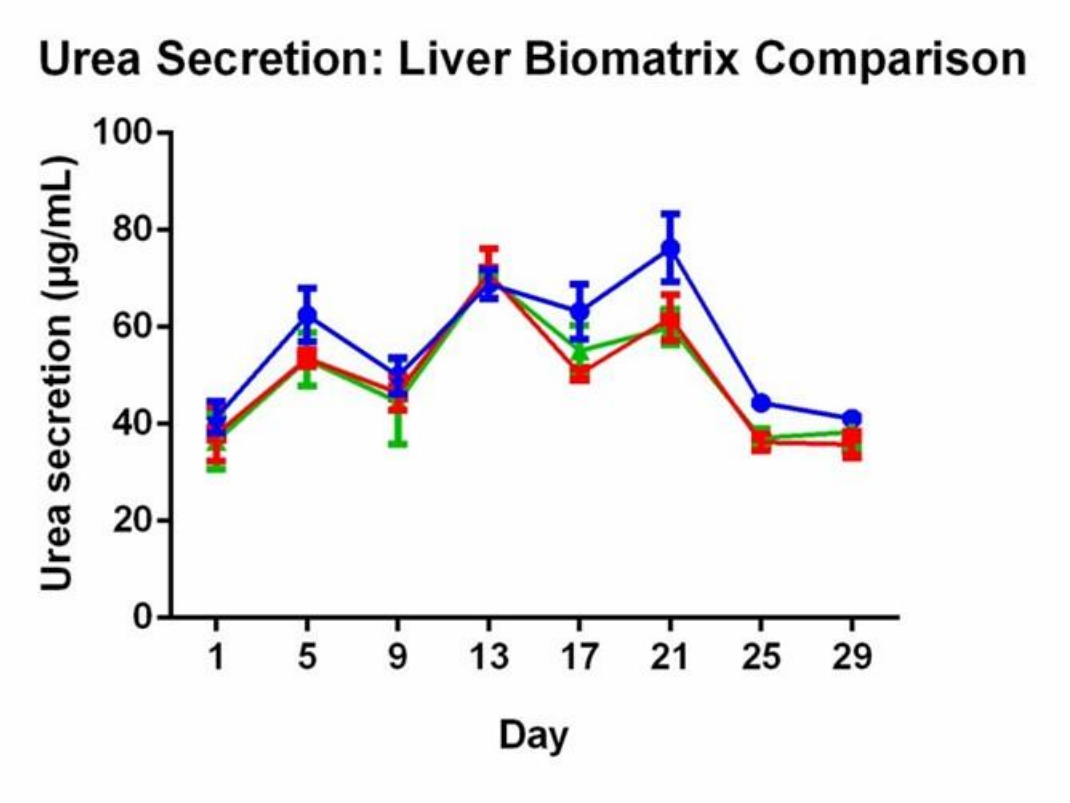

Figure 26 Urea secretion for liver biomatrix comparison

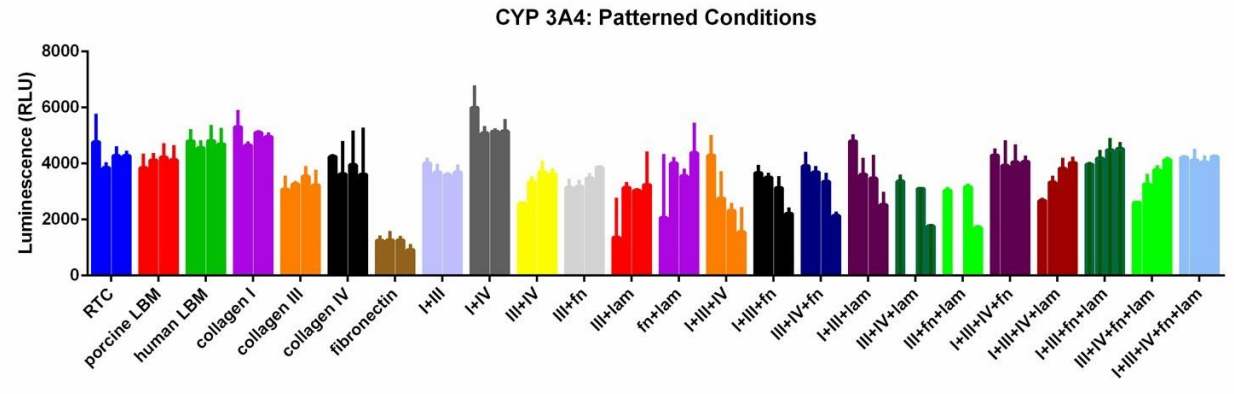

Figure 27 CYP 3A4: patterned conditions

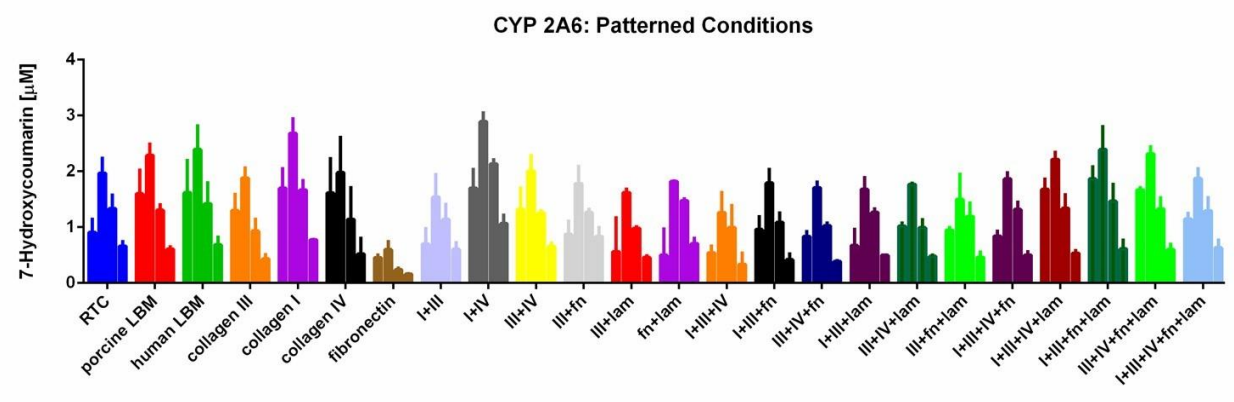

Figure 28 CYP 2A6: patterned conditions

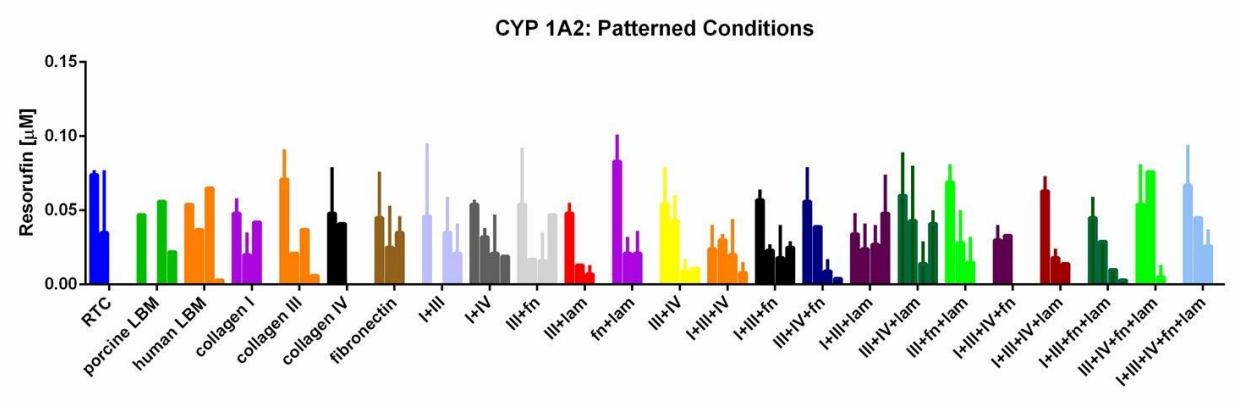

Figure 29 CYP 1A2: patterned conditions

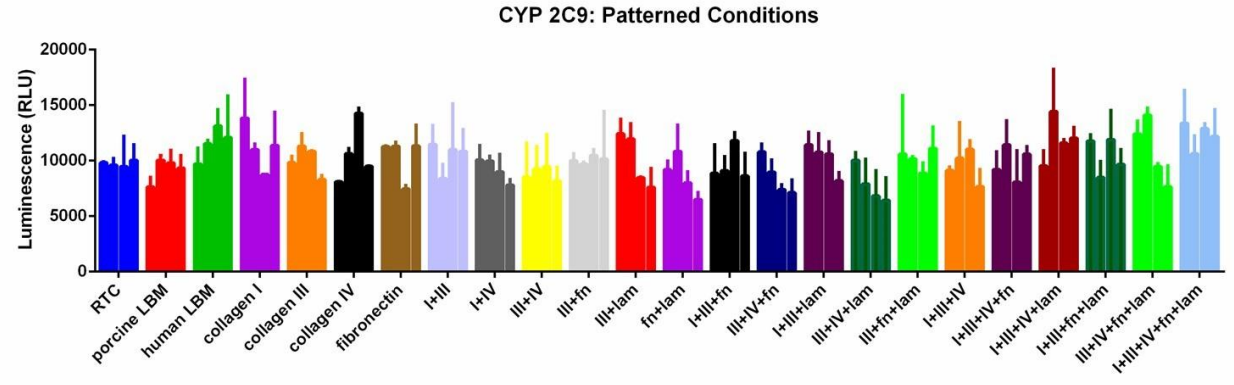

Figure 30 CYP 2C9: patterned conditions

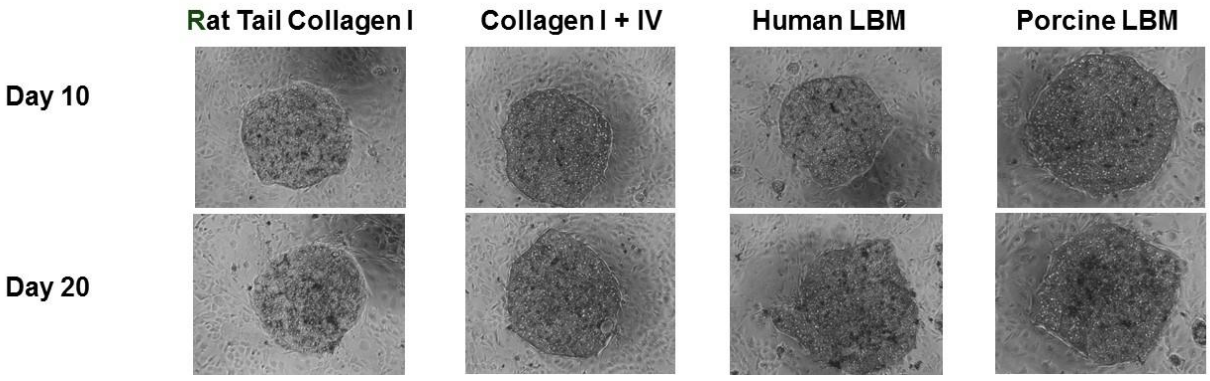

Figure 31 Morphology of rat tail collagen I, collagen I+IV, human and porcine liver iomatrices at days 10 and 20 in culture.

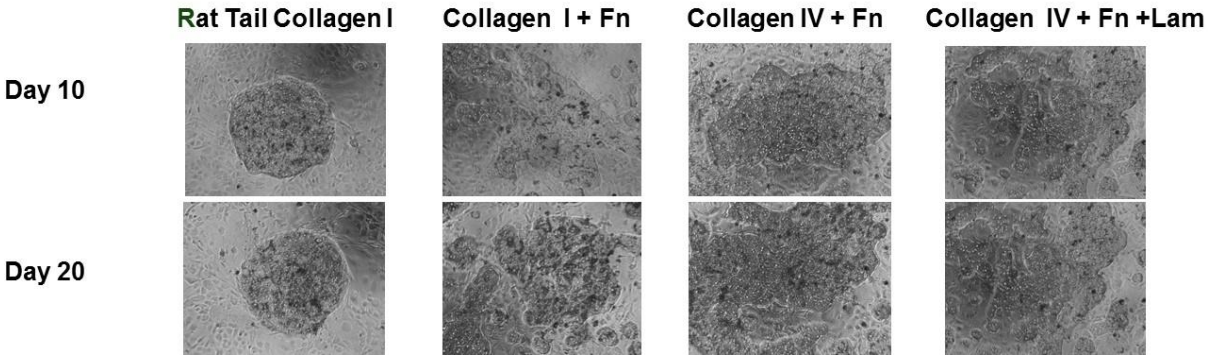

Figure 32 Morphology of rat tail collagen I, collagen I +fibronectin, collagen IV+fibronectin , collagen IV+fibronectin+laminin at days 10 and 20 in culture.

Albumin

Variable	Coefficient	Stdev	t-value	Percent of Effect
Day 5	4.18	0.49	8.57	22%
Day 9	8.24	0.49	16.89	43%
Day 13	9.78	0.49	20.03	51%
Day 17	7.55	0.49	15.47	40%
Day 21	7.27	0.49	14.89	38%
Day 25	3.28	0.49	6.72	17%
Day 29	4.07	0.49	8.34	21%
Rat Tail Collagen	0.61	0.96	0.64	3%
Porcine LBM	-0.14	0.96	-0.14	-1%
Human LBM	0.63	0.96	0.66	3%
Collagen I (25% concentration)	0.55	0.61	0.90	3%
Collagen I (33% concentration)	1.46	0.59	2.48	8%
Collagen I (50% concentration)	2.34	0.68	3.45	12%
Collagen I (100% concentration)	1.97	0.95	2.06	10%
Collagen III (25% concentration)	-0.52	0.59	-0.88	-3%
Collagen III (33% concentration)	-0.42	0.50	-0.84	-2%
Collagen III (50% concentration)	-0.44	0.58	-0.77	-2%
Collagen III (100% concentratior	-2.23	0.99	-2.25	-12%
Collagen IV (25% concentration)	-0.32	0.62	-0.52	-2%
Collagen IV (33% concentration)	-0.49	0.59	-0.83	-3%
Collagen IV (50% concentration)	1.93	0.70	2.74	10%
Collagen IV (100% concentratior	-0.41	0.96	-0.43	-2%
Fibronectin (25% concentration)	-0.22	0.61	-0.36	-1%
Fibronectin (33% concentration)	-0.75	0.58	-1.29	-4%
Fibronectin (50% concentration)	1.04	0.70	1.47	5%
Fibronectin (100% concentration)	-4.93	0.97	-5.11	-26%
Laminin (25% concentration)	-0.26	0.62	-0.42	-1%
Laminin (33% concentration)	-0.08	0.60	-0.13	0%
Laminin (50% concentration)	0.22	0.69	0.32	1%

R-squared: 0.774
Degrees of Freedom: 324

Range	
Low	High
0	19.064

Figure 33 Regression analysis of albumin

The regression that was made assumes that there are no interactions between inputs and that each input is linear in its correlation with the albumin output.

$$Albumin = C_1 Day5 + C_2 Day9 + C_3 Day13 + C_4 Day17 + C_5 Day21 + C_6 Day25 + C_7 Day29 + C_8 RTC + C_9 Procine\ LBM + C_{10} Human\ LBM + C_{11} CollagenI(25\%) + C_{12} CollagenI(33\%) + C_{13} CollagenI(50\%) + C_{14} CollagenI(100\%) + C_{15} CollagenIII(25\%) + C_{16} CollagenIII(33\%) + C_{17} CollagenIII(50\%) + C_{18} CollagenIII(100\%) + C_{19} CollagenIV(25\%) + C_{20} CollagenIV(33\%) + C_{21} CollagenIV(50\%) + C_{22} CollagenIV(100\%) + C_{23} Fibronectin(25\%) + C_{24} Fibronectin(33\%) + C_{25} Fibronectin(50\%) + C_{26} Fibronectin(100\%) + C_{27} Laminin(25\%) + C_{28} Laminin(33\%) + C_{29} Laminin(50\%) + Intercept$$

The output's r-squared value is only 0.774. However, this masks an interesting realization: the non-linear behavior of ECM proteins. In this regression, high levels, but not 100% of collagen I yield positive effects on albumin production. While most important ECM protein according to this model is collagen I, the exact amount of collagen I that should be present will need to be determined in the future. This model shows that compared to 0% collagen I, 50% collagen III produces 2.34 more micrograms of albumin. All other variables, except for number of days both have a small effect and have a high standard devation when compared to the coefficient of the variable. Porcine LBM showed downregulation of 1% and human LBM showed an upregulation of 3%. The presence of rat tail collagen in particular has a slight postive effect, 3%, on the production of albumin.

Based on the albumin regression the top three ECM combinations would be:

Table 1 Albumin top results

Albumin Top Results Based on:	
Regression Prediction	**Graphical Experimental**
Collagen I (50%), Fibronectin (25%), Laminin (25%)	Collagen I (33%), Collagen IV (33%), Laminin (33%)
Collagen I (50%), Collagen IV (25%), Fibronectin (25%)	Collagen I (50%), Collagen IV (50%)
Collagen I (50%), Collagen IV (50%)	Collagen I (33%), Collagen III (33%), Collagen IV (33%)

Urea

Variable	Coefficient	Stdev	t-value	Percent of Effect
Day 5	16.48	2.66	6.20	14%
Day 9	17.09	2.66	6.43	14%
Day 13	46.07	2.66	17.32	39%
Day 17	16.20	2.66	6.09	14%
Day 21	19.38	2.66	7.29	16%
Day 25	-1.87	2.66	-0.70	-2%
Day 29	-4.31	2.66	-1.62	-4%
Rat Tail Collagen	3.64	5.03	0.72	3%
Porcine LBM	-3.47	5.03	-0.69	-3%
Human LBM	-3.19	5.03	-0.63	-3%
Collagen I (25% concentration)	5.90	3.01	1.96	5%
Collagen I (33% concentration)	11.15	3.01	3.70	9%
Collagen I (50% concentration)	20.92	3.56	5.87	18%
Collagen I (100% concentration)	3.12	4.86	0.64	3%
Collagen III (25% concentration)	-1.62	3.13	-0.52	-1%
Collagen III (33% concentration)	-0.47	2.80	-0.17	0%
Collagen III (50% concentration)	0.59	3.13	0.19	0%
Collagen III (100% concentratior	-17.58	5.25	-3.35	-15%
Collagen IV (25% concentration)	0.67	3.14	0.21	1%
Collagen IV (33% concentration)	0.62	3.14	0.20	1%
Collagen IV (50% concentration)	10.83	3.72	2.91	9%
Collagen IV (100% concentratior	-6.44	5.06	-1.27	-5%
Fibronectin (25% concentration)	7.28	5.06	1.44	6%
Fibronectin (33% concentration)	0.51	3.68	0.14	0%
Fibronectin (50% concentration)	0.85	5.06	0.17	1%
Laminin (25% concentration)	-4.07	3.10	-1.31	-3%
Laminin (33% concentration)	-2.18	3.10	-0.70	-2%
Laminin (50% concentration)	-8.91	5.06	-1.76	-8%

R-squared: 0.736
Degrees of Freedom: 308

Range	
Low	High
21.154	139.7

Figure 34 Regression analysis of urea

The regression that was made assumes that there are no interactions between inputs and that each input is linear in its correlation with the urea output.

$$Urea = C_1 Day5 + C_2 Day9 + C_3 Day13 + C_4 Day17 + C_5 Day21 + C_6 Day25 + C_7 Day29$$
$$+ C_8 RTC + C_9 Procine\ LBM + C_{10} Human\ LBM + C_{11} CollagenI(25\%)$$
$$+ C_{12} CollagenI(33\%) + C_{13} CollagenI(50\%) + C_{14} CollagenI(100\%)$$
$$+ C_{15} CollagenIII(25\%) + C_{16} CollagenIII(33\%) + C_{17} CollagenIII(50\%)$$
$$+ C_{18} CollagenIII(100\%) + C_{19} CollagenIV(25\%) + C_{20} CollagenIV(33\%)$$
$$+ C_{21} CollagenIV(50\%) + C_{22} CollagenIV(100\%) + C_{23} Fibronectin(25\%)$$
$$+ C_{24} Fibronectin(33\%) + C_{25} Fibronectin(50\%) + C_{26} Fibronectin(100\%)$$
$$+ C_{27} Laminin(25\%) + C_{28} Laminin(33\%) + C_{29} Laminin(50\%)$$
$$+ Intercept$$

The output's r-squared value is only 0.736. In this regression, up to the 50% concentration, the higher the concentration of collagen I, the higher the urea output. Like in the albumin regression model, the most important ECM protein is collagen I, with 18% upregulation at 50% concentration, with the next one being collagen IV, showing 9% upregulation at 50% concentration. Both porcine and human LBM caused a slight downregulation of 3% each.The presence of rat tail collagen in particular has a slight positive effect on the production of urea, 3%.

Based on the regression the top three ECM combinations would be:

Table 2 Urea top results

Urea Top Results Based on:	
Regression Prediction	**Graphical Experimental**
Collagen I (50%), Collagen IV (25%), Fibronectin (25%)	Collagen I (50%), Collagen III (50%)
Collagen I (50%), Collagen IV (50%)	Collagen I (50%), Collagen IV (50%)
Collagen I (50%), Collagen III (25%), Fibronectin (25%)	Collagen I (33%), Collagen III (33%), Laminin (33%)

CYP 1A2

Variable	Coefficient	Stdev	t-value	Percent of Effect
Day 15	-0.0314	0.0038	-8.37	-33%
Day 23	-0.0374	0.0038	-9.96	-39%
Day 29	-0.0452	0.0038	-12.04	-47%
Rat Tail Collagen	0.0023	0.0091	0.25	2%
Porcine LBM	-0.0041	0.0090	-0.45	-4%
Human LBM	0.0064	0.0091	0.70	7%
Collagen I (25% concentration)	-0.0093	0.0057	-1.63	-10%
Collagen I (33% concentration)	0.0022	0.0057	0.39	2%
Collagen I (50% concentration)	0.0014	0.0067	0.21	1%
Collagen I (100% concentration)	-0.0038	0.0092	-0.42	-4%
Collagen III (25% concentration)	-0.0072	0.0055	-1.31	-7%
Collagen III (33% concentration)	0.0032	0.0048	0.67	3%
Collagen III (50% concentration)	-0.0022	0.0055	-0.40	-2%
Collagen III (100% concentratior	0.0000	0.0094	0.00	0%
Collagen IV (25% concentration)	-0.0065	0.0057	-1.14	-7%
Collagen IV (33% concentration)	0.0014	0.0057	0.25	1%
Collagen IV (50% concentration)	0.0027	0.0067	0.40	3%
Collagen IV (100% concentratior	-0.0085	0.0092	-0.93	-9%
Fibronectin (25% concentration)	-0.0081	0.0057	-1.43	-8%
Fibronectin (33% concentration)	0.0141	0.0057	2.49	15%
Fibronectin (50% concentration)	0.0279	0.0064	4.32	29%
Fibronectin (100% concentration)	0.0009	0.0092	0.10	1%
Laminin (25% concentration)	-0.0033	0.0056	-0.60	-3%
Laminin (33% concentration)	0.0093	0.0056	1.66	10%
Laminin (50% concentration)	-0.0009	0.0067	-0.14	-1%

R-squared: 0.359
Degrees of Freedom: 160

Range	
Low	High
0.000	0.096

Figure 35 Regression analysis of CYP 1A2

The regression that was made assumes that there are no interactions between inputs and that each input is linear in its correlation with the CYP 1A2 output.

$$CYP\ 1A2 = C_1 Day15 + C_2 Day23 + C_3 Day29 + C_4 RTC + C_5 Procine\ LBM + C_6 Human\ LBM + C_7 CollagenI(25\%) + C_8 CollagenI(33\%) + C_9 CollagenI(50\%) + C_{10} CollagenI(100\%) + C_{11} CollagenIII(25\%) + C_{12} CollagenIII(33\%) + C_{13} CollagenIII(50\%) + C_{14} CollagenIII(100\%) + C_{15} CollagenIV(25\%) + C_{16} CollagenIV(33\%) + C_{17} CollagenIV(50\%) + C_{18} CollagenIV(100\%) + C_{19} Fibronectin(25\%) + C_{20} Fibronectin(33\%) + C_{21} Fibronectin(50\%) + C_{22} Fibronectin(100\%) + C_{23} Laminin(25\%) + C_{24} Laminin(33\%) + C_{25} Laminin(50\%) + Intercept$$

The output's r-squared value is 0.359. Unlike other markers, CYP 1A2 production is not significantly affected by any particular ECM protein. However, there are ECM combinations that the model would suggest as being top candidates for the upregulation of CYP 1A2: fibronectin at 33% and at 50% concentrations and laminin at 33% concentration. Porcine LBM caused a 4% downregulation while human LBM resulted in 7% upregulation. Rat tail collagen had a slight positive effect on the production of CYP 1A2, 2%.

Based on the regression the top two ECM combinations would be:

Table 3 CYP 1A2 top results

CYP 1A2 Top Results Based on:	
Regression Prediction	**Graphical Experimental**
Collagen IV (50%), Fibronectin (50%)	Collagen III (25%), Collagen IV (25%), Fibronectin (25%), Laminin (25%)
Collagen I (50%), Fibronectin (50%)	Rat Tail Collagen

CYP 2A6

Variable	Coefficient	Stdev	t-value	Percent of Effect
Day 13	0.7320	0.0990	7.39	24%
Day 21	0.0968	0.0990	0.98	3%
Day 27	-0.0529	0.0990	-0.53	-2%
Rat Tail Collagen	0.0809	0.2419	0.33	3%
Porcine LBM	0.3251	0.2416	1.35	11%
Human LBM	0.4038	0.2403	1.68	13%
Collagen I (25% concentration)	0.3422	0.1445	2.37	11%
Collagen I (33% concentration)	-0.0848	0.1445	-0.59	-3%
Collagen I (50% concentration)	0.4282	0.1721	2.49	14%
Collagen I (100% concentration)	0.6620	0.2363	2.80	22%
Collagen III (25% concentration)	0.2792	0.1400	1.99	9%
Collagen III (33% concentration)	-0.1369	0.1225	-1.12	-5%
Collagen III (50% concentration)	-0.0297	0.1400	-0.21	-1%
Collagen III (100% concentratior	0.0053	0.2470	0.02	0%
Collagen IV (25% concentration)	0.2926	0.1452	2.02	10%
Collagen IV (33% concentration)	-0.1116	0.1452	-0.77	-4%
Collagen IV (50% concentration)	0.5715	0.1730	3.30	19%
Collagen IV (100% concentratior	0.2560	0.2375	1.08	9%
Fibronectin (25% concentration)	0.2423	0.1453	1.67	8%
Fibronectin (33% concentration)	-0.1288	0.1453	-0.89	-4%
Fibronectin (50% concentration)	0.0014	0.1731	0.01	0%
Fibronectin (100% concentration)	-0.7934	0.2377	-3.34	-26%
Laminin (25% concentration)	0.3979	0.1467	2.71	13%
Laminin (33% concentration)	-0.0639	0.1467	-0.44	-2%
Laminin (50% concentration)	-0.0883	0.1751	-0.50	-3%

R-squared: 0.406
Degrees of Freedom: 171

Range	
Low	High
0	3.005

Figure 36 Regression analysis of CYP 2A6

The regression that was made assumes that there are no interactions between inputs and that each input is linear in its correlation with the CYP 2A6 output.

$$CYP\ 2A6 = C_1 Day13 + C_2 Day21 + C_3 Day27 + C_4 RTC + C_5 Procine\ LBM$$
$$+ C_6 Human\ LBM + C_7 CollagenI(25\%) + C_8 CollagenI(33\%)$$
$$+ C_9 CollagenI(50\%) + C_{10} CollagenI(100\%) + C_{11} CollagenIII(25\%)$$
$$+ C_{12} CollagenIII(33\%) + C_{13} CollagenIII(50\%) + C_{14} CollagenIII(100\%)$$
$$+ C_{15} CollagenIV(25\%) + C_{16} CollagenIV(33\%) + C_{17} CollagenIV(50\%)$$
$$+ C_{18} CollagenIV(100\%) + C_{19} Fibronectin(25\%) + C_{20} Fibronectin(33\%)$$
$$+ C_{21} Fibronectin(50\%) + C_{22} Fibronectin(100\%) + C_{23} Laminin(25\%)$$
$$+ C_{24} Laminin(33\%) + C_{25} Laminin(50\%) + Intercept$$

The output's r-squared value is only 0.406. CYP 2A6 production is significantly affected by the concentration of collagen I, causing 11% upregulation at 25% concentration and collagen IV, causing upregulation at 25%, 50%, and 100% concentrations. Porcine LBM caused upregulation of 11% and human LBM caused upregulation of 13%. Rat tail collagen had a slight positive effect on the production of CYP 2A6, 3%.

Based on the regression the top three ECM combinations would be

Table 4 CYP 2A6 top results

CYP 2A6 Top Results Based on:

Regression Prediction	Graphical Experimental
Collagen IV (50%), Fibronectin (25%), Laminin (25%)	Collagen I (50%), Collagen IV (50%)
Collagen I (50%), Collagen IV (50%)	Collagen I (25%), Collagen III (25%), Fibronectin (25%), Laminin (25%)
Collagen I (25%), Collagen IV (25%), Fibronectin (25%), Laminin (25%)	Collagen III (25%), Collagen IV (25%), Fibronectin (25%), Laminin (25%)

CYP 2C9

Variable	Coefficient	Stdev	t-value	Percent of Effect
Day 13	238.20	435.10	0.55	2%
Day 21	-343.40	435.10	-0.79	-3%
Day 27	-1020.40	435.10	-2.35	-8%
Rat Tail Collagen	-234.20	769.50	-0.30	-2%
Porcine LBM	-796.80	774.80	-1.03	-7%
Human LBM	1722.50	759.00	2.27	14%
Collagen I (25% concentration)	960.34	473.33	2.03	8%
Collagen I (33% concentration)	18.09	473.33	0.04	0%
Collagen I (50% concentration)	49.57	562.40	0.09	0%
Collagen I (100% concentration)	1473.76	770.09	1.91	12%
Collagen III (25% concentration)	696.70	452.79	1.54	6%
Collagen III (33% concentration)	-759.17	399.33	-1.90	-6%
Collagen III (50% concentration)	-206.70	452.79	-0.46	-2%
Collagen III (100% concentratior	-13.67	784.26	-0.02	0%
Collagen IV (25% concentration)	739.00	457.70	1.61	6%
Collagen IV (33% concentration)	-1512.20	457.70	-3.30	-13%
Collagen IV (50% concentration)	-1105.70	543.90	-2.03	-9%
Collagen IV (100% concentratior	490.70	744.70	0.66	4%
Fibronectin (25% concentration)	357.60	477.50	0.75	3%
Fibronectin (33% concentration)	-592.80	477.50	-1.24	-5%
Fibronectin (50% concentration)	-680.30	567.30	-1.20	-6%
Fibronectin (100% concentration)	301.50	776.80	0.39	2%
Laminin (25% concentration)	1164.00	466.00	2.50	10%
Laminin (33% concentration)	-515.60	466.00	-1.11	-4%
Laminin (50% concentration)	-548.70	554.60	-0.99	-5%

R-squared: 0.140
Degrees of Freedom: 144

Range	
Low	High
5017	17107

Figure 37 Regression analysis of CYP 2C9

The regression that was made assumes that there are no interactions between inputs and that each input is linear in its correlation with the CYP 2C9 output.

$$CYP\ 2C9 = C_1 Day15 + C_2 Day23 + C_3 Day29 + C_4 RTC + C_5 Procine\ LBM + C_6 Human\ LBM + C_7 CollagenI(25\%) + C_8 CollagenI(100\%) + C_9 CollagenIII(25\%) + C_{10} CollagenIII(100\%) + C_{11} CollagenIV(25\%) + C_{12} CollagenIV(100\%) + C_{13} Fibronectin(25\%) + C_{14} Fibronectin(100\%) + C_{15} Laminin(25\%) + Intercept$$

Although the r-squared value was 0.140, human LBM and collagen I showed significant upregulation of albumin production by 14% and 12% respectively.

Based on the regression the top three ECM combinations would be

Table 5 CYP 2C9 top results

CYP 2C9 Top Results Based on:	
Regression Prediction	**Graphical Experimental**
Collagen I (25%), Collagen III (25%), Collagen IV (25%), Laminin (25%)	Collagen III (25%), Collagen IV (25%), Fibronectin (25%), Laminin (25%)
Human LBM (100%)	Collagen I (25%), Collagen III (25%), Collagen IV (25%), Laminin (25%)
Collagen I (100%)	Collagen IV (100%)

CYP 3A4

Variable	Coefficient	Stdev	t-value	Percent of Effect
Day 13	-305.13	247.58	-1.23	-5%
Day 21	57.07	247.58	0.23	1%
Day 27	-201.37	247.58	-0.81	-3%
Rat Tail Collagen	828.56	425.78	1.95	13%
Porcine LBM	604.18	427.85	1.41	9%
Human LBM	1274.45	419.69	3.04	20%
Collagen I (25% concentration)	726.45	241.07	3.01	11%
Collagen I (33% concentration)	-66.70	241.07	-0.28	-1%
Collagen I (50% concentration)	1326.37	286.43	4.63	20%
Collagen I (100% concentration)	1786.87	392.21	4.56	27%
Collagen III (25% concentration)	-176.80	236.20	-0.75	-3%
Collagen III (33% concentration)	-1200.50	208.30	-5.76	-18%
Collagen III (50% concentration)	-704.50	236.20	-2.98	-11%
Collagen III (100% concentratior	-720.90	409.20	-1.76	-11%
Collagen IV (25% concentration)	169.30	254.60	0.66	3%
Collagen IV (33% concentration)	-804.70	254.60	-3.16	-12%
Collagen IV (50% concentration)	835.30	302.50	2.76	13%
Collagen IV (100% concentratior	365.80	414.20	0.88	6%
Fibronectin (25% concentration)	211.90	233.10	0.91	3%
Fibronectin (33% concentration)	-931.40	233.10	-4.00	-14%
Fibronectin (50% concentration)	-296.50	276.90	-1.07	-5%
Fibronectin (100% concentration)	-2551.80	379.20	-6.73	-39%
Laminin (25% concentration)	35.67	251.37	0.14	1%
Laminin (33% concentration)	-1148.71	251.37	-4.57	-18%
Laminin (50% concentration)	-597.81	299.19	-2.00	-9%

R-squared: 0.470
Degrees of Freedom: 159

Range	
Low	High
7	6514

Figure 38 Regression analysis of CYP 3A4

The regression that was made assumes that there are no interactions between inputs and that each input is linear in its correlation with the CYP 3A4 output.

$$CYP\ 3A4 = C_1 Day13 + C_2 Day21 + C_3 Day27 + C_4 RTC + C_5 Procine\ LBM + C_6 Human\ LBM + C_7 CollagenI(25\%) + C_8 CollagenI(33\%) + C_9 CollagenI(50\%) + C_{10} CollagenI(100\%) + C_{11} CollagenIII(25\%) + C_{12} CollagenIII(33\%) + C_{13} CollagenIII(50\%) + C_{14} CollagenIII(100\%) + C_{15} CollagenIV(25\%) + C_{16} CollagenIV(33\%) + C_{17} CollagenIV(50\%) + C_{18} CollagenIV(100\%) + C_{19} Fibronectin(25\%) + C_{20} Fibronectin(33\%) + C_{21} Fibronectin(50\%) + C_{22} Fibronectin(100\%) + C_{23} Laminin(25\%) + C_{24} Laminin(33\%) + C_{25} Laminin(50\%) + Intercept$$

The output's r-squared value is 0.470. CYP 3A4 production is significantly affected by the concentrations of collagen I, showing upregulation at 25%, 50%, and 100% concentrations and fibronectin, showing 14% downregulation at 33% concentration and 39% downregulation at 100% concenration. Rat tail collagen had a significantly positive effect on the production of CYP 3A4, 13%.

Based on the regression the top three ECM combinations would be

Table 6 CYP 3A4 top results

CYP 3A4 Top Results Based on:	
Regression Prediction	**Graphical Experimental**
Collagen I (50%), Collagen IV (50%)	Collagen I (50%), Collagen IV (50%)
Collagen I (100%)	Collagen I (100%)
Human LBM (100%)	Human LBM (100%)

Because regression analysis is able isolate individual variables, it is possible to detail how other complex ECM protein mixtures, such as porcine and human LBM, compare to the rat tail collagen. The following table details the results.

	Albumin	Urea	CYP 1A2	CYP 2A6	CYP 2C9	CYP 3A4	Average
Rat Tail Collagen	-2%	3%	2%	3%	-9%	13%	2%
Porcine LBM	-3%	-3%	-4%	11%	-15%	9%	-1%
Human LBM	-2%	-3%	7%	13%	9%	20%	7%

Figure 39 Comparison between rat tail collagen, porcine LBM and human LBM

Comparison of average percent effect shows that human LBM is slightly superior to rat tail collagen, which is still preferred over porcine LBM.

3.4 Conclusion

The results of this study yielded several important conclusions. First and foremost, the use of regression analysis proved a superior method of analyzing this data due to its ability to confidently identify top-performing experimental combinations as well as to make predictions about top potential conditions to test in the future. As top results tables for each of the markers show, precise identification of top conditions was possible using regression analysis while the identification of top conditions was problematic using only observational methods.

A particularly interesting realization is that there may be a possibility to modify un-patterned conditions so that they might become top patterned conditions. For example, the regression prediction for best substrate for urea production is Collagen I (50%), Collagen IV (25%), Fibronectin (25%). However, under experimental conditions, these ECM proteins at concentration of 33% each, did not pattern and resulted in unspecific attachment. It seems that slight modifications of ECM protein concetration based on the regression analysis may yield a

top ECM combination for upregulation of urea function. Similar conclusions can be reached by observing non-patterned experimental condition Collagen IV(33%), Fibronectin (33%), Laminin (33%). This condition appears as a predicted top condition for albumin and CYP 2A6 production at the modified concentrations. It should be noted that experimentally it would have been both technically challenging and costly to conduct a screen that would allow to test for a variety of concentrations to troubleshoot non-patterning. The results of the regression models instill hope so that future work that may be done to identify best ECM combinations for the MPCC platform in a cost-effective manner.

Since one of the objectives of this screen was to determined whether the porcine or human LBM could perform as well as the current gold standard, rat tail collagen I, performing a regression analysis was able to give an unequivocal answer. When taking the output of all the assessed functions, human LBM was identified as slightly superior to rat tail collagen. Porcine LBM showed a slight downregulation of 1%. Based on the results of this regression analysis, it is clear that there are superior ways to upregulate certain functions as compared to using rat tail collagen. For example, for future toxicity studies, using Collagen IV(50%) may be considered as it appears as a top prediction in 3 out of 4 CYPs tested here.

The regression model presented here assumes that the effect each input has is linear with respect to the output. As the first step, the degree to which the hepatic functions were affected by the ECM protein concentrations and days in culture were examined. This allowed for the isolation of individual inputs and the assessment of the type and percent of effect produced. While a non-linear behavior could yield a lower p-value, a false conclusion might be made if there is no biological explanation behind this. Therefore, it is important to first examine the data from a linear perspective before moving forward with discerning interactions and non-linear

modeling (Ignotz and Massague 1986). In this study, there were cases where certain ECM combinations were partially patterned or not patterned at all. While all the non-patterned conditioned were excluded from the analysis, instances where there was partial patterning were still used. Therefore, further work may include a method of normalizing the output as a function of cells present to ensure that the desired effect is not due to a difference in cell number. Another next step would be to verify the effect and magnitude of the input when using hepatocyte donors of different genotypes, ethnicities, and disease states. Overall, the presented analysis is the beginning of possibilities that could be done to augment the MPCC model from the ECM perspective.

4. CHITOSAN-HEPARIN POLYELECTROLYTE MULTILAYERS FOR TGFβ DELIVERY IN PRIMARY HUMAN HEPATOCYTE CULTURES

4.1 Motivation

Growth factors (GFs) are molecules that play a critical role in modulating cellular functions such as proliferation, differentiation, cell movement, and ECM remodeling (Matsumoto and Nakamura 1996; Taipale and Keski-Oja 1997). GF binding to ECM is considered to be a regulatory mechanism for GF activity and one that goes awry in liver pathology (Taipale and Keski-Oja 1997; Hayashi 2012). Specifically, continuous TGF-β signaling in liver fibrosis contributes to activation of stellate cells and ECM production (Hayashi 2012). Fibronectin helps to regulate the balance of latent v. active TGF-β, thus maintaining homeostasis in ECM remodeling. GFs bind to carbohydrates known as glycosaminoglycans (GAGs), such as heparin, and are a part of proteoglycans found in the ECM as well as the cell surface (Schlessinger and Lemmon 1995; Ruoslahti et al. 1991). In nature, GF binding to proteoglycans serves to both protect the GFs from degradation as well as to provide a bound reservoir of GFs (Ruoslahti et al. 1991). By contrast, *in vitro* delivery of GFs to cell cultures generally takes places in soluble format and occurs during media changes. As platforms using PHHs represent more physiologically relevant models for developing toxicity screens and novel pharmaceutical agents, it is important to find ways to modulate PHH functions that are also physiologically relevant. In addition, present ways of GF delivery tend to be costly, thus giving more incentive to examine GF delivery methods that are similar to those found in native tissue and that do not require repeat dosing of soluble GFs.

Polyelectrolyte multilayers (PEMs) present itself as an attractive solution due to the spatiotemporal control of the films, ability to incorporate various biomolecules as well as ECM

components, and overall well-controlled biochemical and mechanical properties (Neto et al. 2016). Moreover, prior work demonstrated that in polysaccharide-based PEMs biochemical functions are maintained and conditions such as solution pH and ionic strength can be used to modulate thickness and composition (Boddohi et al. 2010). In the past, heparin – chitosan PEMs were used for growth factor delivery of fibroblast growth factor 2 (FGF-2) to mesenchymal stem cells to study attachment and differentiation response (Almodovar et al. 2010). Chitosan, a linear cationic polysaccharide, can electrostatically interact with negatively charged GAGs such as heparin in a pH-dependent environment, thus making the chitosan-heparin system enticing for mimicking *in vivo* ECM for PHH (Kim et al. 2008).

In this study, first pure hepatocyte and hepatocyte – 3T3-J2 co-cultures were compared in fibronectin-coated and heparin-terminated heparin – chitosan PEMs. The goals were to establish whether the addition of fibronectin improves cell functioning in PEMs as well as to compare pure and co-culture functioning in PEMs. Then the effect of heparin on TGF-β delivery, method of delivery, and response of pure v. co-cultures were assessed.

4.2 Methods

This section was adapted in part from Lin, C. et al. 2017 (Lin et al. 2017).

4.2.1 Fabrication of PEMs And TGF-β Delivery

PEMs were fabricated via layer-by-layer deposition of alternating chitosan and heparin sodium, both prepared in 0.2 M acetate buffer, pH 5.0. The deposition occurred in 5 minute steps of 300 µL of solution for 24-well and 50 µL for 96-well format. Acidified rinse solution at pH 4.0 was used to rinse the plates in between each adsorbed layer. Plates were gently agitated during each step. Since TCPS carries a negative charge, the order of adsorption was always chitosan, which is positively charged, followed by heparin, which is negatively charged. A total

of six layers were adsorbed. Prior to adsorbing recombinant human TGFβ1, PEMs plates were rinsed three times with double distilled water, sterilized with 70% ethanol for an hour, followed by another three washes with double distilled water.

TGF-β was coated at the concentrations of 100 pg/mL, 200 pg/mL, 300 pg/mL, 500 pg/mL, 1000 pg/mL, 5000 pg/mL, 10000 pg/mL. To facilitate adsorption, TGF-β- coated plates were gently agitated for 2 hours and subsequently rinsed twice with double distilled water. Fibronectin was adsorbed at the concentration of 100 μg/mL for 2 hours at 37◦C and was followed by two rinses with double distilled water. TGF-β and fibronectin adsorptions were performed the day of the cell seeding. Dosing with soluble TGF-β occurred on day 3, with subsequent continuous dosing occurring at the media change every other day. Pulse dosing occurred only on day 3.

4.2.2 Cell Culture

Cryopreserved PHHs and 3T3-J2 murine embryonic fibroblasts were seeded in accordance with the procedure outlined in section 3.2.2 of this thesis.

4.2.3 Biochemical Assays

Albumin, urea, CYP 2A6, and CYP 3A4 assays were performed as previously described in section 3.2.3. of this thesis. For albumin and urea analysis, supernatant was collected every other day beginning with day 3 until day 21. For CYPs 2A6 and 3A4 analysis, supernatant was collected on days 7, 13, and 21.

4.2.4 Data Analysis

Linear regression analysis was done using RStudio, version 1.1.423. For regression analysis, each input was treated as a categorical variable. Microsoft Excel and GraphPad Prism 7.0 were used for graphing.

4.3 Results and Discussion

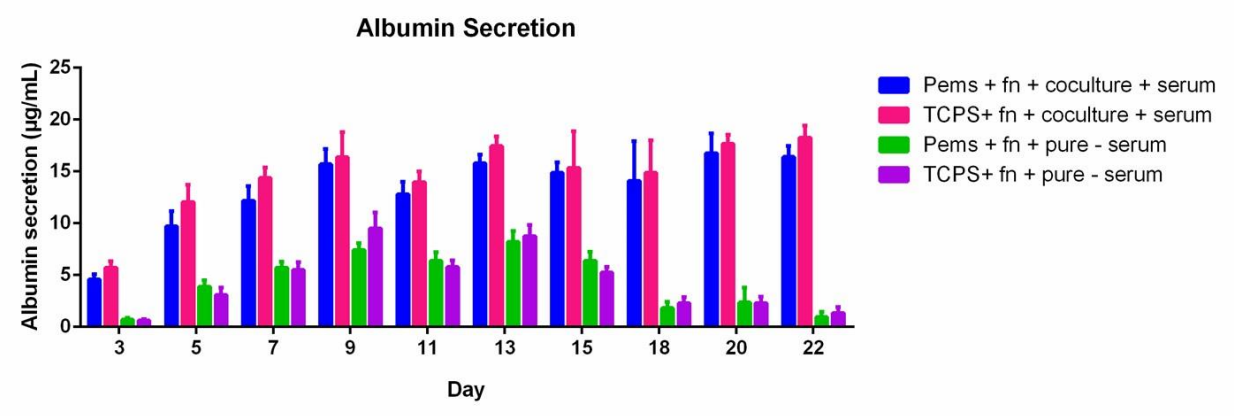

Figure 40 Albumin secretion

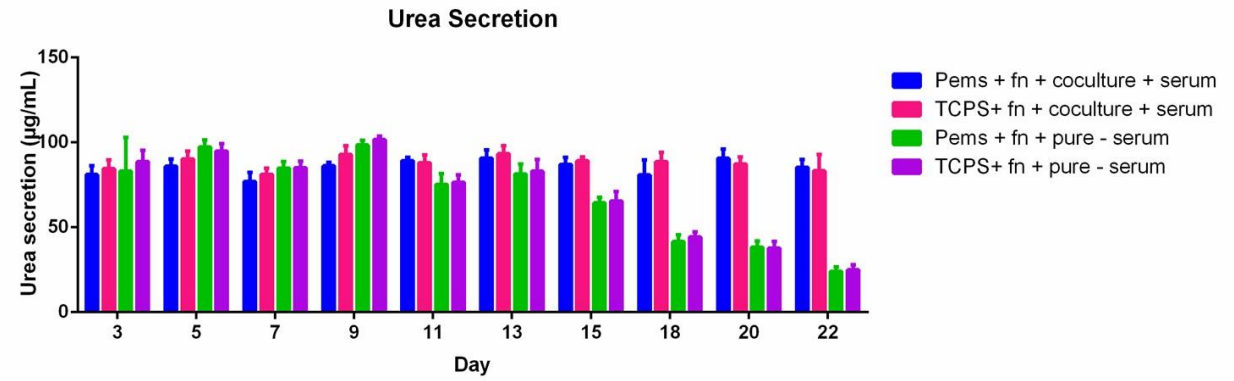

Figure 41 Urea secretion

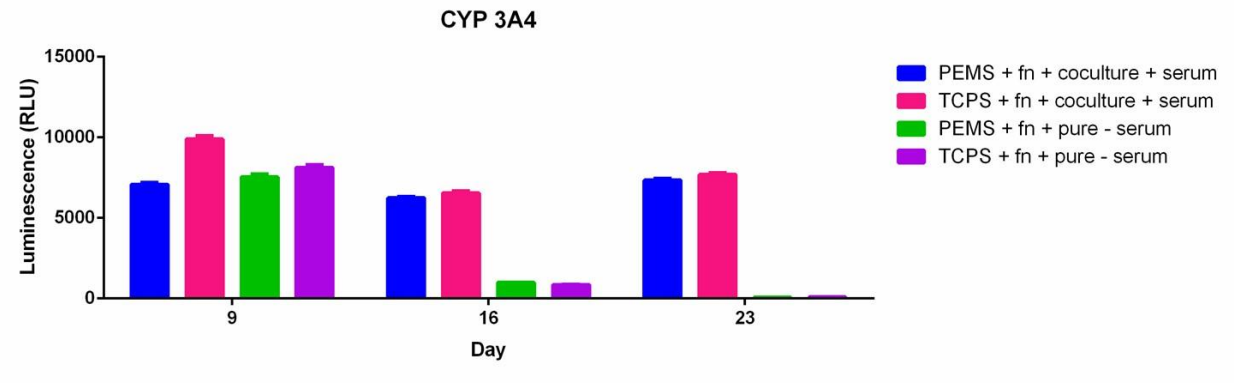

Figure 42 CYP 3A4 secretion

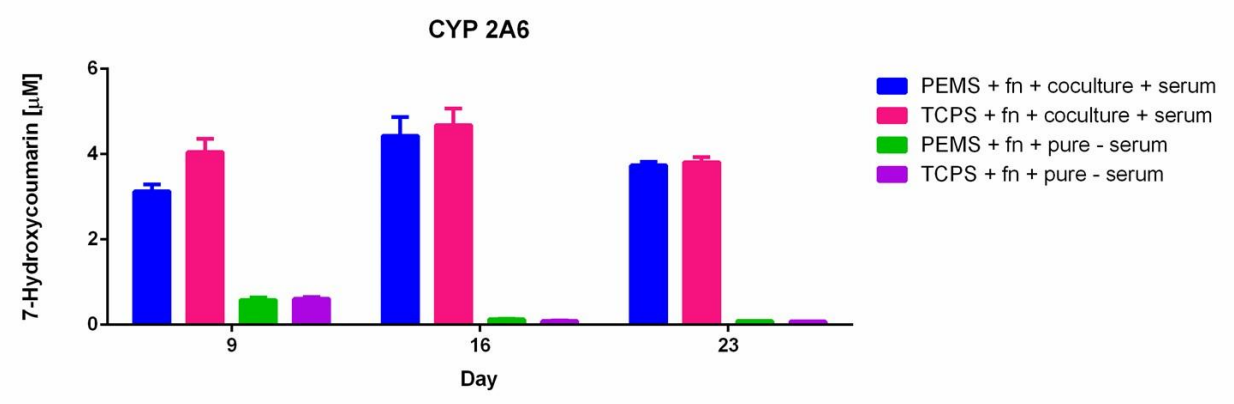

Figure 43 CYP 2A6 secretion

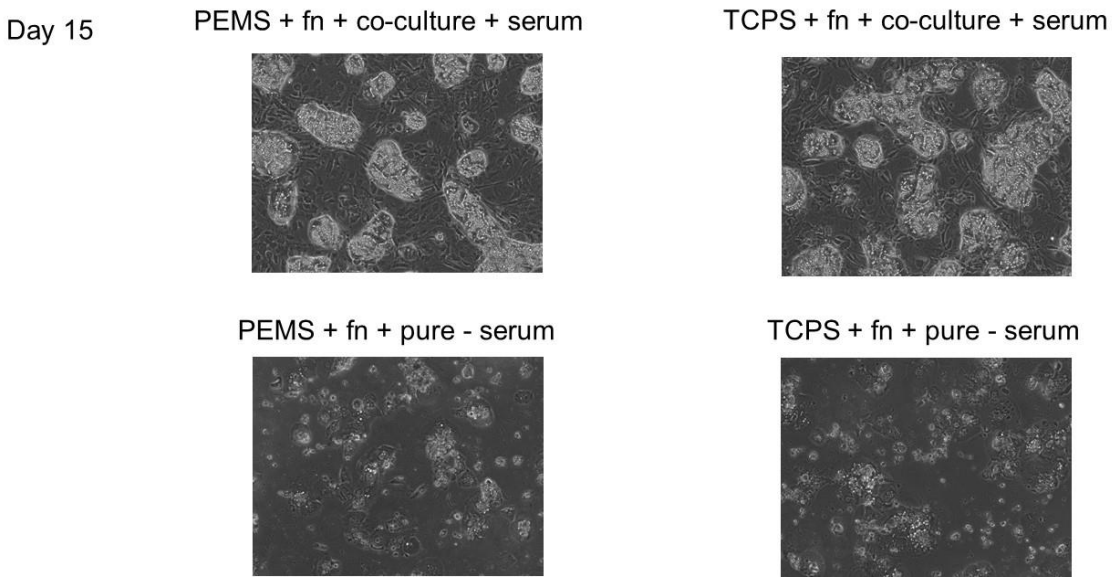

Figure 44 Effect of serum and co-culture at day 15 in culture

In the first part of the study, the effect of fibronectin on cell attachment was studied; cells failed to attach in the absence of fibronectin. The effect of PEMs v. TCPS was also studied; in pure cultures PEMs demonstrated an approximately similar effect as TCPS in albumin and urea production. Similarly, both PEMs and TCPS pure cultures showed a considerable downregulation in function by day 16; approximately sevenfold in CYP3A4 and approximately double in CYP 2A6. Lastly, the effect of co-culture was studied as well as the effect of serum that is present in co-culture medium. By testing PEMs and TCPS conditions that

were coated with fibronectin but did not have serum in media, it was possible to establish that the serum does have a positive effect on co-culture and should be a part of future conditions that contain co-culture. Co-culture conditions on both PEMs and TCPS demonstrated better performance than pure conditions, showing at least double albumin production as compared to monoculture. However, both co-culture and monoculture conditions had similar urea output up until day 18, when monocultures dropped to approximately half of urea output. For both CYPs, co-cultures showed superior performance across all three time points, with co-cultures on TCPS demonstrating slightly better outputs. Imaging also demonstrated similar morphologies between co-culture and pure culture conditions; with co-cultures exhibiting superior morphologies on both substrates. Overall, the necessity of having an ECM protein, such as fibronectin in this study, was verified. While PEMs and TCPS exhibited similar trends, the co-culture conditions in serum-containing media demonstrated superior performance over monoculture.

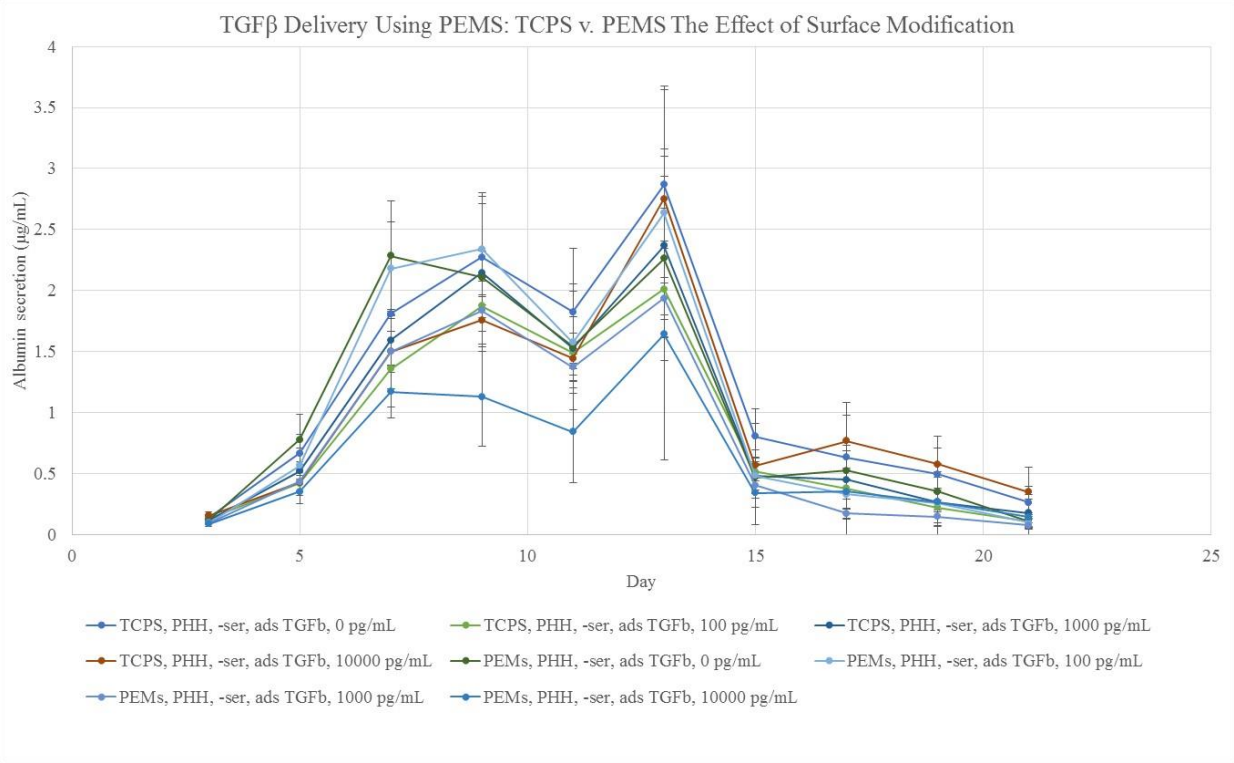

Figure 45 TGF-β delivery using PEMs: TCPS versus PEMs

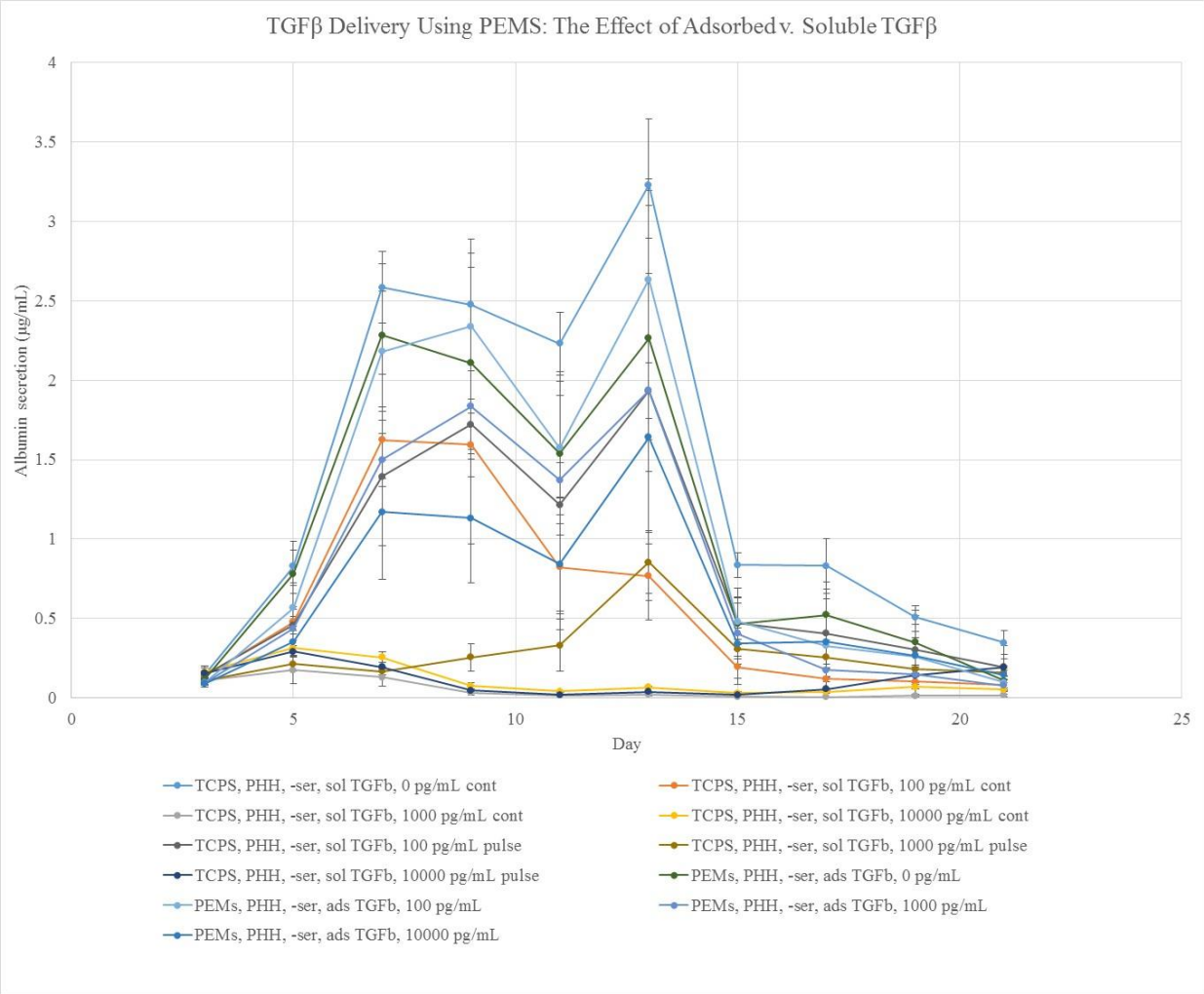

Figure 46 The effect of adsorbed versus soluble TGF-β

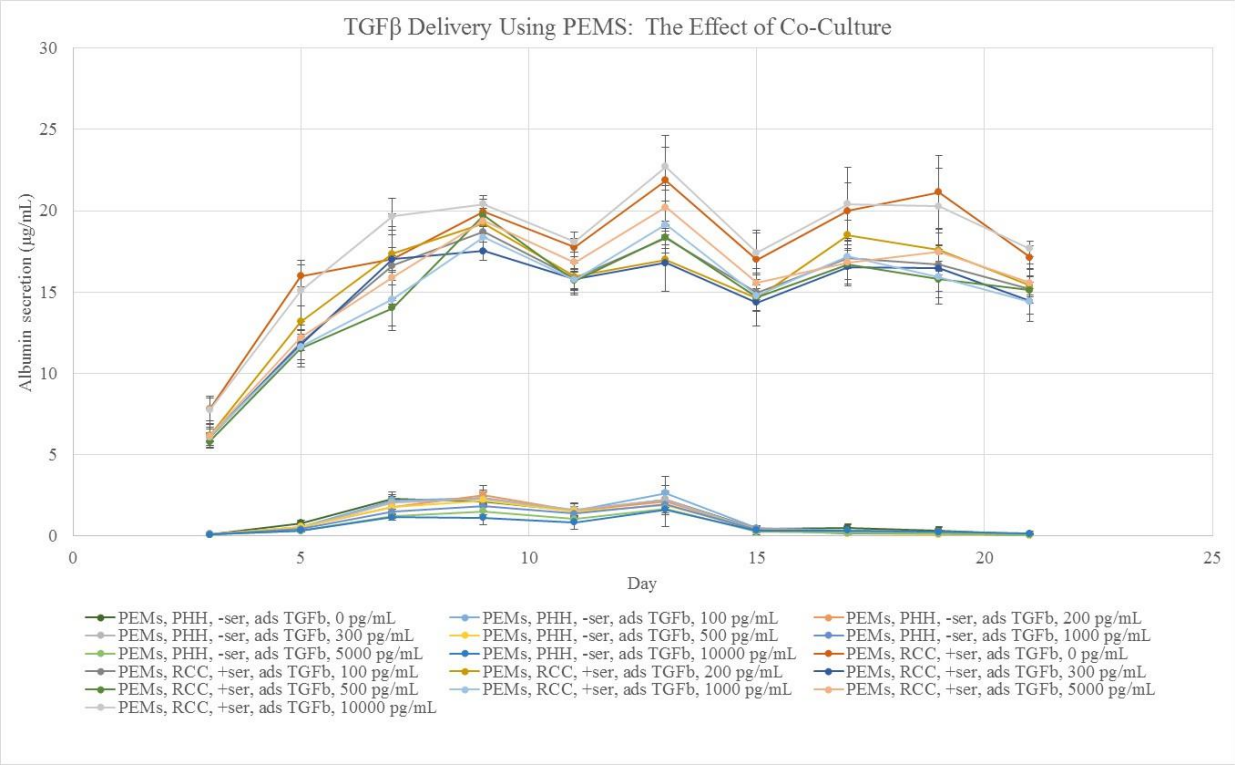

Figure 47 The effect of using PHH versus co-culture

Albumin

Variable	Coefficient	Stdev	t-value	Percent of Effect
Day 5	0.401	0.077	5.21	11%
Day 7	1.461	0.082	17.82	39%
Day 9	1.901	0.078	24.51	50%
Day 11	1.340	0.077	17.40	36%
Day 13	2.093	0.077	27.18	55%
Day 15	0.351	0.077	4.56	9%
Day 17	0.257	0.077	3.34	7%
Day 19	0.152	0.077	1.98	4%
Day 21	0.021	0.077	0.28	1%
PEMS	-0.131	0.042	-3.15	-3%
TGF-β 100	-0.188	0.059	-3.17	-5%
TGF-β 200	-0.101	0.077	-1.31	-3%
TGF–β 300	-0.124	0.077	-1.62	-3%
TGF-β 500	-0.198	0.077	-2.58	-5%
TGF-β 1000	-0.228	0.077	-2.96	-6%
TGF-β 5000	-0.378	0.077	-4.91	-10%
TGF-β 10000	-0.257	0.060	-4.30	-7%

R-squared: 0.862
Degrees of Freedom: 340

Range	
Low	High
0.021	3.795

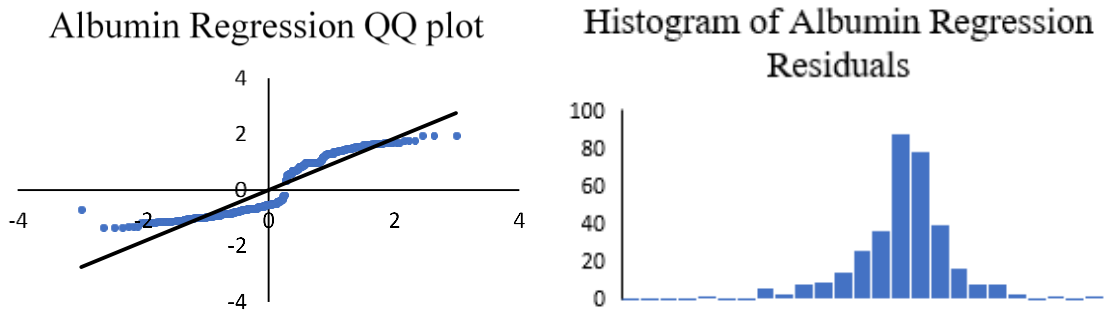

Figure 48 Albumin regression analysis: TCPS versus PEMS

The model for the albumin regression assumes that there is no linearity of the data: that each concentration of TGF-β is assumed to be independent and that each day is treated as an isolated variable, that is coefficient of Day 7 is not related to coefficient of Day 19.

$$Albumin = C_1 Day5 + C_2 Day7 + C_3 Day9 + C_4 Day11 + C_5 Day13 + C_6 Day15 + C_7 Day17 + C_8 Day19 + C_9 Day21 + C_{10} PEMs + C_{11} TGF\beta(100) + C_{12} TGF\beta(200) + C_{13} TGF\beta(300) + C_{14} TGF\beta(500) + C_{15} TGF\beta(1{,}000) + C_{16} TGF\beta(5{,}000) + C_{17} TGF\beta(10{,}000) + Intercept$$

The result shows that the r-squared value is 0.862, which suggests that this regression is a good fit. The histogram of the residuals follows a normal curve distribution. Based on the QQ plot, there is non-linear behavior around the mean within one standard deviation. The x-axis of the QQ plot represent the theoretical normal curve while the y-axis represents the data normalized to the mean. Therefore, the closer the data follows a normal distribution, the more closely it falls along the regression line.

Urea

Variable	Coefficient	Stdev	t-value	Percent of Effect
Day 5	7.43	1.80	4.12	6%
Day 7	27.45	1.94	14.18	23%
Day 9	11.43	1.82	6.29	10%
Day 11	-20.35	1.80	-11.28	-17%
Day 13	-8.73	2.63	-3.33	-7%
Day 15	-30.51	2.63	-11.62	-26%
Day 17	-35.64	1.80	-19.76	-30%
Day 19	-46.37	1.80	-25.70	-39%
Day 21	-58.91	1.80	-32.66	-50%
PEMS	1.32	1.09	1.21	1%
TGF-β 100	1.07	1.46	0.73	1%
TGF-β 200	3.01	2.01	1.50	3%
TGF–β 300	1.61	2.01	0.80	1%
TGF-β 500	1.49	2.01	0.74	1%
TGF-β 1000	4.54	1.46	3.11	4%
TGF-β 5000	0.02	2.01	0.01	0%
TGF-β 10000	5.10	1.47	3.46	4%

R-squared: 0.933
Degrees of Freedom: 292

Range	
Low	High
9.803	128.154

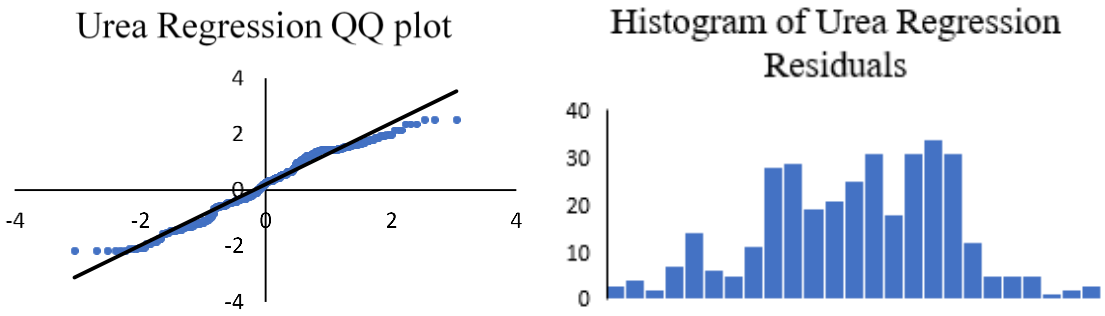

Figure 49 Urea regression analysis: TCPS versus PEMS

As with the albumin regression, the urea regression assumes that there is no linearity of the inputs.

$$Urea = C_1 Day5 + C_2 Day7 + C_3 Day9 + C_4 Day11 + C_5 Day13 + C_6 Day15 + C_7 Day17$$
$$+ C_8 Day19 + C_9 Day21 + C_{10} PEMs + C_{11} TGF\beta(100) + C_{12} TGF\beta(200)$$
$$+ C_{13} TGF\beta(300) + C_{14} TGF\beta(500) + C_{15} TGF\beta(1{,}000) + C_{16} TGF\beta(5{,}000)$$
$$+ C_{17} TGF\beta(10{,}000) + Intercept$$

The result shows that the r-squared value is 0.933, which suggests that there is an excellent predictability of how the final urea output is a function of the initial variables. Also the histogram of the residuals follows a normal curve distribution. However, the distribution is much wider than the distribution of residuals from the albumin regression. The QQ plot shows excellent adherence for the projected line and that the residuals do not skew in one direction or another.

CYP 2A6

Variable	Coefficient	Stdev	t-value	Percent of Effect
Day 13	-0.1408	0.0118	-11.92	-34%
Day 21	-0.1895	0.0117	-16.16	-46%
PEMS	-0.0189	0.0117	-1.61	-5%
TGF-β 100	0.0239	0.0166	1.44	6%
TGF-β 200	0.0411	0.0211	1.94	10%
TGF–β 300	0.0487	0.0211	2.30	12%
TGF-β 500	0.0495	0.0211	2.34	12%
TGF-β 1000	0.0332	0.0166	2.00	8%
TGF-β 5000	0.0030	0.0219	0.14	1%
TGF-β 10000	-0.0071	0.0166	-0.43	-2%

R-squared: 0.728
Degrees of Freedom: 97

Range	
Low	High
0	0.411

Figure 50 CYP 2A6 regression analysis: TCPS versus PEMS

The CYP 2A6 regression assumes that there is no linearity of the inputs.

$$CYP\ 2A6 = C_1 Day13 + C_2 Day21 + C_3 PEMs + C_4 TGF\beta(100) + C_5 TGF\beta(200) + C_6 TGF\beta(300) + C_7 TGF\beta(500) + C_8 TGF\beta(1{,}000) + C_9 TGF\beta(5{,}000) + C_{10} TGF\beta(10{,}000) + Intercept$$

The result shows that the r-squared value is 0.728, which suggests that there is an acceptable predictability of how the final CYP 2A6 is a function of the initial variables. The histogram of the residuals follows a normal curve distribution, but the maximum occurrence of

the residuals is not centered and is slightly shifted to the right. Examining the data from the QQ plot as well, there is a long tail to the left, which suggests that there is an interaction that the model does not take into account.

CYP 3A4

Variable	Coefficient	Stdev	t-value	Percent of Effect
Day 13	30.661	130.295	0.24	1%
Day 21	-2027.778	129.267	-15.69	-54%
PEMS	-28.306	129.267	-0.22	-1%
TGF-β 100	4.167	182.812	0.02	0%
TGF-β 200	68.431	233.040	0.29	2%
TGF–β 300	-13.792	233.040	-0.06	0%
TGF-β 500	-14.125	233.040	-0.06	0%
TGF-β 1000	51.222	182.812	0.28	1%
TGF-β 5000	-295.260	242.021	-1.22	-8%
TGF-β 10000	-98.444	182.810	-0.54	-3%

R-squared: 0.778
Degrees of Freedom: 97

Range	
Low	High
63	3852

Figure 51 CYP 3A4 regression analysis: TCPS versus PEMS

The CYP 3A4 regression assumes that there is no linearity of the inputs.

$$CYP\ 3A4 = C_1 Day13 + C_2 Day21 + C_3 PEMs + C_4 TGF\beta(100) + C_5 TGF\beta(200) + C_6 TGF\beta(300) + C_7 TGF\beta(500) + C_8 TGF\beta(1{,}000) + C_9 TGF\beta(5{,}000) + C_{10} TGF\beta(10{,}000) + Intercept$$

The result shows that the r-squared value is 0.778, which suggests that there is some predictive value of how the final CYP 3A4 output is a function of the initial variables. The r-squared value of CYP 3A4 is similar to the r-squared value of CYP 2A6. The histogram of the residuals follows a normal curve distribution, but the maximum occurrence of the residuals is not centered and is slightly shifted to the right. Combined with the QQ plot, the data falls far away from the predicted values at the low end suggesting that the regression is not accounting for interactions that are occurring when the CYP 3A4 production is low.

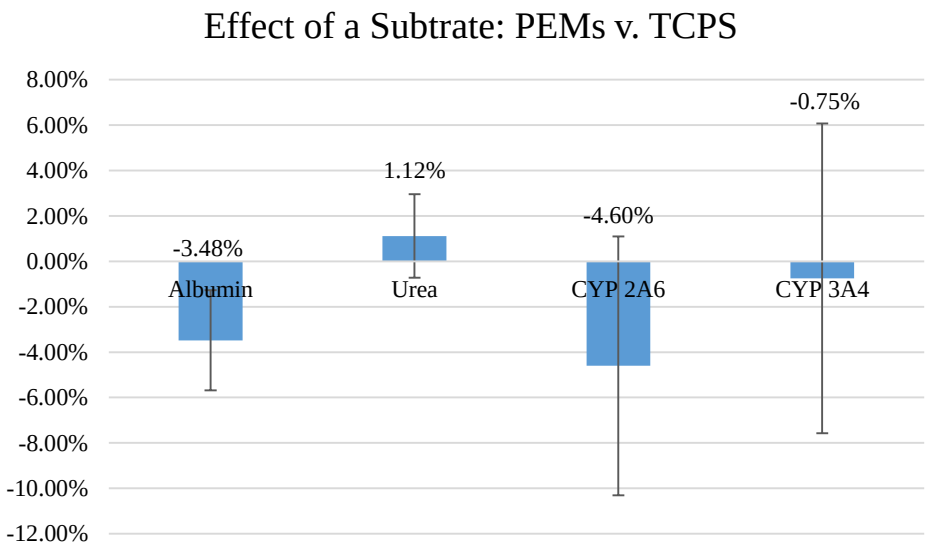

Figure 52 Regression analysis: effect of substrate

The purpose was to study whether heparin has an effect on TGF-β delivery and was done by comparing PHH cultures on PEMS with adsorbed TGF-β in serum free media to PHH cultures on TCPS with adsorbed TGF-β in serum free media. The above figure suggests that urea, CYP 2A6 and CYP 3A4 are not significantly affected by the presence of PEMs within two standard deviations of their means. There is, however, a slight downregulation of albumin production when PEMs are present. The presence of PEMs caused only a 3% reduction in

albumin production. Albumin, urea, CYP 2A6 and CYP 3A4 productions are most affected by the number of days the cells have been in culture. In some cases, the number of days the cells have been in culture can account for over 54% of the total output.

Albumin

Variable	Coefficient	Stdev	t-value	Percent of Effect
Day 5	0.348	0.089	3.92	9%
Day 7	1.111	0.091	12.15	29%
Day 9	1.468	0.089	16.47	39%
Day 11	1.042	0.089	11.74	27%
Day 13	1.635	0.089	18.43	43%
Day 15	0.269	0.089	3.03	7%
Day 17	0.202	0.089	2.27	5%
Day 19	0.115	0.089	1.30	3%
Day 21	0.018	0.089	0.20	0%
PEMS	-0.161	0.060	-2.67	-4%
Adsobred	0.465	0.054	8.55	12%
TGF-β 100	-0.323	0.065	-4.97	-9%
TGF-β 200	-0.324	0.107	-3.03	-9%
TGF–β 300	-0.348	0.107	-3.26	-9%
TGF-β 500	-0.422	0.107	-3.95	-11%
TGF-β 1000	-0.619	0.065	-9.52	-16%
TGF-β 5000	-0.595	0.107	-5.57	-16%
TGF-β 10000	-0.666	0.065	-10.19	-18%

R-squared: 0.687
Degrees of Freedom: 549

Range	
Low	High
0.004	3.795

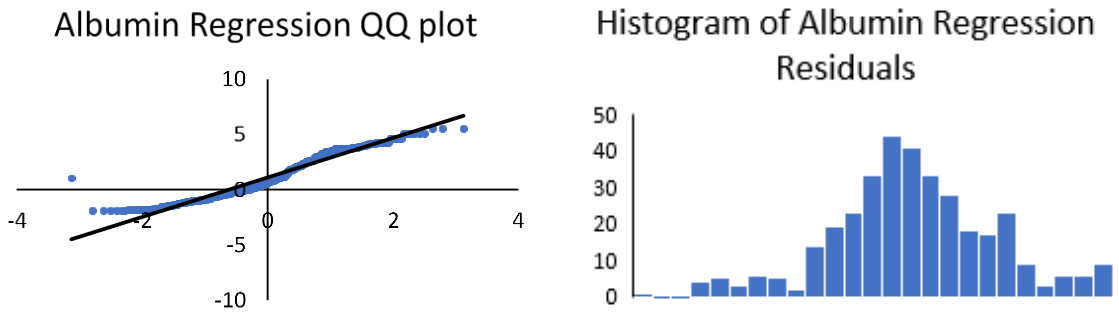

Figure 53 Albumin regression analysis: TGF-β delivery

The albumin regression assumes that there is no linearity of the inputs.

$$Albumin = C_1 Day5 + C_2 Day7 + C_3 Day9 + C_4 Day11 + C_5 Day13 + C_6 Day15 + C_7 Day17 + C_8 Day19 + C_9 Day21 + C_{10} PEMs + C_{11} Adsorbed + C_{12} TGF\beta(100) + C_{13} TGF\beta(200) + C_{14} TGF\beta(300) + C_{15} TGF\beta(500) + C_{16} TGF\beta(1{,}000) + C_{17} TGF\beta(5{,}000) + C_{18} TGF\beta(10{,}000) + Intercept$$

The result shows that the r-squared value is 0.687, which suggests that there is some predictive value of how the final albumin output is a function of the initial variables. The histogram of the residuals follows a normal curve distribution, and the maximum occurrence of the residuals is in the center. This suggests that the regression is good, however it accounts for 68.7 % of the system behavior, with 31.3% unaccounted for. Combined with the QQ plot data, there is no obvious reason why the r-squared value is so low. A possible reason for the r-squared value being low is that the standard deviation of each variable is high and thus too much noise is present in the model.

Urea

Variable	Coefficient	Stdev	t-value	Percent of Effect
Day 5	4.92	2.34	2.10	4%
Day 7	7.48	2.42	3.09	6%
Day 9	-5.71	2.35	-2.42	-5%
Day 11	-30.20	2.34	-12.89	-26%
Day 13	-24.98	2.80	-8.92	-21%
Day 15	-45.70	2.78	-16.44	-39%
Day 17	-47.17	2.34	-20.14	-40%
Day 19	-54.46	2.34	-23.25	-46%
Day 21	-64.22	2.34	-27.42	-54%
PEMS	-1.31	1.72	-0.76	-1%
Adsobred	19.39	1.44	13.48	16%
TGF-β 100	-6.12	1.77	-3.46	-5%
TGF-β 200	-7.71	3.15	-2.45	-7%
TGF–β 300	-9.11	3.15	-2.89	-8%
TGF-β 500	-9.24	3.15	-2.93	-8%
TGF-β 1000	-12.33	1.77	-6.96	-10%
TGF-β 5000	-10.70	3.15	-3.40	-9%
TGF-β 10000	-12.90	1.78	-7.24	-11%

R-squared: 0.815
Degrees of Freedom: 501

Range	
Low	High
9.803	128.154

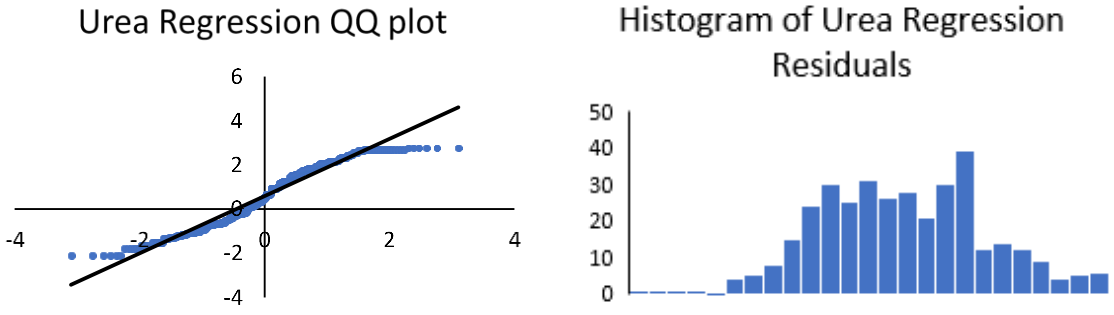

Figure 54 Urea regression analysis: TGF-β delivery

The urea regression assumes that there is no linearity of the inputs.

$$Urea = C_1 Day5 + C_2 Day7 + C_3 Day9 + C_4 Day11 + C_5 Day13 + C_6 Day15 + C_7 Day17$$
$$+ C_8 Day19 + C_9 Day21 + C_{10} PEMs + C_{11} Adsorbed + C_{12} TGF\beta(100)$$
$$+ C_{13} TGF\beta(200) + C_{14} TGF\beta(300) + C_{15} TGF\beta(500) + C_{16} TGF\beta(1{,}000)$$
$$+ C_{17} TGF\beta(5{,}000) + C_{18} TGF\beta(10{,}000) + Intercept$$

The result shows that the r-squared value is 0.815, which suggests that this regression is slightly superior than the albumin regression. The histogram of the residuals follows a normal curve distribution. However, the tail on the leftmost part of the figure is much longer than the right side. This suggests that the regression is good, however it is incomplete in how it accounts for the variables. Combined with the QQ plot, the data suggests that there might be some interactions that are causing a dampening to occur.

CYP 2A6

Variable	Coefficient	Stdev	t-value	Percent of Effect
Day 13	-0.100	0.010	-10.06	-24%
Day 21	-0.146	0.010	-14.73	-36%
PEMS	0.019	0.012	1.52	5%
Adsobred	0.025	0.011	2.27	6%
TGF-β 100	0.009	0.014	0.63	2%
TGF-β 200	0.023	0.022	1.08	6%
TGF–β 300	0.031	0.022	1.43	7%
TGF-β 500	0.014	0.022	0.64	3%
TGF-β 1000	-0.005	0.014	-0.37	-1%
TGF-β 5000	-0.013	0.022	-0.59	-3%
TGF-β 10000	-0.025	0.014	-1.83	-6%

R-squared: 0.634
Degrees of Freedom: 159

Range	
Low	High
0	0.411

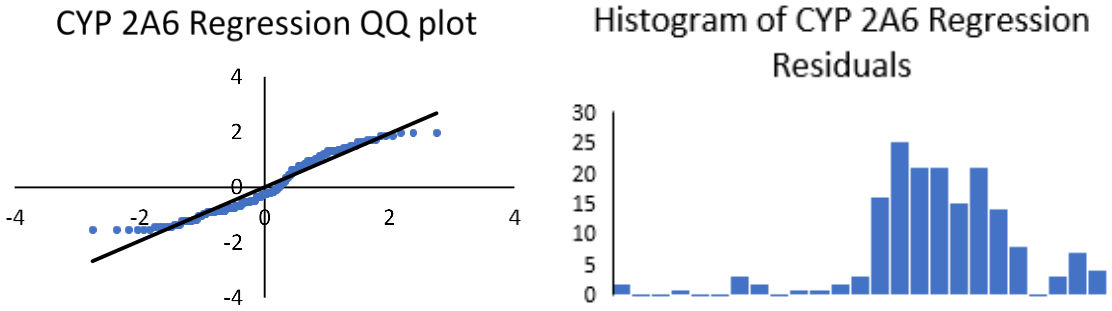

Figure 55 CYP 2A6 regression analysis: TGF-β delivery

The CYP 2A6 regression assumes that there is no linearity of the inputs.

$$CYP\ 2A6 = C_1 Day13 + C_2 Day21 + C_3 PEMs + C_4 Adsorbed + C_5 TGF\beta(100) + C_6 TGF\beta(200) + C_7 TGF\beta(300) + C_8 TGF\beta(500) + C_9 TGF\beta(1{,}000) + C_{10} TGF\beta(5{,}000) + C_{11} TGF\beta(10{,}000) + Intercept$$

The result shows that the r-squared value is 0.634, which suggests that this regression is worse than either albumin or urea. The histogram of the residuals follows a normal curve

distribution. However, as with both urea and albumin, the tail on the leftmost part of the figure is much longer than the right side.

CYP 3A4

Variable	Coefficient	Stdev	t-value	Percent of Effect
Day 13	-98.33	141.16	-0.70	-3%
Day 21	-1716.44	140.46	-12.22	-45%
PEMS	-28.31	176.74	-0.16	-1%
Adsobred	721.76	157.63	4.58	19%
TGF-β 100	-171.97	192.14	-0.90	-4%
TGF-β 200	-339.35	304.96	-1.11	-9%
TGF–β 300	-421.57	304.96	-1.38	-11%
TGF-β 500	-421.90	304.96	-1.38	-11%
TGF-β 1000	-634.22	192.14	-3.30	-16%
TGF-β 5000	-726.76	317.67	-2.29	-19%
TGF-β 10000	-867.97	192.14	-4.52	-23%

R-squared: 0.616
Degrees of Freedom: 159

Range	
Low	High
0	3852

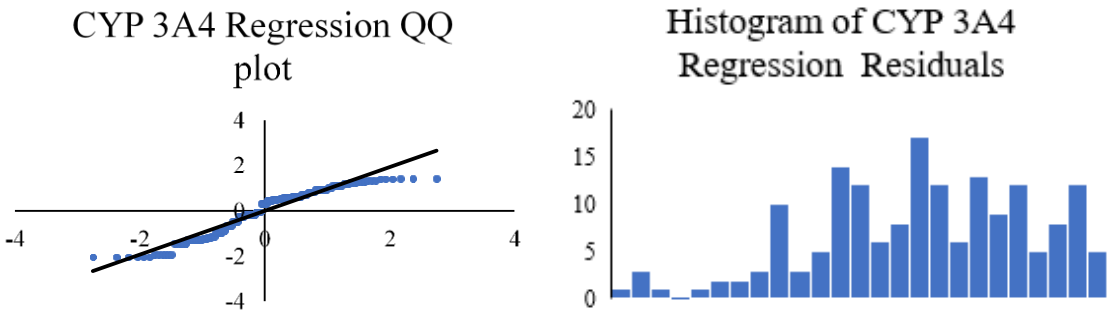

Figure 56 CYP 3A4 regression analysis: TGF-β delivery

The CYP 3A4 regression assumes that there is no linearity of the inputs.

$$CYP\ 3A4 = C_1 Day13 + C_2 Day21 + C_3 PEMs + C_4 Adsorbed + C_5 TGF\beta(100)$$
$$+ C_6 TGF\beta(200) + C_7 TGF\beta(300) + C_8 TGF\beta(500) + C_9 TGF\beta(1{,}000)$$
$$+ C_{10} TGF\beta(5{,}000) + C_{11} TGF\beta(10{,}000) + Intercept$$

The result shows that the r-squared value is 0.616, which is comparable to the r-squared value of CYP 2A6. The histogram of the residuals does not show an obvious pattern and thus it is hard to explain what is going on with this model; perhaps a different, non-linear model should be used instead.

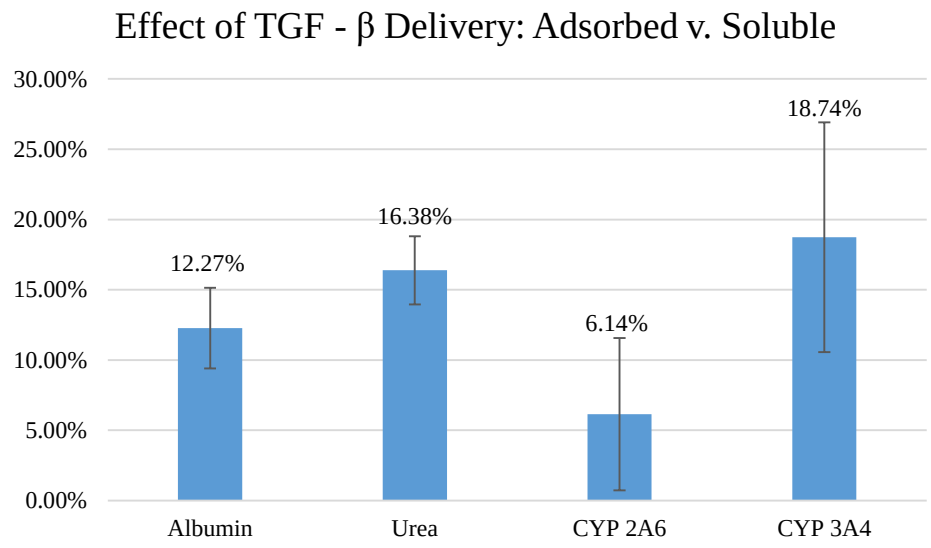

Figure 57 Regression analysis: effect of TGF - β delivery

The adsorbance of TGF-β causes a strong upregulation of each of marker. Also the total effect of the adsorbed TGF-β versus soluble TGF-β is non-trvial, affecting the total ouput of the markers between 6.14% to 18.74%.

Albumin

Variable	Coefficient	Stdev	t-value	Percent of Effect
Day 5	3.42	0.40	8.47	14%
Day 7	5.41	0.42	12.88	22%
Day 9	7.34	0.41	18.11	30%
Day 11	5.63	0.40	13.98	23%
Day 13	7.38	0.40	18.32	30%
Day 15	4.61	0.40	11.45	19%
Day 17	5.80	0.40	14.38	23%
Day 19	5.64	0.40	13.99	23%
Day 21	4.56	0.40	11.31	18%
Co-Culture	14.94	0.18	82.11	60%
TGF-β 100	-1.12	0.35	-3.15	-5%
TGF-β 200	-0.96	0.35	-2.71	-4%
TGF–β 300	-1.41	0.35	-3.96	-6%
TGF-β 500	-1.40	0.35	-3.96	-6%
TGF-β 1000	-1.41	0.35	-3.97	-6%
TGF-β 5000	-1.03	0.35	-2.91	-4%
TGF-β 10000	0.23	0.36	0.65	1%

R-squared: 0.941
Degrees of Freedom: 461

Range	
Low	High
0.021	24.835

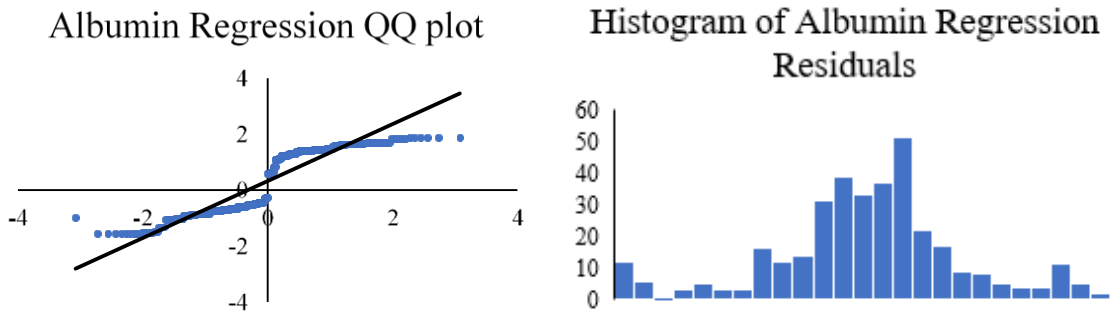

Figure 58 Albumin regression analysis: pure versus co-culture

The model for the albumin regression assumes that there is no linearity of the data.

$$Albumin = C_1 Day5 + C_2 Day7 + C_3 Day9 + C_4 Day11 + C_5 Day13 + C_6 Day15 + C_7 Day17 + C_8 Day19 + C_9 Day21 + C_{10} CoCulture + C_{11} TGF\beta(100) + C_{12} TGF\beta(200) + C_{13} TGF\beta(300) + C_{14} TGF\beta(500) + C_{15} TGF\beta(1{,}000) + C_{16} TGF\beta(5{,}000) + C_{17} TGF\beta(10{,}000) + Intercept$$

The result shows that the r-squared value is 0.941, which suggests that this regression is an excellent fit. The histogram of the residuals follows a normal curve distribution with equally sized tails. Since the QQ plot is not linear, the remainder of the r-squared may be explained via a non-linear function of the inputs.

Urea

Variable	Coefficient	Stdev	t-value	Percent of Effect
Day 5	8.67	2.20	3.93	7%
Day 7	16.60	2.31	7.20	14%
Day 9	12.20	2.22	5.51	10%
Day 11	-4.80	2.20	-2.18	-4%
Day 13	20.01	2.76	7.26	16%
Day 15	-20.07	2.76	-7.28	-17%
Day 17	-22.33	2.20	-10.14	-18%
Day 19	-24.79	2.20	-11.25	-20%
Day 21	-37.60	2.20	-17.07	-31%
Co-Culture	18.16	1.12	16.28	15%
TGF-β 100	-11.02	2.04	-5.40	-9%
TGF-β 200	-15.14	2.04	-7.41	-12%
TGF–β 300	-17.95	2.04	-8.79	-15%
TGF-β 500	-19.73	2.04	-9.66	-16%
TGF-β 1000	-18.36	2.04	-8.98	-15%
TGF-β 5000	-20.19	2.04	-9.88	-17%
TGF-β 10000	-13.24	2.04	-6.48	-11%

R-squared: 0.821
Degrees of Freedom: 413

Range	
Low	High
9.803	131.427

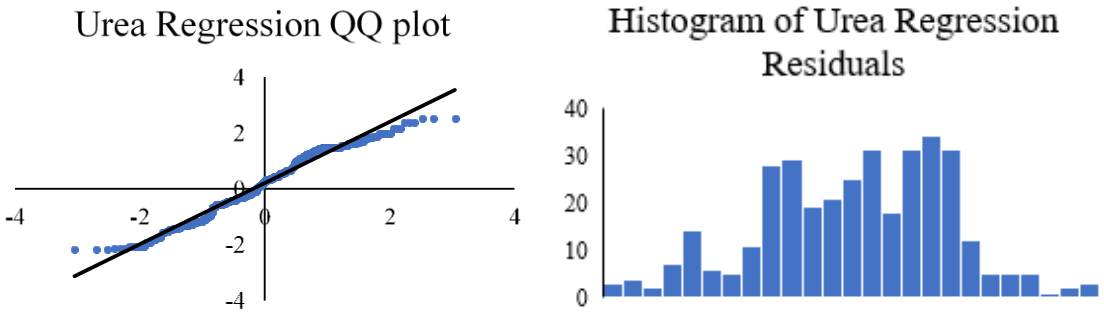

Figure 59 Urea regression analysis: pure versus co-culture

As with the albumin regression, the urea regression assumes that there is no linearity of the inputs.

$$Urea = C_1 Day5 + C_2 Day7 + C_3 Day9 + C_4 Day11 + C_5 Day13 + C_6 Day15 + C_7 Day17 + C_8 Day19 + C_9 Day21 + C_{10} CoCulture + C_{11} TGF\beta(100) + C_{12} TGF\beta(200) + C_{13} TGF\beta(300) + C_{14} TGF\beta(500) + C_{15} TGF\beta(1{,}000) + C_{16} TGF\beta(5{,}000) + C_{17} TGF\beta(10{,}000) + Intercept$$

The result shows that the r-squared value is 0.821, which suggests that there is a good predictability of how the final urea output is a function of the initial variables. The histogram of the residuals follows a normal curve distribution; however, the distribution is much wider than the distribution of residuals from the albumin regression. The QQ plot shows excellent adherence for the projected line.

CYP 2A6

Variable	Coefficient	Stdev	t-value	Percent of Effect
Day 13	0.26	0.08	3.37	7%
Day 21	0.23	0.09	2.56	6%
Co-Culture	2.66	0.07	36.80	67%
TGF-β 100	0.18	0.13	1.43	5%
TGF-β 200	0.17	0.13	1.28	4%
TGF–β 300	0.24	0.13	1.83	6%
TGF-β 500	0.16	0.13	1.20	4%
TGF-β 1000	0.13	0.14	0.96	3%
TGF-β 5000	0.11	0.14	0.81	3%
TGF-β 10000	-0.01	0.13	-0.08	0%

R-squared: 0.933
Degrees of Freedom: 107

Range	
Low	High
0	3.987

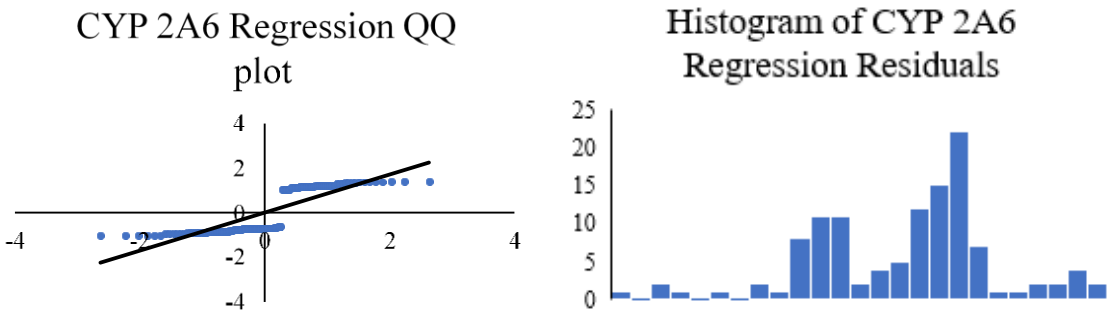

Figure 60 CYP 2A6 Regression analysis: pure versus co-culture

The CYP 2A6 regression assumes that there is no linearity of the inputs.

$$CYP\ 2A6 = C_1 Day13 + C_2 Day21 + C_3 CoCulture + C_4 TGF\beta(100) + C_5 TGF\beta(200) + C_6 TGF\beta(300) + C_7 TGF\beta(500) + C_8 TGF\beta(1{,}000) + C_9 TGF\beta(5{,}000) + C_{10} TGF\beta(10{,}000) + Intercept$$

The result shows that the r-squared value is 0.933, which suggests that there is an excellent predictability of how the final CYP 2A6 is a function of the initial variables. The histogram of the residuals follows a bimodal distribution. Examining the data from the QQ plot, there is poor adherence to the linear projection.

CYP 3A4

Variable	Coefficient	Stdev	t-value	Percent of Effect
Day 13	2772.50	352.30	7.87	19%
Day 21	-443.50	411.60	-1.08	-3%
Co-Culture	7892.70	329.00	23.99	54%
TGF-β 100	-847.50	575.10	-1.47	-6%
TGF-β 200	-865.70	604.80	-1.43	-6%
TGF–β 300	-794.40	593.20	-1.34	-5%
TGF-β 500	-802.20	604.80	-1.33	-6%
TGF-β 1000	-1148.30	618.40	-1.86	-8%
TGF-β 5000	-1032.40	617.00	-1.67	-7%
TGF-β 10000	-345.00	593.50	-0.58	-2%

R-squared: 0.881
Degrees of Freedom: 107

Range	
Low	High
63	14608

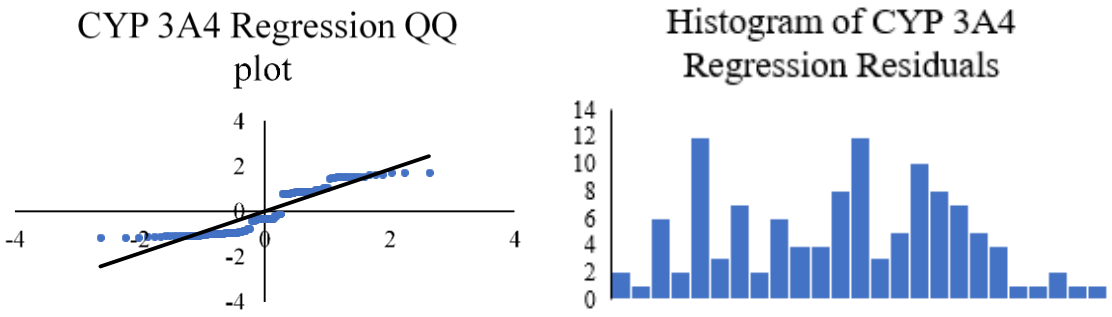

Figure 61 CYP 3A4 Regression analysis: pure versus co-culture

The CYP 3A4 regression assumes that there is no linearity of the inputs.

$$CYP\ 3A4 = C_1 Day13 + C_2 Day21 + C_3 CoCulture + C_4 TGF\beta(100) + C_5 TGF\beta(200) + C_6 TGF\beta(300) + C_7 TGF\beta(500) + C_8 TGF\beta(1{,}000) + C_9 TGF\beta(5{,}000) + C_{10} TGF\beta(10{,}000) + Intercept$$

The result shows that the r-squared value is 0.881, which suggests that there is a predictive value of how the final CYP 3A4 output is a function of the initial variables. The r-squared value of CYP 3A4 is significantly higher than CYP 2A6. The histogram of the residuals

does not follow any distribution. Combined with the QQ plot, the data falls far away from the predicted values and the data does not adhere strongly to the linear expectation as well.

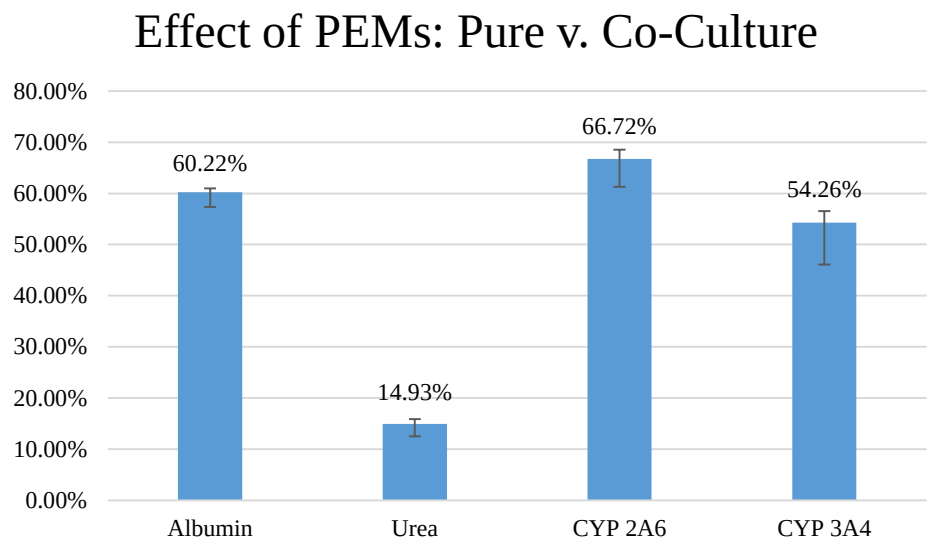

Figure 62 Regression analysis: pure versus co-culture

The presence of a co-culture causes a strong upregulation of each of marker. The total effect of the co-culture is non-trvial causing the total ouput of the markers to increase between 14.93% to 66.72%.

4.4 Conclusion

Multivariant regression modeling was able to successfully isolate and show the contribution of variables to the final output of albumin, urea, CYP 2A6 and CYP 3A4. The analysis further showed that complex modeling may not be needed, as some simple linear regressions were able to achieve an r-squared value of greater than 0.9.

The regressions showed that having a PEMs subtrate had mixed results, and in a majority of cases produced results that showed a downregulation of the desired marker, such as albumin. While the standard deviation was high in all cases, the results showed that there does not seem

to be a justification for having a PEMs substrate in lieu of TCPS for conventional culture; however, PEMs containing heparin are useful for presenting growth factors to hepatocytes in a more physiologically-relevant manner.

While prior work suggested that having TGF-β adsorbed on the surface would be beneficial, it was not until the current work that the benefit was fully understood. For key markers such as albumin and urea, the upregualtion was in excess of ten percent. The standard devations were small enough that the results were significant within 95% for all markers. Prior literature suggested that clustering of growth factor receptors tend to occur around integrin; thus the results were not surprising (Hudson et al. 2017).

The presence of a co-culture was significant and produced upregulation of markers by over 50%. In addition, the regression showed that the co-culture upregulation has relative small standard devations, which is good for the creation of any type of *in vitro* or lab-on-a-chip system. Future work should consider using other ECM proteins that bind to TGF-β, such as collagen IV.

5. CITED LITERATURE

Aleksunes, L. M. & Klaassen, C. D. Coordinated Regulation of Hepatic Phase I and II Drug-Metabolizing Genes and Transporters using AhR-, CAR-, PXR-, PPARα-, and Nrf2-Null Mice. *Drug Metabolism and Disposition* **40**, 1366 (2012).

Allen, J. W., Khetani, S. R. & Bhatia, S. N. In vitro zonation and toxicity in a hepatocyte bioreactor. *Toxicological sciences* **84**, 110-119 (2004).

Almodóvar, J., Bacon, S., Gogolski, J., Kisiday, J. D. & Kipper, M. J. Polysaccharide-based polyelectrolyte multilayer surface coatings can enhance mesenchymal stem cell response to adsorbed growth factors. *Biomacromolecules* **11**, 2629-2639 (2010).

Altrock, E. *et al.* Inhibition of fibronectin deposition improves experimental liver fibrosis. *Journal of hepatology* **62**, 625-633 (2015).

Amacher, D. E. The effects of cytochrome P450 induction by xenobiotics on endobiotic metabolism in pre-clinical safety studies. *Toxicology mechanisms and methods* **20**, 159-166 (2010).

Andria, B., Bracco, A., Cirino, G. & Chamuleau, R. Liver cell culture devices. *Cell medicine* **1**, 55-70 (2010).

Baiocchini, A. *et al.* Extracellular matrix molecular remodeling in human liver fibrosis evolution. *PloS one* **11**, e0151736 (2016).

Bale, S. S., Geerts, S., Jindal, R. & Yarmush, M. L. Isolation and co-culture of rat parenchymal and non-parenchymal liver cells to evaluate cellular interactions and response. *Scientific reports* **6**, 25329 (2016).

Bale, S. S. *et al.* In vitro platforms for evaluating liver toxicity. *Experimental biology and medicine* **239**, 1180-1191 (2014).

Bataller, R. & Brenner, D. A. Liver fibrosis. *The Journal of clinical investigation* **115**, 209-218 (2005).

Berger, D. R., Ware, B. R., Davidson, M. D., Allsup, S. R. & Khetani, S. R. Enhancing the functional maturity of induced pluripotent stem cell–derived human hepatocytes by controlled presentation of cell–cell interactions in vitro. *Hepatology* **61**, 1370-1381 (2015).

Bernardi, M., Maggioli, C. & Zaccherini, G. Human albumin in the management of complications of liver cirrhosis. *Critical Care* **16**, 211 (2012).

Birchmeier, W. Orchestrating Wnt signalling for metabolic liver zonation. *Nature cell biology* **18**, 463 (2016).

Bissell, D. M., Roulot, D. & George, J. Transforming growth factor β and the liver. *Hepatology*

34, 859-867 (2001).

Boddohi, S., Almodóvar, J., Zhang, H., Johnson, P. A. & Kipper, M. J. Layer-by-layer assembly of polysaccharide-based nanostructured surfaces containing polyelectrolyte complex nanoparticles. *Colloids and Surfaces B: Biointerfaces* **77**, 60-68 (2010).

Borst, P., Evers, R., Kool, M. & Wijnholds, J. A family of drug transporters: the multidrug resistance-associated proteins. *Journal of the National Cancer Institute* **92**, 1295-1302 (2000).

Cameron, K. *et al.* Recombinant laminins drive the differentiation and self-organization of hESC-derived hepatocytes. *Stem Cell Reports* **5**, 1250-1262 (2015).

Carlsson, R., Engvall, E., Freeman, A. & Ruoslahti, E. Laminin and fibronectin in cell adhesion: enhanced adhesion of cells from regenerating liver to laminin. *Proceedings of the National Academy of Sciences* **78**, 2403-2406 (1981).

Chen, X. M., O'Hara, S. P. & LaRusso, N. F. The immunobiology of cholangiocytes. *Immunology & Cell Biology* **86**, 497-505 (2008).

Choi, J. & Rubner, M. F. Influence of the degree of ionization on weak polyelectrolyte multilayer assembly. *Macromolecules* **38**, 116-124 (2005).

Clément, B. *et al.* Hepatocytes may produce laminin in fibrotic liver and in primary culture. *Hepatology* **8**, 794-803 (1988).

Costa, R. R. & Mano, J. F. Polyelectrolyte multilayered assemblies in biomedical technologies. *Chemical Society Reviews* **43**, 3453-3479 (2014).

De Bartolo, L. *et al.* Human hepatocyte functions in a crossed hollow fiber membrane bioreactor. *Biomaterials* **30**, 2531-2543 (2009).

Demetris, A. J. *et al.* Functional immune anatomy of the liver—as an allograft. *American Journal of Transplantation* **16**, 1653-1680 (2016).

DiPersio, C. M., Jackson, D. A. & Zaret, K. S. The extracellular matrix coordinately modulates liver transcription factors and hepatocyte morphology. *Molecular and Cellular Biology* **11**, 4405-4414 (1991).

Dooley, S. & Ten Dijke, P. TGF-β in progression of liver disease. *Cell and tissue research* **347**, 245-256 (2012).

Dranoff, J. A. & Wells, R. G. Portal fibroblasts: Underappreciated mediators of biliary fibrosis. *Hepatology* **51**, 1438-1444 (2010).

Du, Y. *et al.* Human hepatocytes with drug metabolic function induced from fibroblasts by

lineage reprogramming. *Cell stem cell* **14**, 394-403 (2014).

Enat, R. *et al.* Hepatocyte proliferation in vitro: its dependence on the use of serum-free hormonally defined medium and substrata of extracellular matrix. *Proceedings of the National Academy of Sciences* **81**, 1411-1415 (1984).

Frantz, C., Stewart, K. M. & Weaver, V. M. The extracellular matrix at a glance. *J Cell Sci* **123**, 4195-4200 (2010).

Friedman, S. L. Liver fibrosis–from bench to bedside. *Journal of hepatology* **38**, 38-53 (2003).

Friedman, S. L. Hepatic stellate cells: protean, multifunctional, and enigmatic cells of the liver. *Physiological reviews* **88**, 125-172 (2008).

Gebhardt, R. & Matz-Soja, M. Liver zonation: Novel aspects of its regulation and its impact on homeostasis. *World journal of gastroenterology: WJG* **20**, 8491 (2014).

Gordillo, M., Evans, T. & Gouon-Evans, V. Orchestrating liver development. *Development* **142**, 2094-2108 (2015).

Gross-Steinmeyer, K. *et al.* Influence of Matrigel-overlay on constitutive and inducible expression of nine genes encoding drug-metabolizing enzymes in primary human hepatocytes. *Xenobiotica* **35**, 419-438 (2005).

Hahn, E., Wick, G., Pencev, D. & Timpl, R. Distribution of basement membrane proteins in normal and fibrotic human liver: collagen type IV, laminin, and fibronectin. *Gut* **21**, 63-71 (1980).

Hamilton, G. A. *et al.* Regulation of cell morphology and cytochrome P450 expression in human hepatocytes by extracellular matrix and cell-cell interactions. *Cell and tissue research* **306**, 85-99 (2001).

Hayashi, H. & Sakai, T. Biological significance of local TGF-β activation in liver diseases. *Frontiers in physiology* **3**, 12 (2012).

Hudson, Shanice V. et al. “Modeling the Kinetics of Integrin Receptor Binding to Hepatic Extracellular Matrix Proteins.” *Scientific Reports* **7**, 12444 (2017).

Ignotz, Ronald A., and Joan Massague. "Transforming growth factor-beta stimulates the expression of fibronectin and collagen and their incorporation into the extracellular matrix." *Journal of Biological Chemistry* **261.9**, 4337-4345 (1986).

Johansson, S., Svineng, G., Wennerberg, K., Armulik, A. & Lohikangas, L. Fibronectin-integrin interactions. *Front Biosci* **2**, d126-d146 (1997).

Jungermann, K. & Keitzmann, T. Zonation of parenchymal and nonparenchymal metabolism in

liver. *Annual review of nutrition* **16**, 179-203 (1996).

Juza, R. M. & Pauli, E. M. Clinical and surgical anatomy of the liver: A review for clinicians. *Clinical Anatomy* **27**, 764-769 (2014).

Kaplowitz, N. Drug-induced liver injury. *Clinical Infectious Diseases* **38**, S44-S48 (2004).

Kaylan, K. B., Ermilova, V., Yada, R. C. & Underhill, G. H. Combinatorial microenvironmental regulation of liver progenitor differentiation by Notch ligands, TGFβ, and extracellular matrix. *Scientific reports* **6**, 23490 (2016).

Khetani, S. R. & Bhatia, S. N. Microscale culture of human liver cells for drug development. *Nature biotechnology* **26**, 120 (2008).

Kim, I.-Y. *et al.* Chitosan and its derivatives for tissue engineering applications. *Biotechnology advances* **26**, 1-21 (2008).

Klein, I. *et al.* Kupffer cell heterogeneity: functional properties of bone marrow–derived and sessile hepatic macrophages. *Blood* **110**, 4077-4085 (2007).

Krebs, H. A. Urea formation in mammalian liver. *Biochemical Journal* **36**, 758 (1942).

Lang, R. *et al.* Three-dimensional culture of hepatocytes on porcine liver tissue-derived extracellular matrix. *Biomaterials* **32**, 7042-7052 (2011).

Leise, M. D., Poterucha, J. J. & Talwalkar, J. A. 1 edn 95-106 (Elsevier).

Lin, C. & Khetani, S. R. Advances in engineered liver models for investigating drug-induced liver injury. *BioMed research international* **2016** (2016).

Lin, C. *et al.* A polyelectrolyte multilayer platform for investigating growth factor delivery modes in human liver cultures. *Journal of Biomedical Materials Research Part A* (2017).

Lin, P., Chan, W. C. W., Badylak, S. F. & Bhatia, S. N. Assessing porcine liver-derived biomatrix for hepatic tissue engineering. *Tissue engineering* **10**, 1046-1053 (2004).

Lin, R. Z. & Chang, H. Y. Recent advances in three-dimensional multicellular spheroid culture for biomedical research. *Biotechnology journal* **3**, 1172-1184 (2008).

Lindros, K. O. Zonation of cytochrome P450 expression, drug metabolism and toxicity in liver. *General Pharmacology: The Vascular System* **28**, 191-196 (1997).

Mak, K. M. & Mei, R. Basement membrane type IV collagen and laminin: an overview of their biology and value as fibrosis biomarkers of liver disease. *The Anatomical Record* (2017).

Martinez-Hernandez, A. & Amenta, P. S. The extracellular matrix in hepatic regeneration. *The*

FASEB journal **9**, 1401-1410 (1995).

Matlin, K. S., Myllymäki, S.-M. & Manninen, A. Laminins in Epithelial Cell Polarization: Old Questions in Search of New Answers. *Cold Spring Harbor perspectives in biology* **9**, a027920 (2017).

Matsumoto, K. & Nakamura, T. Emerging multipotent aspects of hepatocyte growth factor. *The Journal of Biochemistry* **119**, 591-600 (1996).

Moghe, P. V. *et al.* Culture matrix configuration and composition in the maintenance of hepatocyte polarity and function. *Biomaterials* **17**, 373-385 (1996).

Neto, A. I., Vasconcelos, N. L., Oliveira, S. M., Ruiz-Molina, D. & Mano, J. F. High-Throughput Topographic, Mechanical, and Biological Screening of Multilayer Films Containing Mussel-Inspired Biopolymers. *Advanced Functional Materials* **26**, 2745-2755 (2016).

Nguyen-Lefebvre, A. T. & Horuzsko, A. Kupffer cell metabolism and function. *Journal of enzymology and metabolism* **1** (2015).

Ramaiahgari, S. C. *et al.* A 3D in vitro model of differentiated HepG2 cell spheroids with improved liver-like properties for repeated dose high-throughput toxicity studies. *Archives of toxicology* **88**, 1083-1095 (2014).

Reuben, A., Koch, D. G. & Lee, W. M. Drug-induced acute liver failure: results of a us multicenter, prospective study. *Hepatology* **52**, 2065-2076 (2010).

Ruoslahti, E. & Yamaguchi, Y. Proteoglycans as modulators of growth factor activities. *Cell* **64**, 867-869 (1991).

Salomäki, M., Vinokurov, I. A. & Kankare, J. Effect of temperature on the buildup of polyelectrolyte multilayers. *Langmuir* **21**, 11232-11240 (2005).

Sanderson, N. *et al.* Hepatic expression of mature transforming growth factor beta 1 in transgenic mice results in multiple tissue lesions. *Proceedings of the National Academy of Sciences* **92**, 2572-2576 (1995).

Schlenoff, J. B. & Dubas, S. T. Mechanism of polyelectrolyte multilayer growth: charge overcompensation and distribution. *Macromolecules* **34**, 592-598 (2001).

Schlessinger, J., Lax, I. & Lemmon, M. Regulation of growth factor activation by proteoglycans: what is the role of the low affinity receptors? *Cell* **83**, 357-360 (1995).

Schuppan, Detlef. "Structure of the extracellular matrix in normal and fibrotic liver: collagens and glycoproteins." *Seminars in liver disease* **10**, 1-10 (1990).

Seki, S. *et al.* The liver as a crucial organ in the first line of host defense: the roles of Kupffer cells, natural killer (NK) cells and NK1. 1 Ag+ T cells in T helper 1 immune responses. *Immunological reviews* **174**, 35-46 (2000).

Sellaro, T. L. *et al.* Maintenance of human hepatocyte function in vitro by liver-derived extracellular matrix gels. *Tissue Engineering Part A* **16**, 1075-1082 (2009).

Sevior, D. K., Pelkonen, O. & Ahokas, J. T. Hepatocytes: the powerhouse of biotransformation. *The international journal of biochemistry & cell biology* **44**, 257-261 (2012).

Shek, F. W. & Benyon, R. C. How can transforming growth factor beta be targeted usefully to combat liver fibrosis? *European journal of gastroenterology & hepatology* **16**, 123-126 (2004).

Shoulders, M. D. & Raines, R. T. Collagen structure and stability. *Annual review of biochemistry* **78**, 929-958 (2009).

Silva, J. M., Day, S. H. & Nicoll-Griffith, D. A. Induction of cytochrome-P450 in cryopreserved rat and human hepatocytes. *Chemico-biological interactions* **121**, 49-63 (1999).

Si-Tayeb, K., Lemaigre, F. P. & Duncan, S. A. Organogenesis and development of the liver. *Developmental cell* **18**, 175-189 (2010).

Si-Tayeb, K. *et al.* Highly efficient generation of human hepatocyte–like cells from induced pluripotent stem cells. *Hepatology* **51**, 297-305 (2010).

Skardal, A. *et al.* Tissue specific synthetic ECM hydrogels for 3-D in vitro maintenance of hepatocyte function. *Biomaterials* **33**, 4565-4575 (2012).

Stevens, J. L. & Baker, T. K. The future of drug safety testing: expanding the view and narrowing the focus. *Drug discovery today* **14**, 162-167 (2009).

Taipale, J. & Keski-Oja, J. Growth factors in the extracellular matrix. *The FASEB Journal* **11**, 51-59 (1997).

Thomas, R. J. *et al.* The effect of three-dimensional co-culture of hepatocytes and hepatic stellate cells on key hepatocyte functions in vitro. *Cells Tissues Organs* **181**, 67-79 (2005).

Tien, E. S. & Negishi, M. Nuclear receptors CAR and PXR in the regulation of hepatic metabolism. *Xenobiotica* **36**, 1152-1163 (2006).

Wang, S. & Kaufman, R. J. How does protein misfolding in the endoplasmic reticulum affect lipid metabolism in the liver? *Current opinion in lipidology* **25**, 125-132 (2014).

Watanabe, M. *et al.* Maintenance of Hepatic Functions in Primary Human Hepatocytes Cultured on Xeno-Free and Chemical Defined Human Recombinant Laminins. *PloS one* **11**,

e0161383 (2016).

Westerink, W. M. A. & Schoonen, W. G. E. J. Cytochrome P450 enzyme levels in HepG2 cells and cryopreserved primary human hepatocytes and their induction in HepG2 cells. *Toxicology in vitro* **21**, 1581-1591 (2007).

Wierzbicka-Patynowski, I. & Schwarzbauer, J. E. The ins and outs of fibronectin matrix assembly. *Journal of cell science* **116**, 3269-3276 (2003).

Williams, E. J. *et al.* Relaxin inhibits effective collagen deposition by cultured hepatic stellate cells and decreases rat liver fibrosis in vivo. *Gut* **49**, 577-583 (2001).

Xu, C., Li, C. Y.-T. & Kong, A.-N. T. Induction of phase I, II and III drug metabolism/transport by xenobiotics. *Archives of pharmacal research* **28**, 249 (2005).

Zeisberg, M. *et al.* De-differentiation of primary human hepatocytes depends on the composition of specialized liver basement membrane. *Molecular and cellular biochemistry* **283**, 181-189 (2006).

VITAE

EDUCATION

University of Illinois at Chicago
Master of Science in Bioengineering — Expected: May 2018

Bachelor of Science in Bioengineering — May 2017
City Colleges of Chicago STEM Scholar
National Science Foundation Supplemental Fund Recipient, Grant #1230294
Dean's List: Spring 2016, Fall 2016, Spring 2017

EXPERIENCE

Researcher — Chicago, IL
University of Illinois at Chicago – Khetani lab — January 2016 – Present
• Conducted a comprehensive screen of the effects of liver ECM proteins on primary human hepatocyte function
• Constructed heparin-chitosan polyelectrolyte multilayers for growth factor delivery to primary human hepatocytes
• Examined the effects of liver ECM proteins on differentiation and functioning of induced pluripotent stem cells
• Fabricated micropatterned co-cultures for drug clearance testing
• Performed albumin ELISA, urea, and cytochrome P450 assays

Researcher — Evanston, IL
Northwestern University – Notestein group — June 2014 – August 2014
• Studied novel heterogeneous catalytic reactions involving renewable sources
• Researched and performed catalytic runs to optimize thermal epoxidation and photooxidation reactions

Researcher — Chicago, IL
Thermal Conservation Technologies, Inc — May 2013- December 2013
• Designed and built an industry standard reaction chamber for accelerated aging
• Led a research project that examined the effect of rainwater pH on welded 321 stainless steel
• Analyzed surface chemistry, particularly oxidation of 321 stainless steel, over a period of 16 weeks

Research Experience for Undergraduates — Chicago, IL
Illinois Institute of Technology – Brey lab — May 2012- August 2012
• Performed tissue harvesting from Long Evans rats (*Rattus norvegicus*)
• Completed dermal extraction via mechanical and enzymatic means using a technique by Uriel *et al.*

PUBLICATIONS

• Thornburg, Nicholas E., Raimondo, Corrina, Ignacio de Leon, Patricia, Prieto – Centurion, Dario, Schoenfeldt, Nicholas J., Korinda, Andrew W., **Sorokina, Lioudmila V.**, Eaton, Todd R., Notestein, Justin M. "Research Note: Suggested Experimental Methods for Liquid Phase Epoxidation with H_2O_2." Journal of Catalysis (submitted).

• Lin, Christine, Romero, Raimundo **, Sorokina, Lioudmila V.**, Ballinger, Kim R., Place, Laura W., Kipper, Matt J., Khetani, Salman R. "A Polyelectrolyte Multilayer Platform for Investigating

Growth Factor Delivery Modes in Human Liver Cultures." Journal of Biomedical Materials Research Part A (2017).

• Khansari, Maziyar M., **Sorokina, Lioudmila V.**, Mukherjee, Prithviraj, Mukhtar, Farrukh, Shirdar, Mostafa R., Shahidi, Mahnaz, Shokuhfar, Tolou. "Classification of Hydrogels Based on Their Source: A Review and Application in Stem Cell Regulation." JOM (2017): 1-8.

PRESENTATIONS AND POSTERS

• T. Eaton, H.L. Hinton, **L. Sorokina**, et al. "Controlling the titania-silica interface for enhanced (photo)catalytic performance." 249th American Chemical Society National Meeting & Exposition (Presentation)

• **LV Sorokina**, C Negrete, T Higgins, et al. "Corrosion of hermetically welded 321 stainless steel in aqueous solutions" 247th American Chemical Society National Meeting & Exposition (Poster)

• C Negrete, **LV Sorokina**, T Higgins, et al. "Accelerated aging of stainless steels for vacuum insulation panel applications" 247th American Chemical Society National Meeting & Exposition (Poster)

• **L.V. Sorokina**, M. Vaicik , T. Waller, et al. "Pegylation of Dermal Extract Hydrogels" Biomedical Engineering Society Annual Meeting 2012 (Poster)

ADDITIONAL

• Member of Society of Women Engineers — September 2014 – Present
• Member of Biomedical Engineering Society — August 2012 – Present
• Proficient in R, Matlab, SolidWorks, Microsoft Office
• Fluent in Russian, beginner French